Microwave Photonic Radars

Shilong Pan, *Senior Member, IEEE, Fellow, OSA*, and Yamei Zhang, *Member, IEEE*

(Invited Tutorial)

***Abstract*—As the only method for all-weather, all-time and long-distance target detection and recognition, radar has been intensively studied since it was invented, and is considered as an essential sensor for future intelligent society. In the past few decades, great efforts were devoted to improving radar's functionality, precision, and response time, of which the key is to generate, control and process a wideband signal with high speed. Thanks to the broad bandwidth, flat response, low loss transmission, multidimensional multiplexing, ultrafast analog signal processing and electromagnetic interference immunity provided by modern photonics, implementation of the radar in the optical domain can achieve better performance in terms of resolution, coverage, and speed which would be difficult (if not impossible) to implement using traditional, even state-of-the-art electronics. In this tutorial, we overview the distinct features of microwave photonics and some key microwave photonic technologies that are currently known to be attractive for radars. System architectures and their performance that may interest the radar society are emphasized. Emerging technologies in this area and possible future research directions are discussed.**

***Index Terms*—Radars, microwave photonics, LO generation, waveform generation, mixing, filtering, analog-to-digital conversion, beamforming, interference cancellation, analog signal processing, synthetic aperture, radar imaging, photonic integration.**

I. Introduction

RADAR, the acronym of RAdio Detection And Ranging, is regarded as the primary and popular method for all-weather, all-time and long-distance target detection, imaging, classification and recognition [1]. By radiating radio frequency (RF) signals into the free space through a transmitter and collecting the echoes with a receiver, the information (e.g., distance, altitude, image, direction, and speed) of the targets can be extracted after de-chirping, auto-correlation or other algorithms [1]. Traditionally, radars are realized with pure electronic technologies, which now suffer severely from the limited bandwidth, few functions, low speed, and poor resolution, making them difficult to detect and identify low-attitude, low-speed and small targets for civil applications in the complex electromagnetic environment. To deal with these issues, photonics-based technologies were introduced to radars thanks to the distinct features of modern photonics, such as broad bandwidth, flat response, low loss transmission, multidimensional multiplexing, fast analog signal processing, highly coherent pulse source and electromagnetic interference (EMI) immunity [2]–[7]. Typical microwave photonic subsystems like optoelectronic oscillators (OEOs), broadband waveform generators, optical beamforming networks (OBFN), microwave photonic mixers, real-time Fourier transform (RTFT) systems, and photonic analog to digital convertors were developed and optimized for possible application in radars [8]–[13]. Besides, different architectures of microwave photonic radars were proposed recently, which demonstrated the exceptional reconfigurability, multiple functionalities, wide area distribution, and high-resolution imaging capability enabled by the photonics.

This tutorial firstly overviews the unique features of microwave photonics that are attractive for radars, which is presented in Section II. Then, in Section III several microwave photonic technologies that are known interesting to the radar society are reviewed, including photonic local oscillation (LO) generation, photonic radar waveform generation, microwave photonic mixing and channelization, microwave photonic filtering, optical beamforming, optical RTFT, photonic analog-to-digital conversion (ADC), and co-site interference cancellation. In Section IV, recent advancement on the microwave photonic radars is introduced, with an emphasis on the system architectures and the achieved performance. The possible future research directions in this area are discussed in Section V.

II. The Features of Microwave Photonics

In a conventional microwave system, microwave or intermediate frequency (IF) signals are distributed or processed in the electrical domain using electronic components, as shown in Fig. 1(a). To take benefits from modern photonics, broadband electrical-to-optical (EO) and optical-to-electrical (OE) conversions are introduced to the system so that the signals can be transmitted in an optical fiber or processed in the optical domain using optical devices, as shown in Fig. 1(b).

EO conversion with a bandwidth of several or tens of gigahertz can be implemented by a direct-modulated laser diode (LD) or a continuous-wave (CW) laser source together with an external modulator. For an LD, the output optical power would increase linearly with the drive current in a certain range, so EO

Manuscript received February 15, 2020; revised March 25, 2020 and May 1, 2020; accepted May 5, 2020. Date of publication May 7, 2020; date of current version October 1, 2020. This work was supported in part by the National Key R&D Program of China under Grant 2018YFB2201803, in part by the National Natural Science Foundation of China under Grant 61901215 and Grant 61527820, and in part by the Fundamental Research Funds for the Central Universities. *(Corresponding authors: Shilong Pan and Yamei Zhang.)*

The authors are with the Key Laboratory of Radar Imaging and Microwave Photonics (Nanjing Univ. Aeronaut. Astronaut.), Ministry of Education, Nanjing University of Aeronautics and Astronautics, Nanjing 210016, China (e-mail: pans@nuaa.edu.cn; zhang_ym@nuaa.edu.cn).

Color versions of one or more of the figures in this article are available online at https://ieeexplore.ieee.org.

Digital Object Identifier 10.1109/JLT.2020.2993166

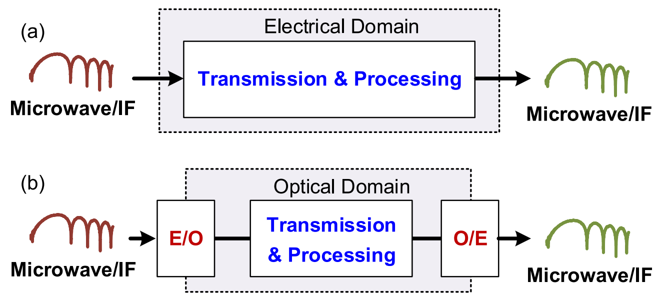

Fig. 1. Schematic diagrams of (a) a conventional microwave system and (b) a typical microwave photonic system.

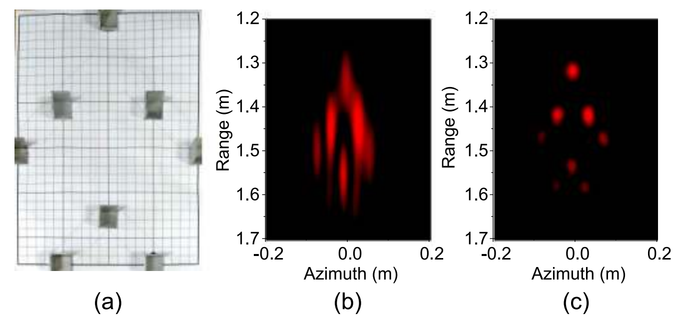

Fig. 2. (a) The target consisting of eight reflectors, and microwave images achieved by (b) a 2-GHz bandwidth radar and (c) an 8-GHz bandwidth radar.

conversion can be easily realized if the LD is properly biased and the drive current to the LD is controlled by a microwave or IF signal. In the external modulation scheme, the phase, intensity or polarization of the CW light from the laser is modulated at an electro-optic modulator (EOM) by changing the refractive index, gain (absorption) coefficient or birefringence of the material in the modulator according to the input electrical signal. Compared with the external modulation, direct modulation is more energy-efficient and cost-efficient, but it is usually difficult to provide a large bandwidth, a high gain, and a large dynamic range that are required by radars. Therefore, EO conversion in the following refers to external modulation unless specified. The broadband OE conversion can be realized by either photovoltaic or photoconductive effect, which converts the optical power into an electrical current. Different types of photodetectors (PDs) are developed to achieve the OE conversion [14], including waveguide PD, uni-traveling carrier PD (UTC-PD), velocity-matched distributed PD, traveling-wave PD and so on [15].

The parameters of the devices for the EO/OE conversion have fundamental impacts on the performance of the microwave systems, such as the link gain, bandwidth, dynamic range, signal to noise ratio (SNR), and conversion efficiency. Thanks to the fast development of the optoelectronic devices, the relative intensity noise (RIN) of the LD, which affects the noise floor of the microwave photonic system, has been improved from −135 dB/Hz in the 1980s to the current −168 dB/Hz [16], [17]; the linewidth, which could be converted into microwave amplitude, phase, or frequency noises in different microwave photonic systems, has been declined from 7.5 GHz to 0.01 Hz [14], [18]; and the output power, which is associated with the gain of the system, has been boosted from several mW to 2 W [19], [20]. The half-wave voltage of the EOM has been reduced from 84 to 0.8 V [21], [22], and its 3-dB bandwidth has been grown from 1 to 500 GHz [23], [24]. In addition, PDs with high responsivity and large bandwidth are also available. For example, UTC-PDs with a 3-dB bandwidth of over 300 GHz [25], a responsivity of 1.02 A/W [26], or an output power as high as 22 dBm [27] has been reported. Besides, arrayed laser [28], arrayed modulator [29] and arrayed PD [30] are also commercially available.

With the improved performance of microwave photonic devices, the amplifier-less microwave photonic link could reach a 12.7-dB gain and a noise figure of less than 5.7 dB [31], and the spurious-free dynamic range (SFDR) could exceed 130 dBc·Hz$^{2/3}$, making microwave photonics highly potential for radar applications. In the past few decades, many unique features of microwave photonics have been revealed which may not be achievable using traditional, even state-of-the-art electronics. Some of these features are obvious and well accepted by the researchers on radars, while some are not fully utilized to form intriguing techniques at the current stage.

A. *Broad Bandwidth*

Bandwidth is of great importance to radars, which directly determines the range resolution and the functionalities (or reconfigurability) of the system. Generally, the range resolution of a radar is expressed as,

$$L_{\mathrm{RES}} = c/2B \tag{1}$$

where c is the speed of light in vacuum, and B is the bandwidth of the radiated signal. As can be seen, the range resolution is inversely proportional to the bandwidth of the transmitted signal [32], so broad bandwidth could lead to high-resolution radar imaging. Fig. 2 shows the microwave images achieved by radars with different bandwidths. The target in Fig. 2(a) is an abstract aircraft composed of eight corner reflectors, which are placed on a rotator with a speed of 360°/s, and the reconstructed images in Fig. 2(b) and (c) are achieved with radars with 2-GHz and 8-GHz bandwidths, respectively. As can be seen, the eight reflectors can be differentiated through the 8-GHz bandwidth radar while the 2-GHz bandwidth one can only obtain a blurred figure. Further increase the bandwidth may enable multispectral radar imaging of complex targets.

Besides, the functions of radars are highly diverse, including air traffic control [33], landing guidance [34], radar astronomy [35], earth exploration [36], aircraft/vehicle anti-collision [37], outer space surveillance [38], meteorological precipitation monitoring [39], altimetry [40], ground-penetrating [41], battle-field surveillance [42], target tracking [43], fire control [44], and so on. Several of these functions may be required in a single platform. Taking radars for autonomous driving as an example, the future self-driving vehicle may call for ultrahigh-resolution imaging, pre-crash warning, chassis-to-ground monitoring, and driver vital-sign monitoring simultaneously or alternately [45]. As different radar functions have their best operation frequency bands, RF frontends with wide bandwidth are the basis of multi-functional or reconfigurable radars.

In addition, for a given emitting power a broadband signal will have small power spectral density, which is beneficial for radars in relation to anti-jamming and anti-intercept [46]. Moreover, broadband radars may decrease the "dead zone" (an area that cannot be detected by a radar) at close ranges since short pulses can be applied.

In traditional radar, the microwave signal is generated and processed in the electrical domain. The signal manipulation capability of a microwave system is connected with the relative bandwidth which is defined as the ratio of the signal bandwidth and the center frequency [47]. For a traditional microwave system, the center frequency is generally around tens of gigahertz. Taking a signal centered at 10 GHz as an example, when its instantaneous bandwidth is 1 GHz, the relative bandwidth is 10%. On the other hand, for a microwave photonic system, the center frequency is ∼193 THz, so the relative bandwidth of the 1-GHz signal is only ∼0.0005%. That is to say, the broadband signal in the electrical domain can be regarded as a very narrow-band signal in the optical domain. Therefore, photonic systems hold an excellent broadband microwave signal handling capability. One such example is optical fiber. The OFS AllWave optical fiber and Corning Ultra optical fiber have a low transmission loss from 1285 to 1625 nm, corresponding to a flat magnitude response of ∼48.8 THz (or ∼25% relative bandwidth) [48], [49].

B. High-Performance Signal Transmission

Transmission lines are widely used in radars, especially arrayed radars, distributed radars, and radars requiring remote signal processing. Optical fiber is regarded as the best medium for information transmission on account of its ultra-low transmission loss (∼0.2 dB/km), light weight (∼60 g/km), low cost and immunity to EMI. The thermal coefficient of delay of the fiber is <5 parts per million (ppm)/°C (some specially-designed fiber may reach a thermal coefficient of delay of < 0.5 ppm/°C), which is a factor of 3∼10 lower than the best coaxial cable [50], [51]. More importantly, optical fiber supports bidirectional transmission, which ensures delivery of ultra-stable frequency and timing reference signals to distributed transceivers since accurate feedback loop can be easily established [52]–[54]. With this feature, an optical link with a transmission distance of 1840 km and a frequency transfer stability at the level of 10^{-19}/day was achieved [54].

As early as the 1970s, NASA successfully applied the radio-over-fiber (RoF) technique in its Deep Space Network (DSN), to deliver RF references to different antennas separated by more than 10 km [55]. In February 2000, a length of ∼60-m long fiber was used to connect two radar transceivers carried by the Space Shuttle Endeavour, enabling the successful mapping of Earth from the 233-km orbit [56].

The high-performance optical signal transmission can also enable a number of new applications for radar systems. The low loss and small dispersion optical fiber can serve as a broadband delay line with a large amount of delay but ignorable loss for radar target simulators, to test radars on aircrafts and ships. With phase-derived ranging enabled by bidirectional transmission, accurate length of a long fiber can be achieved with a resolution of 0.001 ps [57], [58], ensuring precise analog signal processing in the optical domain due to the fact that time delay is one of the essential elements of analog signal processing. By inserting a length of optical fiber into a microwave oscillator together with EO and OE converters, an unprecedented high-Q optoelectronic cavity would be formed, which can generate a high-purity and low-phase-noise microwave LO signal (see OEOs in Section III). Besides, the bidirectional transmission capability of fiber leads to the invention of fiber Bragg gratings (FBGs) [59], which enables a number of advanced signal processing functions for radars.

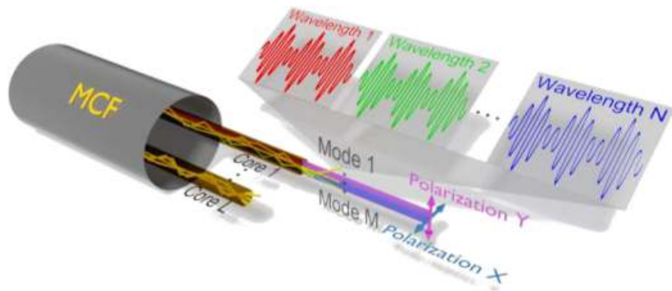

Fig. 3. Illustration of the multi-dimensional multiplexing in microwave photonics. MCF: multi-core fiber.

C. Multi-Dimensional Multiplexing

Active electronically scanned array (AESA) [60], [61] and multiple-input multiple-output (MIMO) [62], [63] radar systems, which are the dominant form of today's radars, are assembled with hundreds, thousands, or even tens of thousands of transmit/receive (T/R) modules. If there is a strategy of multiplexing in the system, the number of the required components would be significantly decreased, leading to a dramatic reduction of cost, size, weight, and power (SwaP) [64]. In addition, frequency response mismatches and other defects among different channels would be minimized. Previously, different types of multiplexing methods were developed for radars (especially for MIMO radars) in the electronic domain, such as time-division multiplexing (TDM), frequency-division multiplexing (FDM) and code-division multiplexing (CDM) [65]–[69].

Photonics would provide additional degrees of freedom for performing multiplexing, which opens the possibility for large-scale, broad-bandwidth, and large dynamic range arrayed radar with reduced hardware resources, as shown in Fig. 3.

One well-known optical multiplexing technique is wavelength-division multiplexing (WDM), which takes benefit from tens-THz available bandwidth of optical devices and is now widely applied in optical communications [70]. Researchers on microwave photonics have already employed WDM to establish different kinds of microwave photonic systems, such as high-performance OBFNs [71], multichannel mixing [72], multichannel RF delivery [73], microwave photonic filtering [74], compressive sensing [75] and so on.

Polarization is another dimension for multiplexing, which has been investigated in a variety of microwave photonic systems for signal generation, transmission, processing, control and measurement [76]–[83]. Thanks to the broadband polarization modulation and mature polarization manipulation, polarization multiplexing is very interesting for coherent operations, but one possible limitation is its sophisticated demultiplexing which usually requires adaptive tracking of the polarization states in the system [84].

Recently, another optical multiplexing technology, i.e., spatial division multiplexing (SDM), was proposed and extensively studied to break the capacity limitation of optical communication systems [85]–[88]. In an SDM system, optical devices such as multi-core fibers (with tens of cores), multi-mode fibers (with thousands of modes) and few-mode fibers are usually employed [89]–[95]. With a pair of fan-in and fan-out modules, optical signals can be coupled into different cores of a multi-core fiber (MCF) and split from the fiber into a number of single-mode fibers (SMFs) [96]. For multi-mode fiber or few-mode fibers, a device named photonic lantern is employed to translate the signals into different transmission modes [97], [98]. The application of SDM technology in microwave photonic systems for multi-LO generation, signal transmission, spectral sensing, filtering, and beamforming was previously investigated [99]–[102]. One primary concern for exploiting SDM in microwave photonics is its severe inter-channel crosstalk due to the limited isolation between different cores or modes [103].

D. Broadband Analog Signal Processing

Analog signal processing is usually a part of the RF frontend in radars. The results are achieved in real time and the functions are always elementary. Examples contain filtering, mixing, phase shifting, frequency division and multiplying, time stretching or compressing, sensitivity time control and so on. Other advanced signal processing functions have to be carried out in the digital domain since digital signal processing (DSP) is flexible, repeatable and accurate. However, DSP would encounter significant challenges when handling broadband signals because of high power consumption, unacceptable latency, and the high-cost and low-performance ADCs at high frequencies [104]. Therefore, the role of analog signal processing should be pronounced for broadband radars.

In electrical analog signal processing systems, signals are processed by passing them through circuits consisting of capacitors, resistors, inductors, delay lines, operational amplifiers, transistors, and other nonlinear devices, which would have a limited bandwidth due to the finite frequency response of these devices [105]. In the optical domain, however, we can implement the analog signal processing in different manners. In particular, we have optical frequency combs (OFCs) or ultrashort optical pulses spreading in a spectral range of several THz. With a programmable filter to shape the spectrum and an EOM to load the microwave signal, the signal can be easily stretched or compressed in a dispersive element. Based on this operation, Fourier transform [106]–[108], pulse coding [109], [110], sampling and quantization [111]–[113], filtering [114]–[116], and time reversal [117] can be achieved. In addition, the spectral lines of the OFCs can be separated in the spatial domain using an optical diffraction grating. Then, spatial light modulators can be used to process the signal. Because of the line-by-line spectral manipulation capability of the SLMs, any linear signal processing function can be potentially executed. Typical examples include correlation [118], spatial Fourier transform [119], [120], matrix calculation [121] and mode shaping [122], [123].

Other broadband analog signal processing based on CW lasers was also reported, such as phase shifting [124]–[126], mixing [10], [127], phase coding [128], [129], filtering [130]–[132], Fourier transform [133], [134], and frequency multiplication [135]–[137], which exhibits excellent flexibility and reconfigurability as well. The combination of OFCs and CW-based signal processing would further enhance the signal processing with parallel processing capability, which not only reduces the number of devices but also improves the inter-channel consistency.

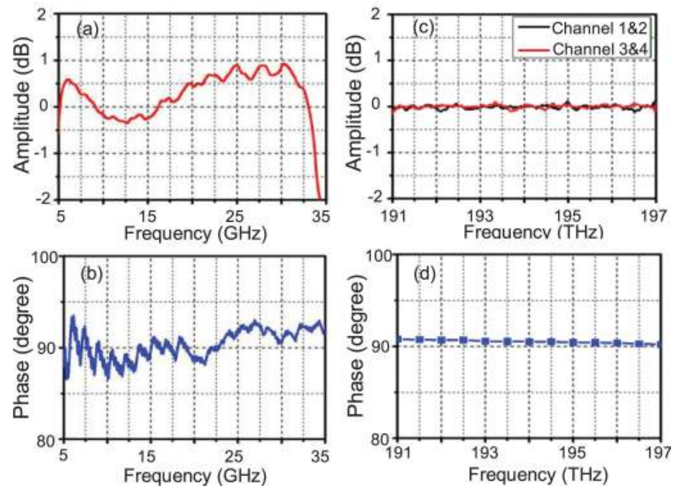

Fig. 4. Frequency responses of (a, b) an electrical 90° hybrid and (c, d) an optical 90° hybrid.

E. Flat Magnitude and Phase Responses

Radars always demand high receiver sensitivity and large dynamic range, which, however, are usually degraded by receiver noise, nonlinearity, inter-/inner-channel crosstalk, and image interference [138]–[140]. The noise or interference out of the radar's frequency band of interest can be easily removed by a filter, while the in-band interference which occupies part or full of the frequency band with the signal-of-interest (SOI) is difficult to be removed. The most effective way for in-band noise and interference mitigation is coherent cancellation, of which a signal with the same power but complementary phase to the undesirable signal is coherently combined with the original signal [138]–[140]. To obtain such a signal, devices with flat and tunable magnitude and phase responses are needed. However, in the electrical domain, the response flatness of a device can only be maintained in a very narrow bandwidth. As an illustration, Fig. 4(a) and (b) show the frequency response of an electrical 90° hybrid. As can be seen, in a 30-GHz frequency range the variation of the phase reaches 7° and that of the power is greater than 3 dB.

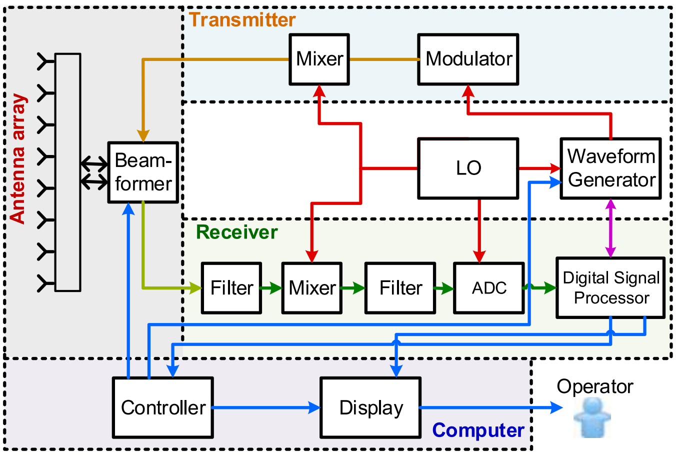

Fig. 5. Block diagram of a typical radar system.

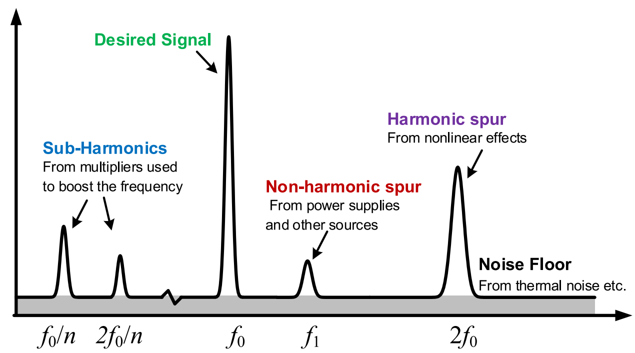

Fig. 6. Typical electrical spectrum of an LO signal.

Thanks to the flat magnitude and phase response of optical devices, it is quite easy to realize broadband signal phase shifting and power manipulating with very small frequency-dependent variations. One example is illustrated in Fig. 4(c) and (d), showing the frequency responses of a commercial optical 90° hybrid. The power and phase variations are 0.1 dB and 1° over a 6-THz frequency range, which is much better than its electrical counterpart. The excellent amplitude-phase consistency would enable wideband noise and interference cancellation in the optical domain.

Previously, coherent cancellation is explicitly or implicitly used in many microwave photonic systems, such as high-linearity analog optical links [141]–[145], image-reject mixers [10], [146]–[152], co-site interference cancellation [153]–[159], and frequency multipliers [160]–[162] to suppress the noise, undesirable nonlinear components, interference and image frequencies. For example, a linearized analog optical link with the third-order intermodulation distortion (IMD3) component suppressed by 40 dB was built in [142]; an image-reject mixer with an image-rejection ratio of 25 dB for a 1.2-GHz instantaneous bandwidth linearly frequency-modulated (LFM) signal was realized in [150] (as a comparison, the instantaneous bandwidth of an electrical image-reject mixer is less than 160 MHz [146]); a 30-dB co-site interference cancellation ratio over 9.5 GHz frequency range was obtained in [156] (while for electrical method the maximum reported bandwidth is only 120 MHz [163]); and an optical link with the common-mode noise suppressed by 15 dB over an 18-GHz frequency range was implemented in [164].

F. Highly Coherent Pulse Source

Thanks to the high-frequency nature of the light wave, ultrashort pulses down to a few femtoseconds can only be generated in the optical domain. Ultrashort pulses have many unique attributes that may enable the radar system to have some extreme performance [165]. First, the picosecond or femtosecond pulse-width could provide ultrahigh time resolution for time-domain manipulation of microwave signals like sampling, switching, time-delay control, and pump-probe measurement. The ultrashort pulses also lead to a bandwidth on the order of THz, which could enable flexible frequency-domain processing of microwave signals. More importantly, the spectral lines of ultrashort pulse trains exhibit ultra-stable phase and magnitude relationships, i.e., the spectral lines are ideally coherent, otherwise, all the spectral components cannot be concentrated into a time scale of picoseconds or femtoseconds. With the high coherence, microwave signals with ultra-low phase noise would possibly be generated, and time-to-frequency and frequency-to-time mapping is also enabled, as has been mentioned in Part D of this section. In addition, for a given pulse energy, the peak power of an ultrashort pulse would be very high, which could easily stimulate various nonlinear effect, and may enable nonlinear microwave signal processing although works on this topic are rarely found in the literature.

Previously, the highly coherent pulse source was employed for developing a number of new techniques for radar applications, such as low-noise microwave signal generation [166], [167], optical sampling and ADC [112], [168], [169], Fourier transform [170], [171], phase detection [172]–[174], time delay measurement [175], synchronizations [173], [176], etc. Most of them can achieve extreme performance in some aspects which is impossible for pure electronic approaches.

III. Microwave Photonic Technologies For Radars

Due to the aforementioned features, microwave photonics attracted considerable interest from the radar and optical societies since the 1960s [4], [177]–[183]. A number of photonics-based techniques have been developed over the past few decades, ranging from LO signal generation, waveform modulation, up- and down-conversion, distribution, beamforming, filtering, to analog-to-digital conversion, which covers almost all the RF modules in radars as shown in Fig. 5 except for antennas and amplifiers. Early studies were mainly focused on analog optical links for distributing RF/LO signals or for implementing time delays, which are considered as the basis of microwave photonic systems. These works were well summarized in [6], [184]. Some of the recent advancement on this topic is also described in Section II, so this section will pay more attention to other microwave photonic technologies that are known interesting for radar applications, including photonic LO generation,

TABLE I
PERFORMANCE COMPARISON OF DIFFERENT PHOTONIC LO GENERATION METHODS

	Method	Frequency [GHz]	PN@10kHz [dBc/Hz]	Long-term Stability	SSR [dB]
[190]	Optical frequency multiplication	up to 100	depends on ref. signal and degrades with 20lg(N)	depends on ref. signal	depends on ref. signal
[191]	Optical phase-lock loop	up to 1000	depends on ref. signal and loop parameter	depends on ref. signal	/
[192]	Brillouin oscillator	21.7	-90	5×10^{-12}	about 70
[193]	Sideband-injection-locked laser	36	-102	/	about 82
[194]	Kerr frequency comb oscillator	9.9	<-121	10^{-10}	> 60
[166]	Optical-to-radio frequency division	12	<-173	6.5×10^{-16}	/
[174]	Optical-microwave synchronization	10	<-145	depends on MLL	/
[195]	Optoelectronic oscillator	10	<-150	$<10^{-12}$	about 140

PN: phase noise; SSR: spur suppression ratio

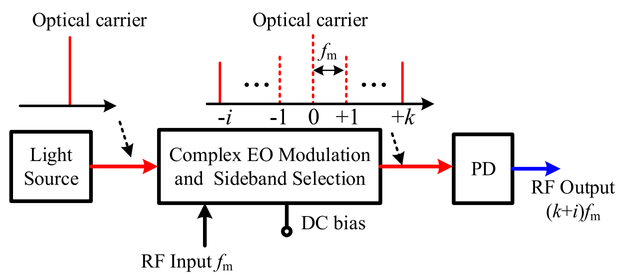

Fig. 7. Photonic LO generation based on optical frequency multiplication.

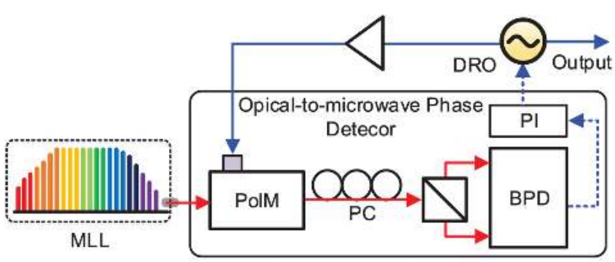

Fig. 8. Photonic LO generation based on an optical-to-microwave phase detector. MLL: mode-locked laser; PolM: polarization modulator; PC: polarization controller; BPD: balanced photodetector; PI: proportional-integral controller; DRO: dielectric resonator oscillator.

photonic radar waveform generation, photonic mixing and channelization, microwave photonic filtering, optical beamforming, photonic analog-to-digital conversion, optical real-time Fourier transform, and optical co-site interference cancellation.

A. Photonic LO Generation

As an essential part of radars, an LO generator provides reference signals for waveform generation, up- and down-conversion, synchronization, and timing for ADCs, digital-to-analog conversions (DACs) and DSP modules. The frequency stability and spectral purity of the LO signal provide the performance baseline for coherent radar systems in which the received signals are "phase compared" to the transmitted waveform. Short-term frequency stability of the LO is usually denoted as phase noise, which is particularly important for radars to extract Doppler information from weak echo signals under a heavy-clutter or hostile jamming environment [185]–[187]. For commercial-available 10-GHz electronic LOs, the phase noise can reach <-105 dBc/Hz@ 1-kHz frequency offset or <-115 dBc/Hz@ 10-kHz frequency offset. Long-term frequency stability can be evaluated using Allan frequency deviation, which is critical for long-distance radars and multi-static radars, i.e., the frequency of the LO should maintain the same if the echo is received with a large time delay or out of sync. The Allan deviation for a typical 10-GHz commercial RF source is $<1\times10^{-11}$@1s. Spurious level is another key parameter of the LO source which is related to the false alarm probability of a radar system. The spectral purity of the LO is usually degraded by the harmonics, sub-harmonics, and non-harmonic spurs, as shown in Fig. 6. All of them should be suppressed to <-50 dBc for a practical radar.

Conventional high-frequency LO signals are generated mainly based on frequency multiplication of a low-frequency electronic oscillator such as oven-controlled crystal oscillator and atomic clock. If the low frequency signal is expressed as $E_1(t) = \cos[2\pi ft+\phi_0(t)]$, where f is the frequency and $\phi_0(t)$ is the phase noise, the LO signal after frequency multiplication with a factor of n can be written as $E_2(t) = \cos\{n\times[2\pi ft+\phi_0(t)]+\phi_1(t)\} = \cos[2\pi nft+n\phi_0(t)+\phi_1(t)]$, where $\phi_1(t)$ is the auxiliary phase noise introduced by the frequency multiplier. As can be seen, the phase noise of the generated signal is increased by more than n times (or $> 20\lg(n)$ dB). In addition, the spur level is usually high, which demands filters with high out-of-band rejection and suitable electromagnetic compatibility design. There are also many types of resonators for low phase noise signal generation, such as dielectric resonators, ceramic coaxial resonators, metamaterial Möbius strips resonators [188], and so on. However, these techniques are frequency limited as their Qs degrade with frequency.

Photonics has been introduced to the generation of LO signals since the early 1960s [189], and many methods were proposed and studied, such as those using optical frequency multiplication [190], optical phase-lock loops [191], Brillouin oscillators [192], sideband-injection-locked lasers [193], Kerr frequency comb oscillators [194], optical-to-radio frequency division [166], optical-microwave synchronization [174], and OEOs [195]. However, only a few of them can meet the high requirements of radar systems when considering the phase noise, frequency stability, purity, complexity, and reliability. Table I

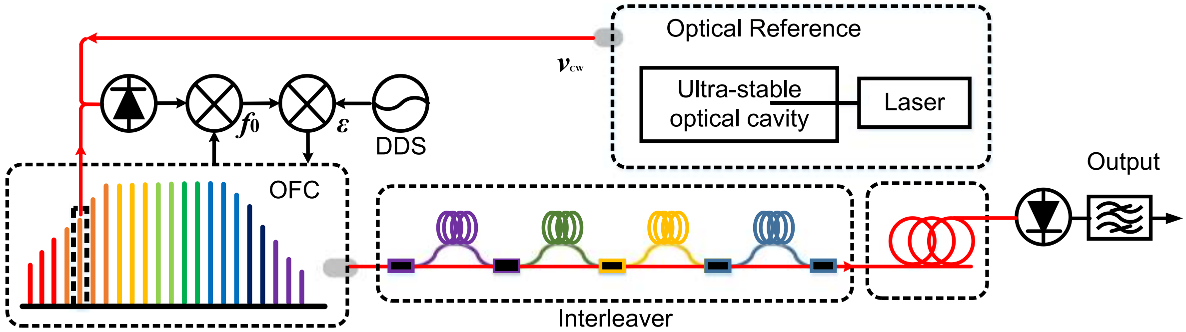

Fig. 9. Photonic LO generation based on optical-to-radio frequency division. DDS: direct digital synthesizer; OFC: optical frequency comb.

shows the performance comparison of different photonic LO generation techniques. As can be seen, the methods based on optical frequency multiplication, optical-to-radio frequency division, optical-microwave synchronization, and OEOs can achieve comparable or superior performance as compared with the electronic implementations.

Optical frequency multiplication is generally realized by beating the selected sidebands of the optically-modulated signal after EOM [196]–[199], as shown in Fig. 7. Sideband selection is usually accomplished by adjusting the DC biases of the EO modulator or inserting an optical filter. In this way, LO signals with frequencies that are twice [196], four times [197], eight times [161], even twenty-four times [198] of the input low-frequency RF signal can be successfully generated, with other harmonics largely suppressed. It should be noted that the quality of the output frequency is determined by the input signal, and its phase noise is deteriorated by $20\lg(n)$ dB, which does not overcome the limitations of electrical approaches.

The spectral lines from a mode-locked laser (MLL) exhibit high phase consistence, by which pulses with sub-ps pulse width are formed [165]. Selecting and beating two of these spectral lines would lead to the generation of microwave signals with very low phase noise. However, the carrier variations and other defects in the PDs would drastically raise the phase noise. To overcome this problem, optical-microwave synchronization based on an optical-microwave phase detector is a promising solution [174], [199]. Fig. 8 shows a typical scheme of RF generation based on the optical-microwave synchronization [174]. The phase detector contains a polarization modulator (PolM) and a balanced photodetector (BPD). By tuning the DC bias and the polarization controller, the output is proportional to the phase difference between the optical pulse and zero-crossing positions of a microwave signal under test. With a proportional-integral servo system as a feedback loop, the phase of the microwave signal will be locked to the optical pulse. An 8-GHz microwave signal with a phase noise of −138 dBc/Hz @10 kHz and −165 dBc/Hz@10 MHz was experimentally generated. Based on a similar principle, an X-band signal synthesizer was established using an optical-microwave phase detector, a dielectric resonator oscillator and a direct digital synthesizer (DDS) [200], showing a phase noise of −145 dBc/Hz @ 10 kHz for a 10-GHz carrier frequency. Besides, the generated signal can be tuned from 9 to 10 GHz with an integrated RMS timing jitter between 7.6 fs and 9.1 fs.

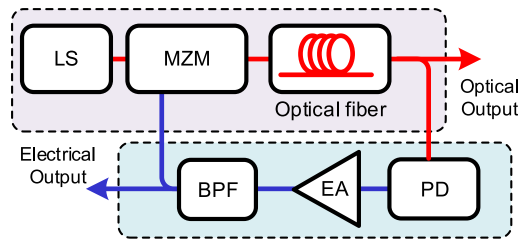

Fig. 10. Functional block diagram of an OEO. LS: laser source; MZM: Mach-Zehnder modulator; PD: photodetector; EA: electrical amplifier; BPF: band-pass filter.

Optical-to-radio frequency division is another photonic LO generation method to take advantage of the phase consistence of the MLL spectral lines. A typical setup is shown in Fig. 9 [166]. A fiber-based OFC is phase locked to a narrow linewidth CW reference laser which is locked to an ultra-stable Fabry-Perot cavity via the Pound-Drever-Hall technique, realizing optical division with high performance. By using high-linearity low-noise PD, finely controlling the amplitude-to-phase noise conversion and managing the link dispersion and pulse width, the phase noise of the 12-GHz harmonics from the fiber-based OFC is optimized. An ultra-pure 12-GHz microwave signal with a frequency stability of lower than $6.5\times e^{-16}$ @ 1s and a recorded low phase noise of < -173dBc/Hz@10 kHz is achieved.

OEO is considered as one of the most promising photonic LO generation approaches for radar applications [201]. Fig. 10 shows the functional block diagram of an OEO. A CW light from a laser source passes through a Mach-Zehnder modulator (MZM) and a long optical fiber, and is then converted into an electrical signal at a PD. The generated electrical signal is amplified, filtered and finally fed back to the RF port of the MZM, forming an oscillation loop. The phase noise of a single-loop OEO can be briefly given by

$$S_{\varphi}(f) = noisefloor - 10\lg\left[\left(1 - \frac{f_{\text{osc}}}{f_{\text{osc}} + j2Qf} e^{-j2\pi f n_r L/c}\right)^2\right] \quad (2)$$

where f_{OSC} is the oscillation frequency, f is the frequency offset from f_{OSC}, and Q, L, and n_r are the quality factor of the electric filter, fiber length, and fiber refractive index, respectively. As can be seen from Eq. (2), the phase noise is determined by the noise floor of the system and the fiber length. Previously,

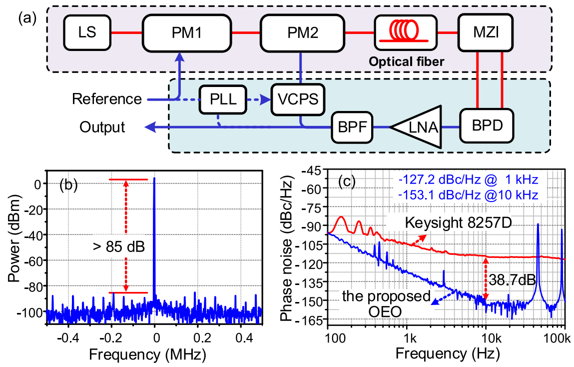

Fig. 11. Experimental results of the OEO based on coherent noise cancellation. (a) Schematic diagram. (b) Electrical spectrum and (c) phase noise of the generated 10-GHz signal. LS: laser source; PM: phase modulator; MZI: Mach-Zehnder interferometer; LNA: low-noise amplifier; BPF: bandpass filter; PLL: phase-locked loop; VCPS: voltage-controlled phase shifter.

the phase noise of the OEO was reduced mainly by using a long optical fiber. As a case in point, a length of 16-km optical fiber was inserted in a 10-GHz OEO to achieve a phase noise of −163 dBc/Hz @ 6 kHz [202]. However, ultra-small free spectral range (FSR) would be resulted if a long optical fiber is employed, leading to a great challenge for sidemode suppression. Although ultra-narrow optical filters like whispering gallery mode (WGM) resonators [203] or Fabry-Perot (FP) etalons [204] have been developed to suppress these sidemodes, it is a vital problem to let the optical source have the same wavelength drift with these optical filters.

To achieve low phase noise oscillation with relatively-short length fiber, we have proposed a coherent noise cancellation method to reduce the noise floor of the OEO [205]. As shown in Fig. 11(a), a pair of cascaded phase modulators (PMs) is applied to expand the output optical spectrum and keep the optical power in the optical fiber constant, which reduces the intensity noise induced by the nonlinear effects in the optical fiber. A reference signal for injection locking and the oscillation signal of the OEO are introduced to the two PMs, respectively. A dual-output Mach-Zehnder interferometer is inserted to convert the phase modulation into two complementary intensity modulations which are then detected by a BPD. Because of the complementary intensity modulations and the balanced detection, the common-mode intensity noise of the link will be largely suppressed. Based on this approach, a 10-GHz signal with a phase noise of < −153 dBc/Hz @ 10 kHz is achieved using a 4.4-km optical fiber, which is 38.7-dB lower than that of a commercially available signal generator (Keysight 8257D). The sidemode suppression ratio reaches 85 dB by means of the injection locking process, as shown in Fig. 11. The frequency stability of the OEO is around 10^{-12}. The main unstable factors are related to the temperature, humidity, variation etc. With temperature and variation controlling and feedback loops, the stability can be further improved.

B. Photonic Radar Waveform Generation

The performance of a radar largely depends on the waveform applied in the system. Suitable waveform will make a radar having the desired resolution in range and velocity since the waveform determines the delay-Doppler response of a radar system. Also, advanced waveforms would improve spectrum efficiency, obtain high pulse energy with low peak power, or enable advanced signal processing. Different kinds of waveforms have been exploited in radars, such as LFM signals, nonlinearly frequency-modulated signals, phase-coded signals with binary sequences or polyphase sequences, frequency-coded waveforms, and orthogonal FDM (OFDM) signal (also known as multicarrier waveforms), as shown in Fig. 12.

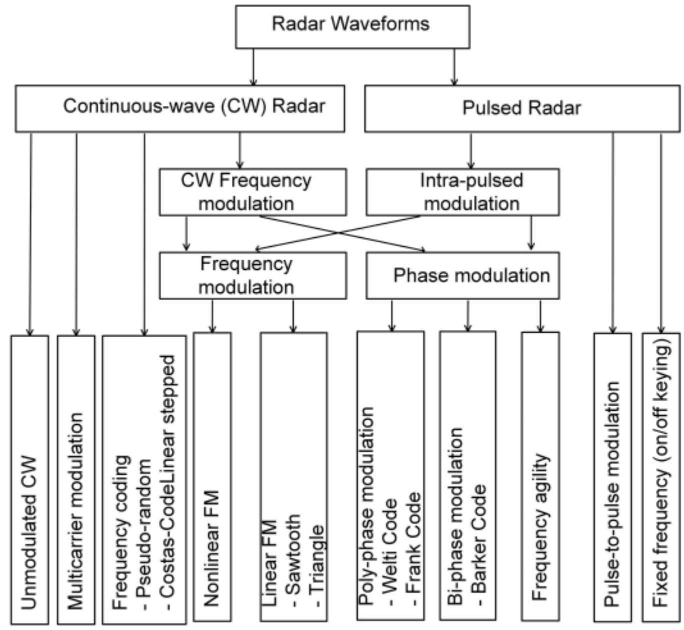

Fig. 12. Typical waveforms used in radars.

Traditional electrical systems generate the waveforms either in the analog domain using a voltage-controlled microwave oscillator, or digitally using a DDS. The DDS offers excellent flexibility for programmable waveform generation, but it suffers from the limited instantaneous bandwidth which is usually less than 2 GHz. In order to break through the bandwidth limitation of the electrical approaches, photonics-based microwave waveform generation has been proposed. Benefiting from the high frequency and large bandwidth of optical devices, microwave photonic technologies open the possibility of radar signal generation with high frequency, broad bandwidth and large time-bandwidth product (TBWP). In general, photonics-based microwave waveform generation methods can be divided into five categories: spectral shaping and frequency-to-time mapping [206]–[212], externally optical injection of a semiconductor laser [213]–[216], photonic microwave frequency multiplication [160], [217], [218], optical frequency-time stitching [219], and photonic digital-to-analog conversion (DAC) [220], [222]. The comparison of the key performances of the main methods for radar waveform generation are illustrated in Table II.

In the spectral shaping and frequency-to-time mapping method, an optical ultrashort pulse generator, an optical spectral shaper, and a dispersive element are needed, as shown in Fig. 13 [9], [223]. The optical spectrum of the ultrashort optical pulse is

TABLE II
PERFORMANCE COMPARISON OF DIFFERENT PHOTONIC RADAR WAVEFORM GENERATION METHODS

Methods	Key advantages	Drawbacks
Spectral shaping and frequen-cy-to-time mapping	Large bandwidth (37.4 GHz in [212]); high flexibility	Small time duration (~10 ns), poor linearity
Externally optical injection of semi-conductor laser	Large bandwidth (up to 12 GHz,10-22 GHz); large TBWP (1.2×10^5) [213,214]	Limited frequency stability, low phase co-herence
Photonic microwave frequency mul-tiplication	Large bandwidth (12 GHz in [218]), high linearity (depends mainly on the electrical signal generator)	Requiring a low-frequency electrical wave-form generator with high performance
Optical frequency-time stitching	Large bandwidth and TBWP (10 GHz and 5×10^4, respectively in [219]); in-creased linearity	Complicated structure, requiring high-precision amplitude and phase controlling
Photonic DAC	High flexibility	Limited ENOB (3.49 in [220]), poor linearity, small dynamic range (only 22.8 dB)

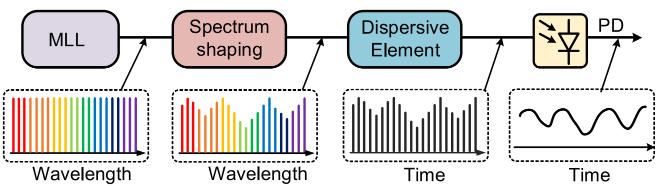

Fig. 13. Schematic diagram of the microwave photonic radar waveform generator based on spectral shaping and frequency-to-time mapping.

firstly shaped according to the profile of the desired waveform with an optical spectral shaper such as superimposed chirped FBG [206], Sagnac loop filter [207], tilted FBG [208], phase-shifted Lyot optical filter [209], differential group delay element [210], and optical programmable processor [211], [212]. The shaped spectrum is then mapped into the time domain via the dispersive element. After optical-to-electrical conversion in a PD, microwave waveforms are generated. The instantaneous bandwidth of the generated signals can reach 37.4 GHz [212]. However, this method suffers severely from the limited time duration (usually <10 ns), which is not suitable for radar applications with long-distance detection.

In the photonic waveform generation method based on externally optical injection of a semiconductor laser, an optical carrier with a dynamical amplitude variation is injected into a semiconductor laser, as shown inFig. 14 [213]–[216]. Under proper injection conditions, period-one (P1) oscillation state can be invoked through undamping the relaxation resonance. The injection light pulls the intracavity field oscillation of the slave laser by locking the optical phase of the laser. Meanwhile, the necessary gain for the slave laser is reduced by the optical injection. According to the antiguidance effect, the refractive index inside the cavity changes, resulting in the redshift of the cavity resonance. Therefore, the output spectrum of the slave laser is dominated by two frequency components, i.e., the regenerated optical carrier and injection-shifted cavity mode. After optical-to-electrical conversion, a microwave signal can be generated. Since the cavity resonance shift depends on the gain reduction which is determined by the injection strength, the beating microwave frequency is also dependent on the injection strength. Therefore, by shaping the amplitude of the injected optical signal, the instantaneous frequency of the generated

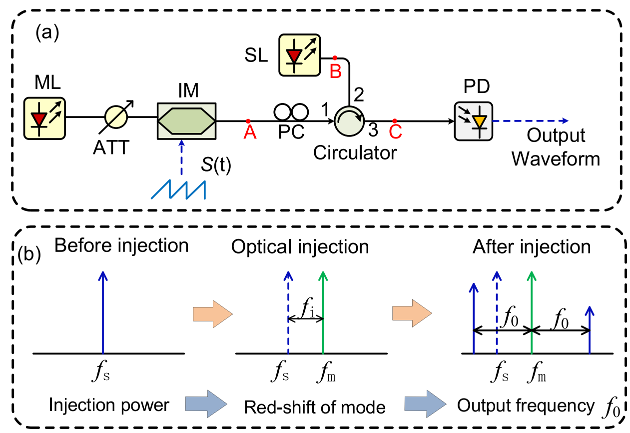

Fig. 14. (a) Schematic diagram of the microwave photonic waveform generator based on externally optical injection of a semiconductor laser, and (b) illustration of its operation principle. ML: master laser, ATT: optical attenuator; IM: intensity modulator; SL: slave laser.

microwave signal would be programmed accordingly. For instance, when the injection light has a linearly increased optical amplitude, a linearly chirped microwave waveform would be generated. If the injected optical signal is coded by a sequence, a frequency-coded waveform would be produced. Previously, the LFM waveforms with a center frequency tuning from $\sim$10 to $\sim$67 GHz, an instantaneous bandwidth of 12 GHz, and a TBWP of.$\times10^5$ were generated [213], [214]. The generation of a frequency-hopped waveform with a stepped linear sequence or a Costas sequence was also reported [216].

This scheme has several advantages over generation schemes based on a femtosecond pulsed laser or high-speed electrical AWG, i.e., low cost, simplicity, reconfigurability and large TBWP. However, the P1 oscillation frequency is sensitive to the fluctuation of optical injection parameters, resulting in limited frequency stability and chirp repeatability of the generated microwave waveform. In addition, since the regenerated optical carrier and the lasing cavity mode are not strictly phase locked, the phase coherence of the generated waveforms is not satisfactory.

Photonic microwave frequency multiplication is a straightforward way for broadband radar waveform generation, in which a low-frequency and narrow-band radar signal is generated in the electrical domain with high quality, and then frequency

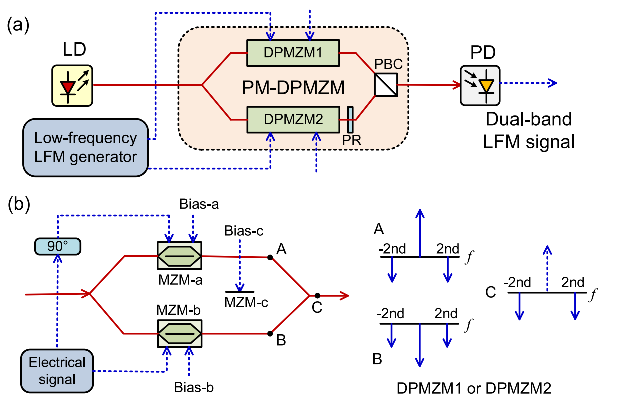

Fig. 15. (a) Dual-LFM signal generation based on photonic microwave frequency multiplication, and (b) illustration of the operation in each DPMZM.

multiplied in the optical domain with high performance [160], [217], [218]. The main difference between the electrical and optical frequency multiplications is that the optical method has an intermediate state in the optical domain, so we can remove most of the undesirable frequency components by applying wideband coherent cancellation or using an optical filter. A large-bandwidth and high-frequency waveform with a low spur level can thus be generated. Fig. 15 shows a typical optical frequency quadrupler based on a dual-parallel MZM. When an electrical signal is introduced to the sub-MZMs of the dual-parallel MZM, different-order sidebands will be generated together with the optical carrier because of the electro-optical nonlinearity of the MZMs. The odd-order sidebands are firstly removed by biasing the sub-MZMs at the maximum transmission point. Then, the optical carrier is eliminated by coherent cancellation with the help of an electrical 90° hybrid, leaving only the two second-order sidebands. Beating the sidebands in a PD, a frequency-quadrupled microwave signal is obtained with other harmonics largely suppressed. With this scheme, a dual-band LFM radar signal (18∼22 GHz, 28∼32 GHz) was produced based on a low-frequency electrical dual-band signal (4.5∼5.5 GHz, 7∼8 GHz) [160]. Thanks to the high quality and high stability of the generated signal, several ultrahigh-resolution imaging radars were built based on this method [147], [217], [218], [224]–[228].

Optical frequency-time stitching is another interesting waveform generation method that takes advantage of both electronics and photonics, in which channelized LFM signals are first generated and then stitched in both the time and frequency domains to form a large-bandwidth LFM signal [220]. The channelized LFM signals can be obtained by using two OFCs with different frequency spacings. One of the OFCs is modulated by an intermediate-frequency (IF) LFM signal via carrier-suppressed single-sideband modulation, and the other one is frequency shifted by an optical frequency shifter. Then the modulated signal OFC and the frequency-shifted local OFC are combined and sent into a wavelength-division demultiplexer to divide the signal into multiple channels. Each channel has one comb line from the signal OFC (carrying the low-frequency waveform) and one comb line from the local OFC. Due to the different frequency spacings of the two OFCs, multiple sub-LFM signals with different center frequencies can be generated in different channels. By introducing proper time delays to these sub-LFM signals and combing them, a frequency-stepped LFM signal can be obtained. Particularly, when the bandwidth of the IF-LFM signal is equal to the space difference of the comb, a new LFM waveform with multiplied bandwidth and time duration could be generated. As a result, a reconfigurable multi-band LFM signal with large TBWP is obtained. Since the frequency variation in each sub-LFM signal keeps unchanged and the bandwidth of the combined signal is multiplied by N times, where N is the channel number, the linearity of the output signal would be enhanced by N times. In an experiment, LFM signals with frequencies from DC to 10 GHz and from 20 to 30 GHz over a 5-μs time duration were produced, and the TBWP of the generated signals is multiplied by 25 times [219].

Analogous to electronic DACs, photonic DAC is another effective approach for flexible radar waveform generation. The basic principle is to design digital sequences according to the required waveform, and then use it to drive a parallel-weighted [229]–[238] or serial-weighted [239]–[241] optical link. Taking the parallel weighted photonic DAC as an example, an optical carrier or pulse train is divided into N channels. The nth channel is set to have an equivalent power that is 2^n times the power of the first channel, which is modulated by the nth sequence and eventually summed in a PD with other modulated channels. After an electrical filter, a radar waveform can be generated. The prominent advantage of the waveform generation based on a PDAC is the superior flexibility, i.e., both the temporal duration and waveform profile can be arbitrarily designed. For example, in [220], triangular, parabolic, rectangular and sawtooth waveforms are generated using a 2.5-GSa/s and 4-bit photonic DAC. In [221], a 4-GHz LFM signal is realized based on a 4-bit DAC. The system is further optimized to generate a W-band LFM signal with a bandwidth of 8 GHz and a time duration of 9.9 μs [222], which is applied for radar imaging. However, the photonic DACs at the present stage usually have a small effective number of bits (ENOB), leading to a poor linearity and small dynamic range.

In addition to these methods, radar waveforms can also be generated with photonic microwave phase modulation [124], [161], [242], photonic microwave delay-line filtering [243], heterodyning of a fixed wavelength and a wavelength-swept laser [244] and so on. These methods are not discussed in detail here due to their limited phase coherence, system complexity, poor stability or small TBWP at the current stage, but they are likely to contribute to radar applications after certain improvement.

C. Microwave Photonic Mixing and Channelization

Frequency mixer is one of the essential parts of radars. In the transmitter, mixers are needed to upconvert the wave-form generated at the IF band to the desired RF band; while at the receiver, the mixers are required to down-convert the received RF signal to the baseband or IF band since the ADCs and DSP units usually have insufficient bandwidth to directly process the RF signals. To meet the requirement of future multifunctional or reconfigurable radars, mixers should be capable of processing

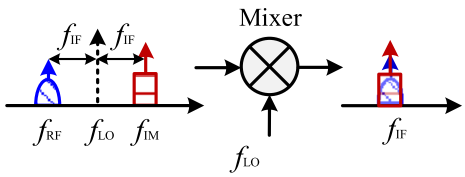

Fig. 16. Evolution of the image interference in a frequency mixer

large-bandwidth signals with high conversion efficiency, low mixing-spur level, and large dynamic range.

Although a lot of wideband mixers have been developed using pure electronics, they always generate a large number of undesired mixing components (15-dB LO and RF to IF isolation for a 4-44 GHz commercially available electrical mixer [10]). Filters can remove some of the mixing spurs, but they may not work if the input signal has a wide bandwidth. In that case, the mixing spurs and the desired output might overlap in the spectrum. As a result, the operational instantaneous bandwidth and the dynamic range of the mixer are still limited (i.e., IF instantaneous bandwidth limited to no more than 3 GHz [10]), leading to multi-stage frequency converters together with filters employing to today's radar systems to ensure a sufficiently high dynamic range, favorable conversion efficiency, and acceptable mixing-spur suppression [245]–[247].

To overcome the above problem, microwave photonic mixers with the potential to provide high mixing performance have attracted significant interests [248]. In principle, any nonlinear effect in the optical or electro-optic devices can be applied to implement frequency mixing. Such device includes a semiconductor optical amplifier (SOA) [249], an electro-absorption modulator [250], a directly-modulated laser [251], an external modulator [252] and so on. A comprehensive review of these mixers can be found in [10].

It should be noted that conventional photonic microwave mixers are usually implemented through heterodyne structures, which can be easily interfered with by image signals, as shown in Fig. 16. This could create at least two problems for modern radars. First, the noise from the image frequencies can easily pollute the noise figure of the receiver by 3 dB. Second, the signals at the image frequency would dramatically lower the sensitivity and dynamic range of the receiver or even jam it.

To deal with the problem, considerable efforts have been devoted to implementing the image-reject mixer [253]. Table III shows the performance of typical microwave photonic image-reject mixers in the literature, which can be divided into two main categories, i.e., pre-filtering and phase cancellation.

With an optical filter [254] or an electrical filter [255] placed before a conventional mixer, the image interference can be directly removed with a large image rejection ratio. For instance, by using two cascaded electrical bandpass filters, a microwave photonic mixer with an image rejection ratio of >150 dB was reported [255]. One critical problem associated with the pre-filtering method is the limited bandwidth and the strict requirement on the sharp edge of the filters, which impedes their application in multifunction or reconfigurable radars.

TABLE III
PERFORMANCE COMPARISON OF DIFFERENT MICROWAVE PHOTONIC IMAGE-REJECT MIXERS

	Method	BW [GHz]	IRR [dB]	CE [dB]	SFDR [dB·Hz$^{2/3}$]
[254]	Optical filtering	8~18	20	-47~-35	107
[255]	Electrical filtering	0.8~8.8	150	3-8	106
[256]	Hartley	5.6~32	60	-15	120
[257]	Hartley	10~40	60	-20	NA
[151]	Hartley	10~40	57.2	-9~-5	108
[146]	Balanced Hartley	Over 40	60	6-dB higher than [256]	NA

BW: bandwidth; IRR: image-rejection ratio; CE: conversion efficiency; SFDR: free dynamic range

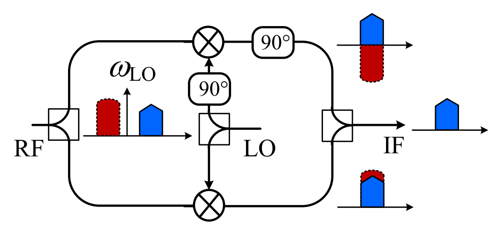

Fig. 17. Schematic diagram of the image-reject mixer based on Hartley architecture. RF: radio frequency, LO: local oscillation, IF: intermediate frequency.

On the other hand, phase cancellation based on Hartley architecture can realize the image-reject mixer without using a filter. Fig. 17 illustrates the principle of the Hartley architecture. A pair of quadrature LO signals are mixed with the input RF signals to generate two quadrature IF signals, which are then combined by a low-frequency 90° hybrid. The purpose of the two 90° phase shifts in the upper path is to let the IF signal from the image out of phase and those IF signals from the wanted signals in phase. In this way, the desired IF signals are enhanced while the downconverted image is suppressed. Since this kind of image-reject mixer uses phase differences of the signals to realize the image rejection, broadband mixing can be achieved if the frequency responses of the devices are flat, which is exactly one key feature of microwave photonics. Previously, a microwave photonic image-reject mixer with an image rejection ratio of ~60 dB and an operational frequency range of ~40 GHz was successfully achieved [151], [256], [257].

The image-reject mixer, however, can only suppress the images while the mixing spurs caused by the nonlinear effect still exist. For instance, the 2nd-order harmonic mixing spur between the RF and image is usually close to or even overlap with the desired IF signal for wideband radars. To eliminate the image and other mixing spurs simultaneously, recently we proposed a new image-reject mixing architecture, i.e., balanced Hartley architecture [146], as shown in Fig. 18. The modulated RF and LO signals are respectively sent to the signal port and LO port of the 90° optical hybrid, and phase shifts of 0, $\pi/2$, π and $3\pi/2$ are introducing to the input signals. The phase cancellation is first realized by the balanced detection, which removes the undesirable mixing spurs and common-mode noises. Then, a second phase cancellation is implemented by using an electrical 90° hybrid, by

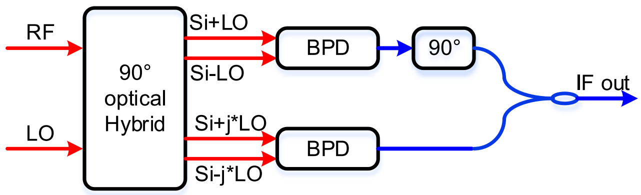

Fig. 18. The balanced Hartley architecture for image-reject mixers [146].

which the image interference is eliminated. With this structure, a photonics-based radar using balanced I/Q de-chirping in the receiver was reported [225], achieving an image-rejection ratio higher than 30 dB. The spurs caused by the baseband envelope and the frequency mixing between radar echoes with different time delays were successfully eliminated.

Photonics-based image-reject mixers can be applied in coherent optical RF channelizers to avoid spectrum aliasing, which is a crucial problem associated with the traditional optical channelizer based on directly spectrum slicing [258] and comb filtering-based spectrum slicing [259], [260]. The optical RF channelizer, which slices a broadband RF signal into multiple consecutive narrowband sub-channels, would be an effective preprocessor for multiband or broadband radars to relieve the requirement of high sampling rate and large dynamic range ADCs [261]. Fig. 19 shows the schematic diagram of the coherent optical RF channelizer based on a microwave photonic image-reject mixer. Two OFCs are employed. The signal OFC, which consists of a number of optical carriers with different wavelengths, is modulated by the received wideband RF signal, leading to many copies of the RF input in the optical domain. Then, the RF-modulated optical signal is combined at an optical 90° hybrid with the local OFC which has a frequency spacing that is slightly different from the signal OFC. Two waveshapers are used to split the signals at the I and Q ports into multiple channels. In each channel, the I and Q signals are detected by two PDs, combined by a low-frequency electrical 90° hybrid and then low pass filtered. Because of the low pass filtering, only the frequency components around the spectral lines in the local OFC is downconverted. The spectrum aliasing problem, which is the same as the image interference, is suppressed by the image-reject photonic microwave mixing. As a result, optical RF channelization with all the information in the input signal maintained is achieved. In an experiment, a five-channel optical channelizer with an operational frequency range of 13–18 GHz and an image-rejection ratio of 25 dB was demonstrated [262]. In addition, a microwave channelizer using a dual-output image-reject mixer based on the balanced Hartley architecture was demonstrated recently [263], which further improves the channelization performance.

D. Microwave Photonic Filtering

Filters that can remove the out of band noise, spurs and interference are essential components in radar systems. Thanks to the flexibility of DSP, most of the advanced filters for radars are realized in the digital domain. However, due to the insufficient dynamic range of the ADC, analog filters are still indispensable in the RF frontend, especially for broadband radars. While electronic filtering is a well-established function for low-frequency signals, the filter parameters such as insertion loss, passband flatness, edge steepness, and out-of-band rejection would worsen with the center frequency. Besides, reconfigurable or programmable filters are difficult to achieve using pure electronic approaches, so high-speed switches with filter banks have to be applied in multiband, multifunctional or software-defined radars.

Microwave photonic filters would be interesting for radars if other microwave photonic techniques have been already used in the system [3], [264]–[266]. In that case, no additional EO/OE conversion loss is introduced. Moreover, realizing the analog filter in the optical domain can benefit from the distinct features brought by the photonic technologies. For instance, because of the low loss (independent of the RF signal frequency) and light weight of the optical fiber, a very long time delay can be introduced to the microwave photonic filters, so the Q value can be made high. In addition, the broad bandwidth of the optical devices would allow the microwave photonic filters to be used for multichannel filtering with excellent consistency between different channels based on optical multiplexing technologies.

In general, a microwave photonic filter can be realized by weighting, delay, and sum of the optical signals in multiple taps, which can be divided into finite impulse response (FIR) filters and infinite impulse response (IIR) filters according to the number of taps [267], [268]. Because of the square-law detection of the PDs, positive-coefficient microwave photonic filters can be easily realized [269]–[271], which can only perform low pass filtering. In order to overcome this issue, microwave photonic filters with a negative coefficient were developed by introducing a 180° phase difference between two adjacent taps based on complementary modulation or balanced photodetection, etc., which can realize bandpass filtering [272]–[274]. However, as the center frequency of the filter tuned, the 3-dB bandwidth and FSR are also changed. To achieve a tunable microwave photonic filter without affecting the shape of the frequency response, complex coefficient microwave photonic filters are implemented by changing the phase of the taps. Previously, complex coefficient taps were obtained by stimulated Brillouin scattering (SBS) [275], a phase-shift FBG [276], non-uniformly spaced delay lines [277], 2-D liquid crystal on silicon [278], an SOA with slow and fast light effects [279], an all-optical differentiator [280], or a silicon-on-insulator microring resonator [281]. However, these systems suffer from the small operation bandwidth or stringent control of the wavelength and amplitude of the optical carrier. In addition, full FSR-range tunability is hard to implement because of the difficulties to perform the full 360° phase shift. To remedy this, a full FSR range tunable microwave photonic filter with complex coefficients was proposed by using a PolM [282], [283], a dual-parallel MZM (DPMZM) [284], or a dual-drive MZM (DDMZM) [285]. As an example, Fig. 20 shows the schematic diagram of a full FSR-range tunable MPF with all complex coefficients [282], [283]. The full 360° phase shifts are realized by a multi-channel microwave photonic phase shifter [125], which is composed of a laser source, a PolM, three wavelength-division multiplexers,

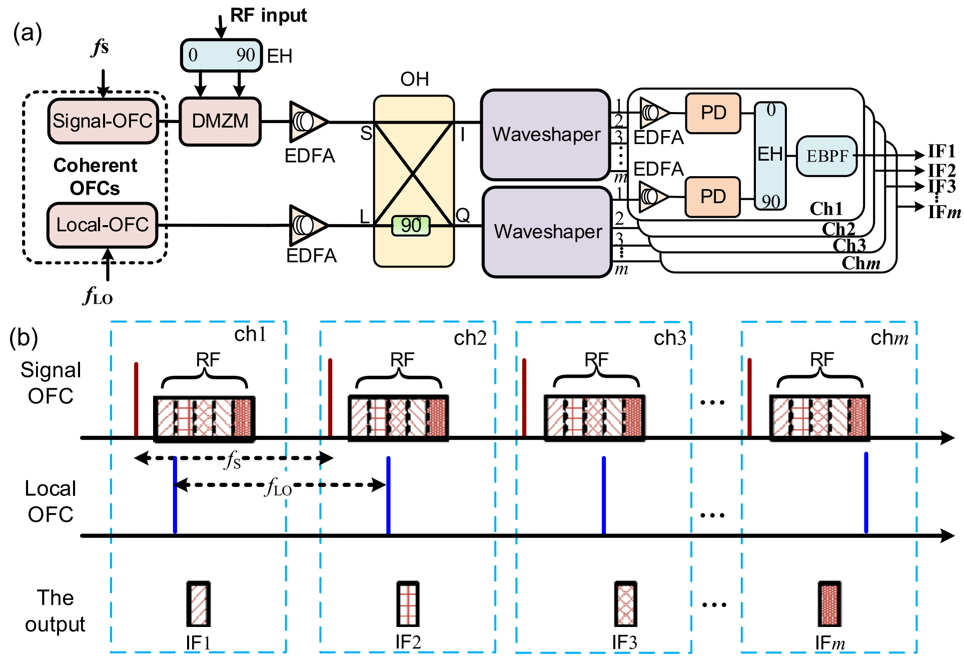

Fig. 19. (a) Schematic diagram of the optical RF channelizer based on a multichannel image-reject mixer [262]. (b) Illustrations of the optical and electrical spectra at different points of the channelizer. DMZM: dual-drive MZM; EDFA: erbium-doped fiber amplifier; OH: optical hybrid; EH: electrical hybrid; EBPF: electrical bandpass filter.

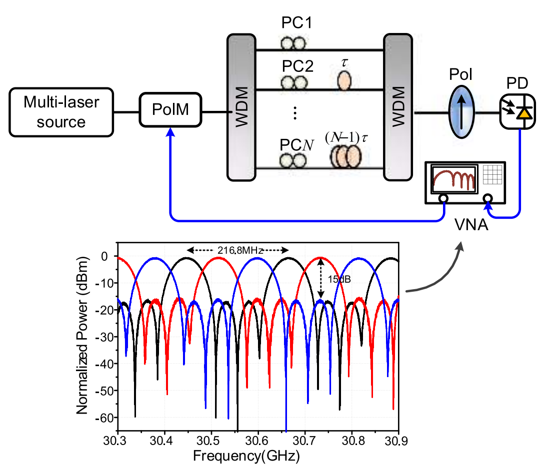

Fig. 20. A multi-tap microwave photonic filter with all complex coefficients [283]. WDM: wavelength division multiplexers; Pol: polarizer; VNA: vector network analyzer.

a number of polarization controllers and polarizers, and a PD. By simply controlling the polarization controller in each tap, the phase of the RF signal can be tuned independently in the range from -180°to 180°. Thus, the frequency response of the filter can be tuned over the full FSR-range while maintaining the shape unchanged. The 3-dB bandwidth is easily tuned by adjusting the time difference between adjacent taps since the FSR is the inverse of the time difference. When the time difference is very small (∼0.1 ns or smaller), the 3-dB bandwidth can be larger than 10 GHz. However, since the system is polarization-based, temperature and variation controlling circuits may be required for practical applications.

In order to overcome the limitation of periodic filtering characteristics, some single or multi-passband microwave photonic filters were reported [265], [286]-[288]. A single-passband microwave photonic filter based on SBS and a fiber-ring resonator was realized in [286]. The maximum Q-factor, 3-dB bandwidth and center frequency tuning range of the microwave photonic filter were $\sim 1.7\times 10^4$, 825 ± 125 kHz and 2–16 GHz, respectively. In [288], a dual-passband microwave photonic filter with tunable passbands and invariant shape was realized based on phase-modulation to intensity-modulation conversion by the SBS effect, where two cascaded DPMZMs were employed to generate a two-tone pump with programmable frequencies. The two passbands of the proposed filter are freely tuned from 0–9.644 GHz, and the out-of-band rejection ratio and 3-dB bandwidth were larger than 25 dB and smaller than 55 MHz, respectively.

In recent years, integrated microwave photonic filters have also drawn significant interests due to the compact size, low cost, and low power consumption [289]–[295]. Many methods have been demonstrated for integrated microwave photonic filtering, such as those based on ring resonators [289], waveguide grating [290], Mach-Zehnder interferometer [291], integrated Kerr frequency combs [292], [293], and SBS effect [294], [295], etc. Taking [290] as an example, an integrated filter enabling narrow flat-top passband with steep roll-off and wide stopband was realized using a third-order distributed feedback resonator, and employed to introduce a 20-GHz frequency shift to a 5 Gbit/s data signal with large sideband SNR, strong carrier rejection, and low spurious sideband level. The high performance of the integrated microwave photonic filters may pave the way for the practical application of microwave photonic filters in radar systems.

E. Optical Beamforming Network

Beamforming network for phased array antennas is one of the earliest radar subsystems in which microwave photonic solutions are seriously considered. Initial proposals of the optically controlled RF beamforming can be dated back to the 1970s [296] and pioneer demonstration can be found in the literature since the 1990s [11], [297]–[299]. The major advantage of realizing a beamforming network using microwave photonics is the low loss delay lines with large achievable range and broad bandwidth, which can radically solve the beam squint problem (i.e., the main lobe direction is frequency dependent) of a phase shifter-based array excited by wideband signals.

The key components in the OBFNs are optical delay lines, in which the delays of RF signals are controlled through optical approaches. A typical optical delay line consists of a laser source, an EOM, an optical delay element and a PD [300]. The phase response of the delay element should be linear and tunable over the operational optical band so that an RF frequency response with a controllable linear phase, i.e., constant delay over a broad bandwidth, can be obtained. Several optical delay tuning mechanisms and the corresponding structures have been reported. Changing the effective total length of an optical path through optical switches is the most intuitive method for delay tuning, in which the fixed optical paths to be selected can be implemented by both the discrete optical fibers [301] and the integrated waveguides [302]. To fill the gaps between discrete time delays that are limited by the switch-based optical delay elements, devices capable of continuous or quasi-continuous delay tuning have also been proposed, which includes vector-sum operation [303], [304], mechanically-adjusted free space optics [305], Fourier-domain optical processors [306], tunable chirped FBGs [307], thermally-tuned integrated ring resonators [308], or pump-managed nonlinear optics such as SBS [309], etc. Obviously, a continuously-tunable optical delay line with a large delay range can be achieved through the joint use of the switch-based optical delay elements and the continuous-controlled ones [310]. Optical delay lines can also be realized by employing dispersive optical delay elements and wavelength-tunable lasers or an OFC [311]–[316], in which the phase response of the dispersive element can be regarded as linear over the band around the optical carrier. By adjusting the dispersion parameter or the wavelength of the optical carrier, the RF delay can be controlled since the effective phase response of the optical dispersive element is changed.

Based on the optical delay lines, an OBFN for squint-free beam steering can be established. One of the goals in the combination of multiple optical delay lines is to use limited optical devices to realize the delay control of a large number of RF signals, which is required by large arrays and multi-beamforming systems. Owing to the intrinsic advantage of broad bandwidth provided by optical solutions, the reuse of optical devices and the parallel control of multiple RF signals can be easily achieved through the WDM technique. For example, an OBFN that can independently and simultaneously steer two wideband beams was proposed [317]. The structure of the OBFN is shown in Fig. 21, in which the delay elements with progressive dispersion

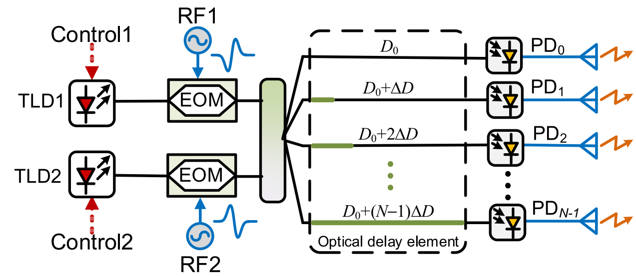

Fig. 21. Schematic diagram of the OBFN that can independently and simultaneously steer two wideband beams [317]. TLD: tunable laser diode; EOM: electrooptic modulator.

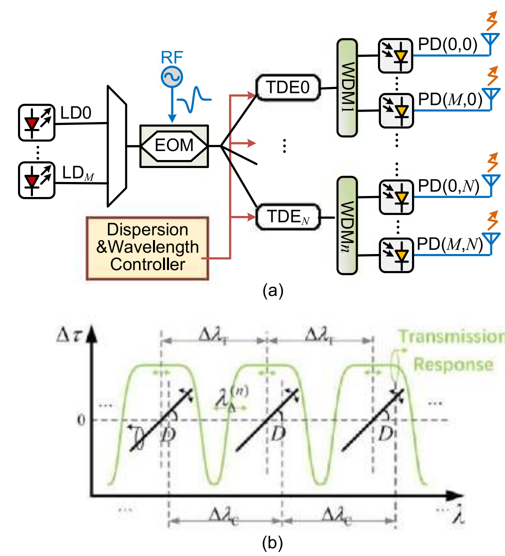

Fig. 22. (a) Structure of a typical 2D OBFN [318] and (b) the response of a tunable dispersive element used in the 2D OBFN. TDE: tunable dispersive element.

parameters are used to generate stepped delays needed by the antenna array. The directions of the two beams are controlled by two wavelength-tunable lasers. Here, all the dispersive delay elements are shared by the two RF beams. The concept of device reuse can also be applied to the beamforming network for planar arrays [318]. As shown in Fig. 22, based on the WDM technique, N FBG-based tunable dispersive elements and M wavelength-fixed laser sources are sufficient to construct the kernel part of a 2D OBFN for an $M\times N$ array. By programming the dispersion parameters and the wavelength offsets of the tunable dispersive elements, time delays for different antenna elements can be controlled to form the required two-dimension delay steps, enabling the beam steering in both azimuth and elevation directions.

Recently, researchers made significant progress on the photonic integrated circuits, which may enable the large-scale application of the OBFN. For example, a fully integrated RF-in-RF-out 1×4 OBFNs with built-in lasers, modulators, delay elements, and detector arrays have been realized through the hybrid integration using Si_3N_4 and InP platforms [319]. Two structures of the OBFNs were demonstrated. The first one based on switches achieved a delay range of 1.3 ns over a bandwidth

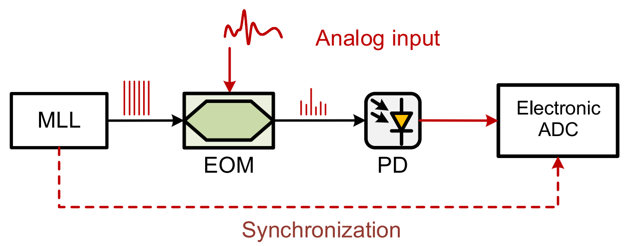

Fig. 23. Block diagram of the photonic sampling ADC.

of 8 GHz, and the second one based on ring resonators realized a delay range of 1.8 ns and a bandwidth of 2.2 GHz.

It is worth noting that OBFNs with large RF bandwidths put forward the requirement of modified methods in modeling, measurement and performance evaluation since the traditional methods were derived under narrow-band conditions. Several new concepts have been proposed to analyze the characteristics of wideband OBFNs, including the impulse response analysis with integrated array pattern [320], the frequency-dependent array factor with correlation-maximum array pattern [300] and the generalized pattern multiplication approach [321]. A time-domain approach for the measurement of the wideband pattern has also been reported, through which the nonlinearity in an OBFN and its negative impact on the RF signals are addressed.

F. Photonic Analog-to-digital Conversion

With the growing demands such as multi-functional and software-defined operation, it becomes a common consensus that as many signal processing functions as possible should be implemented in the digital domain. Thus, high-performance ADCs are essential to bridge the radar frontends and the DSP modules. The evolution of the radar systems is demanding ADCs with a high sampling rate, a broad analog bandwidth, and a high ENOB. Simultaneously satisfying the three requirements is quite challenging for state-of-the-art electronic ADCs.

By virtue of the large bandwidth of photonic devices and the low timing jitter of MLLs, photonic techniques can remarkably enhance the performance of electronic ADCs [13]. In the last few years, extensive efforts have been devoted to the design and implementation of photonic ADCs, in which photonic techniques play the role of an analog sampler with ultra-low timing jitter, signal pre-processor or quantizer. Here, we focus on two major kinds of photonic ADCs that have already been tried in microwave photonic radar systems, i.e., ADCs with photonic sampling and those with photonic pre-processing

In the optical domain, an MLL can produce pulses with a sub-ps pulse width and a timing jitter in the order of tens of femtosecond, which can be considered as the Dirac delta functions and are ideal to sample the analog signals. The basic structure of the photonic sampling ADC is shown in Fig. 23 [322]. Ultrashort pulses from an MLL are intensity-modulated by the input analog signal, so the sampled values of the analog signal are represented by the peak intensities of the modulated optical pulses. The optical pulses are then sent to a PD to perform the optical-to-electrical conversion, in which the peaks of the obtained electrical pulses are quantized by an electronic ADC

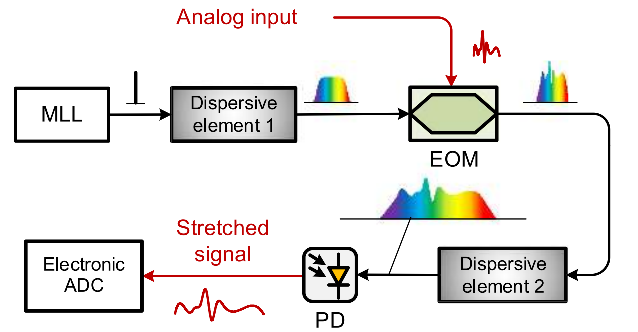

Fig. 24. Block diagram of the photonic time-stretch ADC.

synchronized with the MLL. Photonic sampling ADCs can bring about notable improvement to both the ENOB and the analog bandwidth of an electronic ADC. Since the photonic sampling process does not change the time duration of the signal to be converted, the photonic sampling ADC can handle an analog signal with a large pulse duration or even a continuous-wave signal.

Although the photonic sampling cannot improve the sampling rate of an electronic ADC directly, which leads to a limited instantaneous bandwidth, the photonic structure can realize the serial-to-parallel conversion of the pulse sequence with minor modification. As a result, the sampling rate of multiple electronic ADCs can be aggregated. A typical example of such photonic sampling ADC is the one in the microwave photonic radar reported in [323], [324]. A switching matrix consisting of three dual-output MZMs is used to divide the sample sequence into four parallel channels, so the equivalent sample rate of the system is multiplied by four.

Another kind of photonic ADC applies photonic techniques to pre-process the analog signals, making them easier to be converted into the digital domain. Stretching the signal in the time domain to slow the signal waveform down is an intuitive pre-processing method. Fig. 24 illustrates the principle of the photonic time-stretch ADC [325]. An ultrashort optical pulse with a broad spectrum is firstly generated by an MLL and pre-chirped in the first dispersive element. Then, by modulating the pre-chirped pulse with the analog signal to be processed, the time-domain waveform of the analog signal is mapped to the spectrum of the chirped pulse. Through the second dispersive element, the modulated optical pulse is further chirped, during which the pulse along with the carried analog signal is stretched in the time domain. Thus, a stretched replica of the input analog signal can be obtained at the output of the PD, which is much easier to be processed by an electronic ADC. In fact, if a stretch factor of M is realized by the photonic time-stretch system, both the equivalent sampling rate and the analog bandwidth of the electronic ADC can be multiplied by M. Besides, the noise induced by the timing jitter during sampling can also be suppressed since the signal waveform is significantly slowed by the photonic time-stretch process. Previously, a photonic time-stretch ADC with distributed Raman optical amplification was demonstrated, in which an equivalent sampling rate of up to 10 Tsample/s and a stretch factor up to 250 were realized [169].

Improvements and modifications of the photonic time-stretch ADC have been proposed to compensate for the nonlinearity [326] and the dispersion-induced RF power fading [327]. A microwave photonic radar system using photonic time-stretch ADC in the receiver was also proposed with a stretch factor of ∼5 [328], in which the direct sampling of X-band radar echoes was achieved.

Photonics-based periodic extension of the analog signal can also be employed to enhance the performance of an electronic ADC. If the analog signal to be converted is periodic, the ADC sampling rate as low as the repetition frequency of the signal is sufficient to acquire the waveform, providing that a minor difference between the sampling period and the signal period is introduced. This concept is similar to the principle of an equivalent time sampling oscilloscope, in which the sampling rate of the oscilloscope is far below the Nyquist rate required by the analog signal. Although the analog signal to be converted is usually aperiodic and can hardly use the aforementioned principle of equivalent sampling, we can resort to photonic techniques to perform the periodic extension. Both the linear scheme [329] and the loop-based structure [330], [331] have been proposed to repeat the signal in the time domain, in which the advantage of a large time delay with low loss provided by optical fibers is exploited.

Thanks to the high equivalent sampling rate brought by the photonic time-stretching or periodic extension, photonic ADCs with pre-processing can be used to convert signals with large instantaneous bandwidths. However, these processes enlarge the time slot occupied by the signal and could thus lead to the severe time-domain aliasing. One of the solutions is to divide the analog signal into multiple time slots and then process them using a parallel structure. Several demonstrations based on this method have already been reported [332], [333].

G. Real-Time Optical Fourier Transform

Fourier transform for fast electrical spectrum analysis is of great importance for cognitive radars [334]. Conventionally, Fourier transform is implemented using an ADC followed by the digital fast Fourier transform (FFT) algorithm [335]. However, FFT suffers from small processing bandwidth limited by the ADC or intolerable latency due to the enormous amount of data. To enable broadband cognitive radars, photonics-based approaches for Fourier transform, especially optical RTFT, have been proposed. The optical RTFT maps the spectrum of an unknown RF signal into the time domain, thus enabling real-time serial detection by analyzing the optical profile with time at the output, without the cumbersome FFT process. Typically, RTFT can be realized using dispersive elements or a frequency-shifted loop.

The concept of dispersion-based RTFT comes from the space-time duality, which refers to the similarity between the diffraction of an electromagnetic beam and the dispersive propagation of an electromagnetic pulse [336]. In the space domain, Fraunhofer diffraction realizes the Fourier transform of the input beam. Similarly, in the time domain, when a short optical pulse passes through a dispersive medium, the pulse will be broadened and

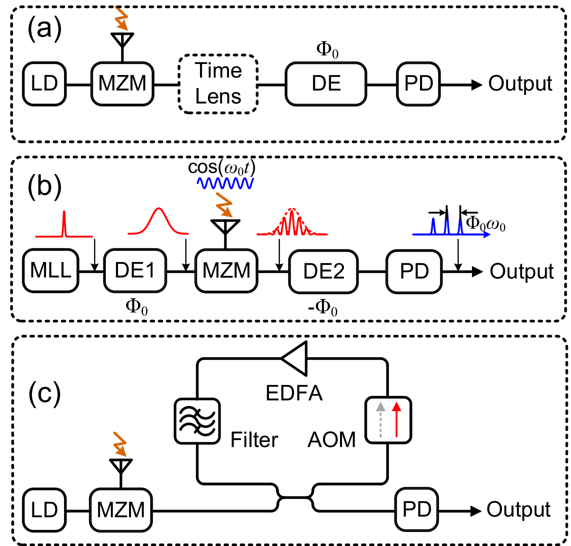

Fig. 25. Schematic diagram of three typical RTFT systems. (a) Dispersion-based RTFT; (b) temporal-convolution-based RTFT; and (c) frequency-shifted-loop-based RTFT. DE: dispersive element; AOM: acousto-optic modulator.

the spectrum will be mapped into the time domain. Thus, by modulating an optical source with the electrical signal to be processed, RTFT of the signal will be implemented. The schematic diagram of this method is shown in Fig. 25(a). The dispersive element in the system can be implemented using a length of dispersive SMF [12] or an FBG [337]. However, analogous to the Fraunhofer diffraction, the RTFT method in Fig. 25(a) only works under the condition of far-field dispersion. When the dispersion value is not large enough, time lens would be useful, which offers a quadrature phase shift [336]. It is worth noting that the frequency resolution of the dispersion-based RTFT is limited by the dispersion value of the dispersive element. A better frequency resolution requires a larger dispersion value. To improve the frequency resolution, bandwidth magnification was proposed and a frequency resolution of 60 MHz was experimentally demonstrated [338].

Temporal convolution [339]–[342] is another form of dispersion-based RTFT, as illustrated in Fig. 25(b). In this system, an ultrashort optical pulse from an MLL is temporally stretched by a dispersive element. The stretched pulse is modulated by the RF signal via an MZM and then temporally compressed by a second dispersive element. On the condition that the dispersion of the two dispersive elements is complementary, after OE conversion the spectrum of the electrical signal applied to the modulator is mapped into the time domain at the output of the system. In this method, the observation of the output requires an oscilloscope with a high sampling rate. To overcome this problem, the technologies of temporal amplification [343] and asynchronous optical sampling [344] are utilized. The temporal-convolution based RTFT has the potential for realizing an instantaneous bandwidth as large as several Terahertz and a frequency resolution as low as hundreds of megahertz at the same time.

Another method to implement the RTFT is to use a frequency-shifted loop [133], [134], [345]–[347]. As shown in Fig. 25(c), the electrical signal to be processed modulates an optical carrier and the modulated optical signal is injected into the frequency-shifted loop. In the frequency-shifted loop, the optical signal is frequency shifted by an acousto-optic modulator (AOM) per round. The filter is used to shape the spectrum of the output signal. An erbium-doped fiber amplifier (EDFA) is inserted in the loop to compensate for the cavity loss. On the condition that the frequency-shifted loop works at a proper state, especially the frequency shift per cycle being a multiple of the fundamental cavity frequency, the spectrum of the signal to be processed will be mapped into the time domain and can be observed by an oscilloscope after the optical-to-electrical conversion. Compared with the dispersion-based RTFT schemes, the frequency resolution of this configuration is greatly improved. Meanwhile, this system has the minimal processing latency, which equals to the inverse of the frequency resolution. A frequency resolution of 30 kHz was experimentally demonstrated [133]. Different from the dispersion-based RTFT, the frequency-shifted-loop-based RTFT has no limitation on the time window, thus it can be applied to the measurement of infinitely long signal. However, the operation bandwidth of the frequency-shifted loop-based RTFT is limited to only tens of megahertz, up to the frequency shift of the AOM. To realize a larger bandwidth, some prior information of the frequency band of the signal is required.

H. Optical Co-site Interference Cancellation

In a radar system, when a signal is radiated into the free space via a transmitter, a portion of the radiated signal would be leaked directly to the receiver due to the fact that the transmitter and receiver are very close. This effect is also a long-standing concern of distributed radars. The leakage, usually denoted as co-site interference or self-interference in the literature, would be overlapped with the weak SOI in the same frequency band and is difficult to be removed with a filter [348], which seriously affect the performance of the radar system. One direct way to solve this problem is to let the transmitter and the receiver work at different time slots, but this would introduce a "dead zone" and make the implementation of multifunction radars difficult.

Another way for co-site interference suppression is coherent cancellation, in which a mitigation signal that has the same amplitude and complementary phase to the co-site interference is first produced and then coherently combined with the received signal. One such system is illustrated in Fig. 26. As can be seen, the transmitted signal is split into two paths. One is sent to the antenna for emission while the other is transmitted through an attenuator and a phase shifter. Then, the signal is combined with the received signals consisting of the leaked interference signal and the SOI. By carefully adjusting the attenuator and the phase shifter, the interference signal can be successfully suppressed while the SOI remains.

Traditionally, co-site interference cancellation systems are realized in the electrical domain, which, however, suffer from low frequency and narrow operation bandwidth. The maximum cancellation bandwidth that has ever been reported for pure electronic approaches is only 120 MHz centered at 2.45 GHz [163]. To achieve broadband co-site interference cancellation at high frequency, photonics-based technologies become attractive, and lots of efforts have been devoted to this topic in the past two decades [153]–[159], [349]–[356].

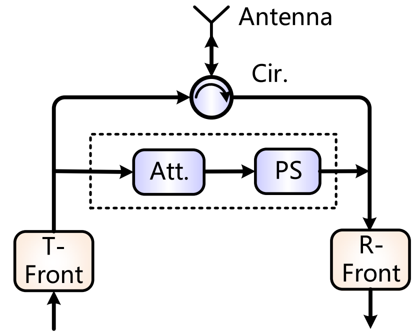

Fig. 26. Schematic diagram of a typical co-site interference cancellation system. PS: phase shifter, Cir: circulator.

A classical photonic co-site interference cancellation system contains two optical links. One is utilized to convey the co-site interference and the SOI captured by the receiver, and the other is employed to produce and regulate the mitigation signal. A fixed π phase shift should be introduced to the replica of the interference signal, which can be implemented via differential detection [353], balun coupling [356], complementary intensity modulations [158], phase-modulation to intensity-modulation conversion [273], or polarization modulation [274]. With a time-delay line and a variable optical attenuator (VOA) to achieve the delay and magnitude matching, the interference can be largely suppressed.

It should be noted that the phase of the signals in the optical links may be changed with the temperature and vibration in the environment. In that scenario, tunable phase shifters implemented in the optical domain to compensate the phase variations become essential. Previously, photonic microwave phase shifters were realized by slow light effect [357]–[361], optical vector sum [362], [363], and external modulation together with optical heterodyne detection [364]–[369]. Fig. 27 shows the key performances of typical microwave phase shifters achieved in the literature. As can be seen, microwave photonic phase shifters based on external modulations have the broadest operational bandwidth and best amplitude-phase consistency as compared with others, which are attractive to the co-site interference cancellation.

The photonic microwave phase shifters based on a DDMZM [355], a DPMZM [155], a PolM [156], a PM [354], or a polarization-division multiplexing (PDM) modulator [350] were tested in the co-site interference cancellation systems, and the performances of the systems are summarized in Table IV.

Most of the reported systems did not consider the scenario that the interference signal is reflected, scattered or diffracted by the surroundings, i.e., the received signals may contain multiple delayed, attenuated and phase-shifted copies of the interference signal. To address this issue, multi-channel interference cancellation with independent phase and magnitude control in each channel was proposed [153], [156]. Fig. 28 shows the schematic diagram of one typical multi-channel interference

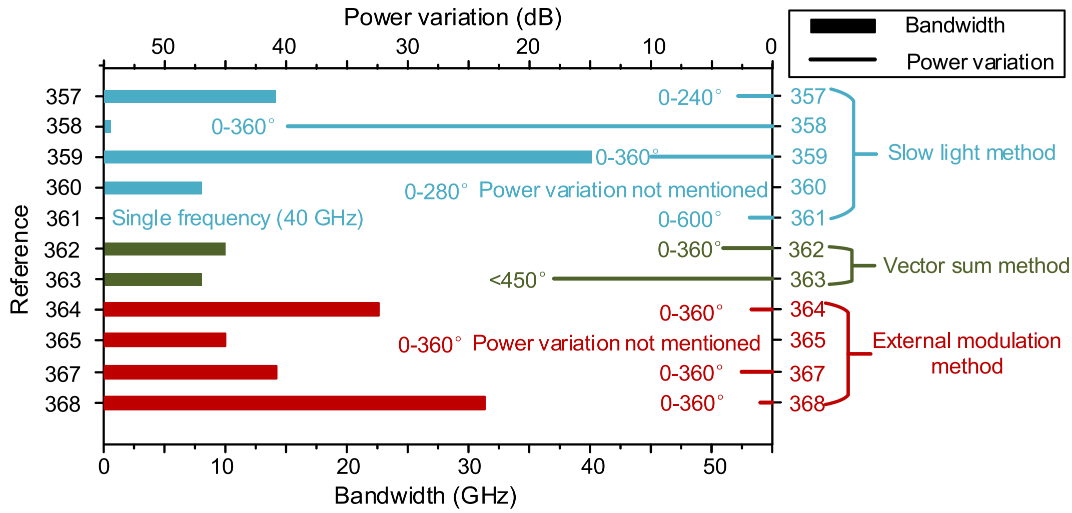

Fig. 27. Performance comparison of typical photonic microwave phase shifters

TABLE IV
PERFORMANCES COMPARISON OF TYPICAL CO-SITE INTERFERENCE CANCELLATION SYSTEMS

Phase-shifting mechanism	Ref.	Bandwidth	Broadband cancellation	Single-frequency cancellation
PDM-DPMZM	[350]	Not mentioned	29 dB @ 200 MHz	58.1 dB @ 15 GHz
PM-based	[354]	Not mentioned	20 dB @ 10 MHz	56 @8 GHz
DPMZM-based	[155]	4 GHz @ 30 dB	Not mentioned	Not mentioned
DDMZM-based	[355]	9 GHz @ 30 dB	25 dB @ 19.5 MHz	Not mentioned
PolM-based	[156]	9.5 GHz @ 30 dB	15 dB @ 4 GHz	Not mentioned

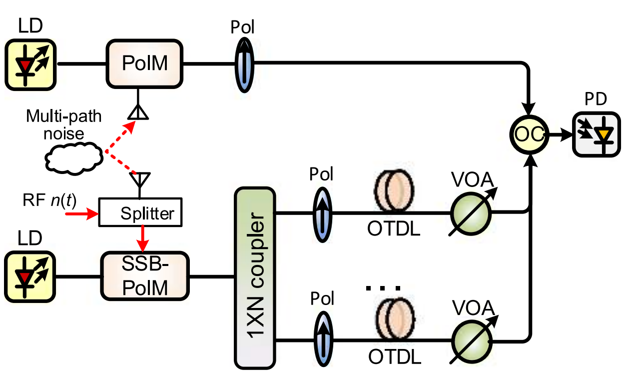

Fig. 28. Optical multipath RF interference cancellation using a PolM-based photonic microwave phase shifter. OTDL: optical time-delay line.

cancellation system [156] using a multichannel polarization-modulation based photonic microwave phase shifter [124], [370]. The upper optical link is employed to carry the SOI signal and the multi-path interferences, and the lower link is utilized to introduce multiple phase-shifted, time-delayed and amplitude-manipulated mitigation signals by adjusting the polarization controller, the time-delay line and the VOA in each path. As a result, interference cancellation with a 20-dB suppression ratio over a 13.3-GHz range (from 3.5 to 16.8 GHz) or a 30-dB suppression ratio over a 9.5-GHz range (from 5.5 to 15 GHz) was demonstrated.

IV. THE ARCHITECTURES OF MICROWAVE PHOTONIC RADARS

The microwave photonic techniques described in Section III can be integrated to realize a radar transceiver, taking advantage of the attractive features of photonics. Fig. 29(a) shows a general block diagram of a microwave photonic radar, which comprises T/R modules, optical modules, and DSP modules. According to the architecture of the optical modules, microwave photonic radars can be divided into two categories, i.e., optoelectronic hybrid structure and all-optical structure.

Fig. 29(b) shows the architecture of the optoelectronic hybrid radar, which is the traditional electronic radar shown in Fig. 5 with one or more subsystems implemented in the optical domain. This structure is well compatible with the current radar systems, so it would be readily accepted by researchers in the radar society and be more likely to be deployed shortly. However, multiple OE and EO conversions would be required if there are two or more optical modules in the system. At the current stage, multiple pairs of OE and EO conversions would introduce considerable loss, noise, and nonlinear components, and therefore significantly degrade the performance of the radar. Moreover, other electronic components in the system would offset the merits obtained by the microwave photonic technologies.

Different from the optoelectronic hybrid radar, an all-optical radar implements all the RF signal generation, transmission, and processing by photonics methods, which is usually built based on an MLL, as shown in Fig. 29(c). In the transmitter, the MLL

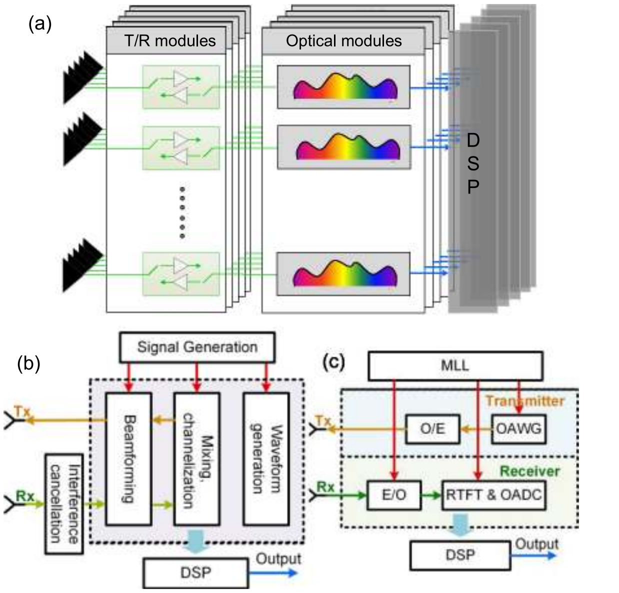

Fig. 29. (a) The architecture of a microwave photonic radar, and the optical modules in (b) an optoelectronic hybrid radar and (c) an all-optical radar. DSP: digital signal processing; OAWG: optical arbitrary waveform generator; O-E: optical-to-electrical conversion; OADC: optical analog-to-digital converter; RTFT: real-time Fourier Transform; E-O: electrical-to-optical conversion.

provides highly coherent optical carriers or ultrashort pulses for broadband radar 0signal generation, and in the receiver, the echo is handled with analog signal processing modules enabled by the ultrashort pulses. The reference signals for the whole radar system is also provided by the MLL. The advantages of the all-optical radar include the dramatically reduced number of OE and EO conversions and some extreme performance brought by the highly coherent pulse source as stated in Section II. But the problem is that most of the ultrashort-pulse based signal processing modules do not have sufficient maturity to support the practical deployment at the current stage.

Based on the two architectures, microwave photonic MIMO radars, multifunction radars and distributed radars were demonstrated.

A. Optoelectronic Hybrid Radar

Early demonstration of the microwave photonic radar based on the optoelectronic hybrid structure can be dated back to the 1990s [11], [298], [371], in which the prototypes of OBFNs were developed and investigated using outfield experiments. Although target detection was not implemented in these works, the systems developed can still be regarded as the optoelectronic hybrid radars because they contain transmitters and receivers by which radar functions can be implemented. In 1991, W. Ng *et al.* from the HRL Laboratories realized the first demonstration of an actual dual-band (1–2.6 GHz and 8–12 GHz) phased array antenna based on an OBFN, verifying the squint-free operation of radars steered by optical delay lines [11]. Later, the system design and performance of an L-band 96-element array controlled by photonics was reported by J. J. Lee *et al.* from the same group. Pulses were propagated through all the RF and optical components. The bandwidth of the system was >550 MHz,

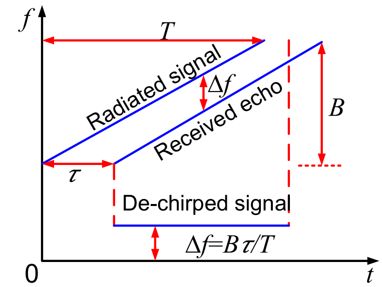

Fig. 30. Illustration of the principle of LFM de-chirping

corresponding to a range resolution of 30 cm for target detection [372]. In 1994, A. Goutzoulis *et al.* from Westinghouse Electric Corporation implemented the field demonstration of a 6-bit fiber-optic true-time delay system for a 2×16 element broadband array antenna [298]. Squint-free beam steering over +45° was demonstrated over the full antenna-limited 0.6–1.5 GHz band. D. Dolfi *et al.* from Thales Research & Technology also reported the experimental demonstration of a two-dimensional optically controlled phased-array antenna operating between 2.7 and 3.1 GHz in 1996 [299]. Time delay scanning between 0° and 20° was realized using free-space propagation and spatial light modulators.

Afterward, other microwave photonic components were tested in radars under development. For instance, analog photonic links were applied in AN/SPQ-9B Advanced Development Model radar operated in the X band to remote the antenna and the transceiver [373]. Outfield measurement showed that the SNR degradation caused by the incorporation of the analog photonic link could be negligible (0.4 dB for transmit and 0.3 dB for receive). In 2013, a chip-scale OEO from OEwaves Inc. was incorporated into the Miniature Hit-to-Kill (MHTK) interceptor designed by Lockheed Martin, which successfully supported the guided test fight [374].

Recently, the broadband nature of the optoelectronic hybrid radar was employed to achieve ultrahigh-resolution radar imaging. In general, radar imaging can be performed by either synthetic aperture radar (SAR) or inverse synthetic aperture radar (ISAR), which uses the movement of radar antenna or the target to create a synthetic aperture, providing finer spatial resolution than the conventional beam-scanning radars. The range resolution is determined by the bandwidth of the radar via $L_R = c/2B$ which is distance independent, and the cross-range resolution is related to the viewing angle θ and the carrier frequency f_c of the radar signal by $L_C = c/2\theta f_c$. Since high cross-range resolution can be achieved by enlarging the viewing angle, the key to improve the two-dimensional resolution is to increase the bandwidth of the radar.

Most of the currently reported optoelectronic hybrid radars for high-resolution imaging are realized through de-chirping processing, where an LFM signal is used as the radar waveform [32], [217], [218], [222], [224]–[228], [323], [375]–[379]. The principle of de-chirp processing of the LFM signal is illustrated in Fig. 30, which is performed by mixing the received LFM echo with the reference LFM signal (i.e., the radiated signal). Assuming the expression of the frequency of the reference LFM

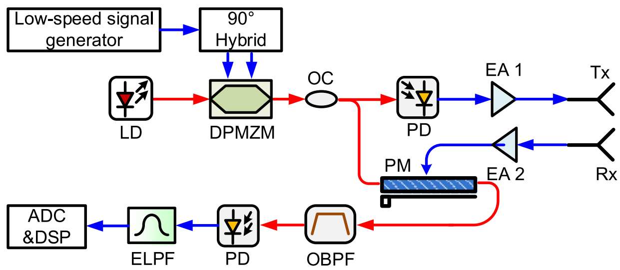

Fig. 31. Schematic diagram of the microwave photonic radar based on de-chirping processing. DPMZM: dual-parallel Mach-Zehnder modulator; OBPF: optical band-pass filter; ELPF: electrical low-pass filter.

signal is $f_T(t) = f_0 + kt$, where f_0 is the initial frequency and k is the chirp rate. For the simplest scenario with a point target, the echo frequency is a replica of the reference frequency with a time delay of τ which could be written as $f_E(t) = f_0 + k(t+\tau)$. Then, the mixing of the echo with the reference leading to $f_{\text{de-chirp}}(t) = f_0 + k(t+\tau) - (f_0 + kt) = k\tau$. $k\tau$ is usually much smaller than f_0, so a low-speed ADC is sufficient to sample the de-chirped signal, which ensures high-speed signal processing in the following stages. If τ is large, then an optical delay line can be used to delay the reference signal, making $f_{\text{de-chirp}}(t) = k(\tau - \tau_0)$, where τ_0 is the delay of the optical delay line. Therefore, the distance between the radiator and the target can be calculated by $L = c\tau/2 = c\tau_0/2 + cT/(2B) \cdot f_{\text{de-chirp}}$, where T is the pulse width of the LFM signal. The range resolution of the radar depends on the full width half maximum of the de-chirped signal ΔB, i.e., $L_R = c\tau/2 = cT/(2B) \cdot \Delta B$. For an ideal case, $\Delta B = 1/T$, so the best resolution that can be achieved is $L_R = c/2B$. If the target or the transmitter is moving, the Doppler frequencies can be resolved from the echoes to obtain the azimuth position of the target.

Fig. 31 shows a schematic diagram of a typical microwave photonic radar architecture based on de-chirping processing [217]. Photonic microwave frequency multiplication (as described in Section III) is applied to achieve the frequency quadrupling of an IF-LFM signal from a low-speed signal generator. The optical frequency-quadrupled signal is split into two parts by an optical coupler (OC). One part is injected into a PD to convert the optical signal into an electrical signal for emission. The other part of the optical signal is introduced to a PM, which is modulated by the radar echo. The PM together with an optical band-pass filter (OBPF) and a PD is used to perform frequency mixing. With an electrical low-pass filter (ELPF) to select the different frequency components, de-chirp processing of the LFM waveform is implemented. The de-chirped signal is sampled by an ADC and then sent to a DSP unit to calculate the image of the target. Based on this architecture, many experiments and field trials have been conducted to achieve high-resolution and real-time imaging [32], [218], [227], [228], [375]. In [32], an LFM signal with a bandwidth of 8 GHz was generated and radar imaging with a range resolution of $\sim$2 cm was achieved. The image resolution was further improved by increasing the center frequency and bandwidth of the LFM signal to the Ka band and 12 GHz, respectively, and a range resolution of $\sim$1.3 cm was achieved [218]. In addition, real-time ISAR or SAR imaging of non-cooperative targets was demonstrated, which successfully achieved the ultrahigh-resolution microwave images or videos of a Boeing 737 airplane [227], an unmanned aerial vehicle (UAV) [375], and Leifeng pagoda [228].

To achieve a higher azimuth resolution of the ISAR imaging without increasing the integration time, a MIMO radar architecture can be applied. Fig. 32 illustrates a microwave photonic $M \times N$ MIMO radar architecture [226], where M LDs with different wavelengths serves as the CW light sources. Each light of them is modulated by an IF-LFM signal at a DPMZM to realize frequency quadrupling. The obtained M-channel frequency quadrupled LFM signals have the same bandwidth but different center frequencies. In the receive end, N receivers are applied to collect echoes of the M transmitted signals. In each receiver, de-chirping and separation of radar echoes from different channels are implemented simultaneously. As a result, M digital signals corresponding to the de-chirped echoes of the M transmitted signals are separately obtained in each receiver. A microwave photonic 2×2 MIMO radar with a 4-GHz bandwidth was established in [226], and the functions of target positioning and direction of arrival estimation were realized.

In order to remove the image-frequency interferences and false targets in the single-channel photonic de-chirping receiver with real-valued outputs used in [32], [218], [226]–[228], [375], a photonics-based radar architecture using in-phase and quadrature (I/Q) de-chirping receiver with balanced detection was proposed [225], as shown in Fig. 33. In the receiver, balanced I/Q de-chirping is conducted based on a 90° optical hybrid, and two BPDs are adopted for the removal of baseband background signals and interferences resulting from the frequency mixing between echoes with different time delays. The key advantage brought by the I/Q de-chirping scheme is the determination of whether the de-chirped frequencies are positive. Thus, targets that are farther or nearer than the observational reference point can be distinguished. Furthermore, the balanced detection is beneficial to boost the amplitude of the de-chirped frequency components. An 8-GHz microwave photonic radar transceiver based on such architecture was built in the K-band for ranging and imaging, which experimentally verified the elimination of the interference induced by image frequency, baseband envelope, and unwanted frequency mixing.

Other optoelectronic hybrid radar architectures based on the de-chirping mechanism were also reported to further improve the radar performance, such as phased array radar [376] and dual-band LFM CW radar [224], [377], and full-polarimetric radar [378].

The optoelectronic hybrid radar architecture can also be used for 3D imaging. In [380], an interferometric inverse synthetic aperture radar was established with an optical arbitrary waveform generator in the transmitter and photonic microwave mixing in the receiver. The system uses the phase differences between two complex-valued 2D images to evaluate the height of each point. To further improve the performance of 3D imaging especially for the height dimension, an equivalent 2D aperture vertical to the radar-target line of sight is necessary. One of the methods to achieve an equivalent 2D aperture is scanning the antenna with a 2D translation stage, which has been adopted in a radar with a photonic W-band millimeter-wave pulse generator

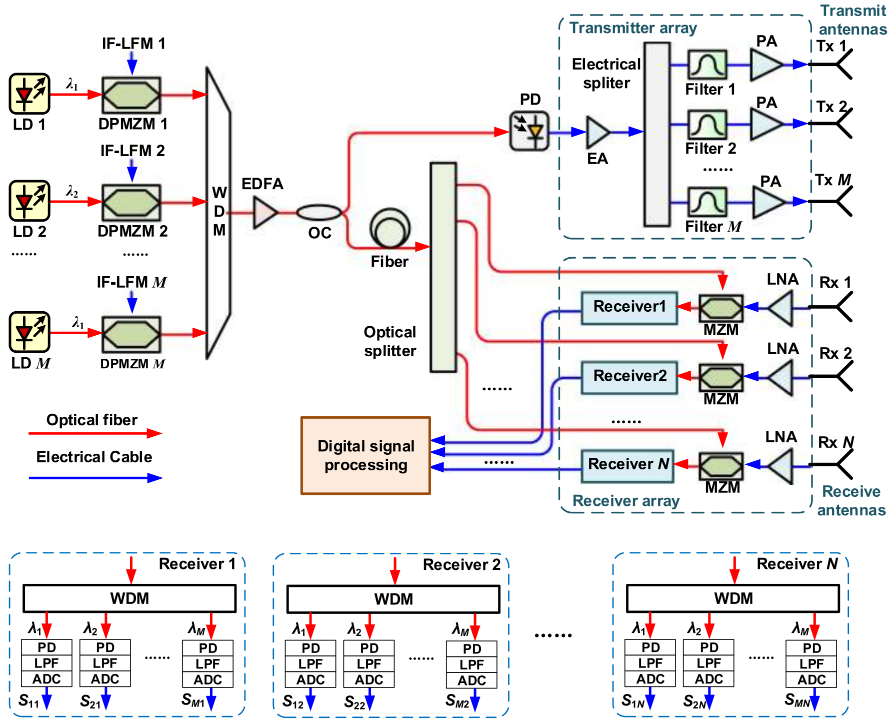

Fig. 32. Schematic diagram of the microwave photonic $M \times N$ MIMO radar architecture. PA: power amplifier.

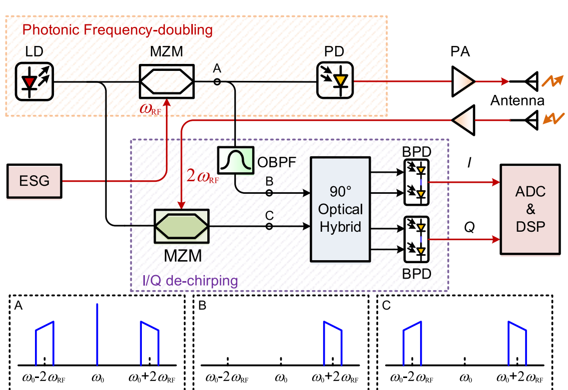

Fig. 33. Schematic diagram of microwave photonic radar architecture using balanced in-phase and quadrature (I/Q) de-chirping receiver.

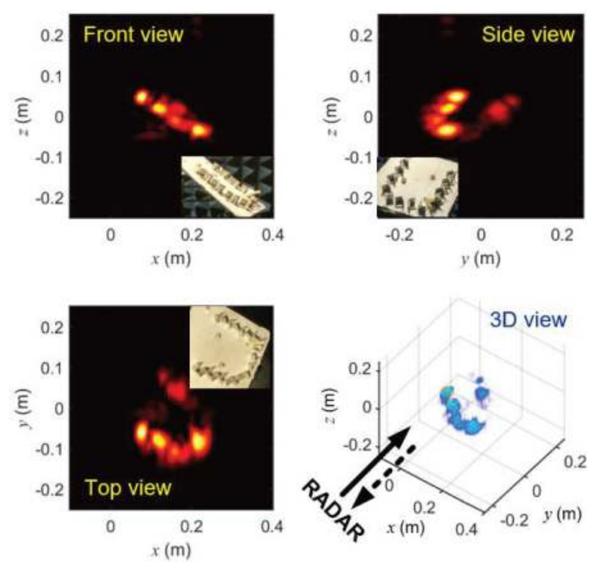

Fig. 34. Experimental results of a microwave photonic 3D inverse synthetic aperture radar [224].

[381]. In addition, similar to the principle of an inverse synthetic aperture radar for 2D imaging, rotating the target around two orthogonal axes can also compose a 2D equivalent aperture. Fig. 34 shows the experimental results of a rotation-based 3D inverse synthetic aperture radar, in which a photonics-based K-band radar transceiver capable of generating and processing LFM signals with a bandwidth of 8 GHz was employed [224].

It is worthy to note that recording a large amount of raw data during a relatively long time for completing the scanning or rotation is almost unavoidable in 3D radar imaging, which puts forward the requirements for fast analog signal pre-processing and high coherence between radar pulses. Fortunately, with key microwave photonics technologies mentioned in section III, microwave photonic radar would achieve more satisfactory 3D images with lower SWaP in the future.

B. All-Optical Radar Architecture

An MLL is the heart of an all-optical radar system which provides a pulse train with ultra-stable repetition rate, ultrashort pulse width, and a large number of spectral lines. As an example, Fig. 35 shows the schematic diagram of the first all-optical radar system demonstrated via a field trial experiment [323]. In the transmitter, two OBPFs are used to select two comb lines from the MLL. One comb line is modulated by a baseband waveform while the other is frequency shifted. The two wavelengths are

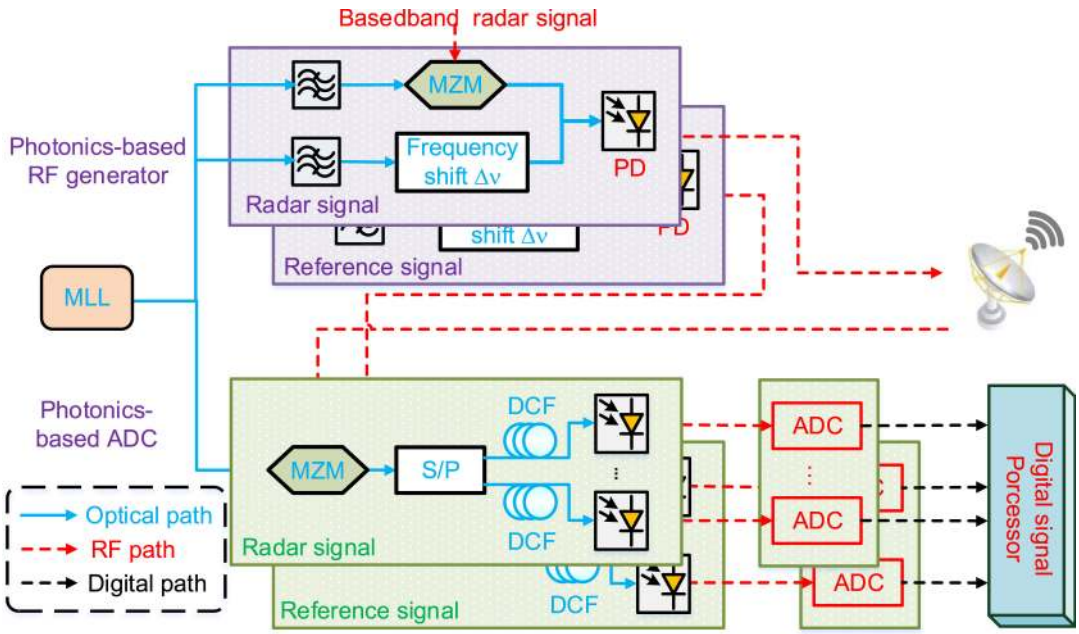

Fig. 35. Schematic diagram of the reconfigurable radar based on all-optical architecture [323]. DCF: dispersion compensation fiber.

then beating at a PD to generate the radar waveform at the desired frequency band. By changing the baseband signal, the waveform of the generated radar signal can be reconfigured, and the center frequency can be switched by selecting two comb lines with different frequency spacing. As a result, radar waveforms with a center frequency from 400 MHz to 40 GHz and a bandwidth of 200 MHz are generated. The bandwidth of the generated waveform is limited by the repetition rate of the MLL, which was 400 MHz in the demonstration. In the receiver, the received echoes are sampled by the ultrashort optical pulses from the same MLL. Then, the sampled signal is transferred to low-speed signals by optical serial-parallel conversion and time stretching. As a result, a low-speed electrical ADC is enough to digitize the signal in each channel. In the field-trial experiment, the feasibility of the all-optical radar was demonstrated. With a 13-bit Barker code radar signal, the range resolution of the radar was around 23 m, and the detection range was about 30 km. The range resolution can be further improved if an IF waveform with a larger bandwidth is employed.

Thanks to the abundant spectral resources of the MLL, the above system can be upgraded to realize dual-band microwave photonic radar for multi-functional operation [379], with the schematic diagram of the transmitter and receiver shown in Fig. 36. In the transmitter, three comb lines of the MLL are selected via optical filters, and one of them is modulated by two IF waveforms with different center frequencies. Combing the three signals and beating them at a PD, multiple radar waveforms are generated. Then, two RF filters with different center frequencies are employed to select the waveforms, which are radiated into the free space via two antennas. In the receiver, the reflected echoes are modulated onto one of the three reference optical comb lines via a modulator and then sent to a PD along with the other two comb lines. Down-conversion of the two radar waveforms is thus realized. The obtained IF signals are sent to an electrical ADC

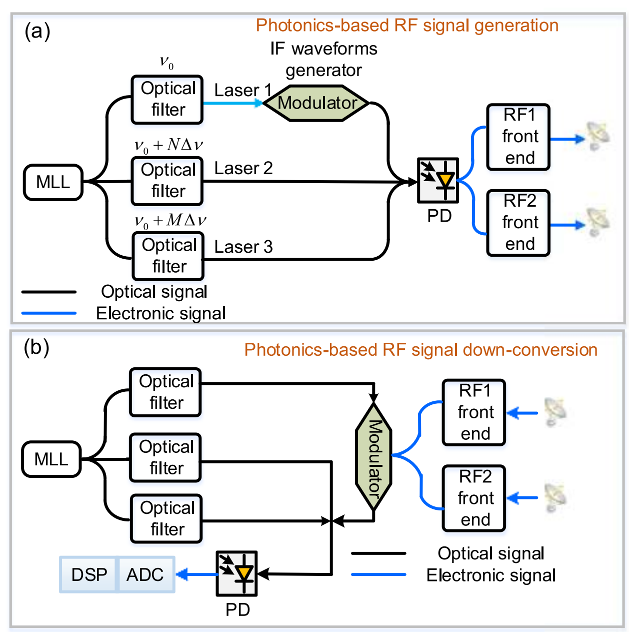

Fig. 36. Schematic diagram of the dual-band microwave photonic radar [379].

and DSP module to extract the ranging information or perform radar imaging.

The structure of dual-band microwave photonic radar can be further simplified to a setup shown in Fig. 37 [382]. Each comb line from the MLL is modulated by the electrical signals in the transmitter and the receiver. Although more unwanted optical frequency components are introduced to the PDs, the comb lines and the sidebands that are used to generate the desired electrical signals are not interfered with each other. Therefore, the microwave photonic radar transceiver without optical filters is feasible. The system has been applied for ISAR imaging [383],

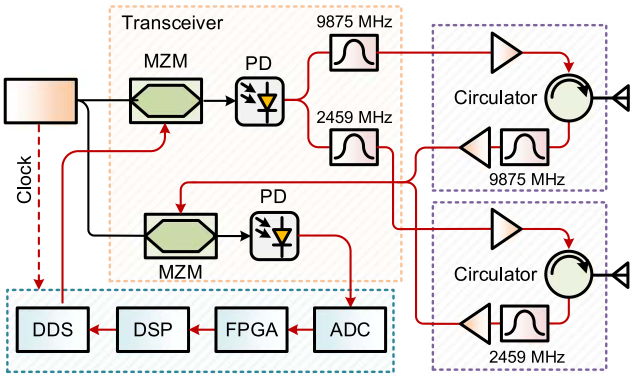

Fig. 37. Schematic diagram of the dual-band microwave photonic radar without optical filters [382].

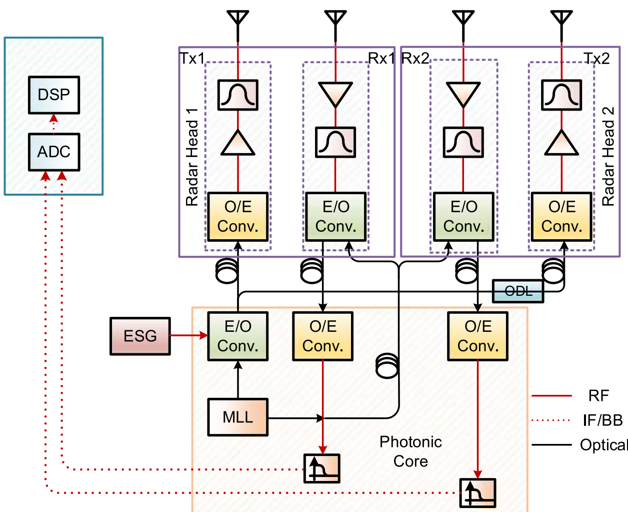

Fig. 38. Structure of the photonics-enabled distributed coherent radar systems with 2×2 MIMO [387].

naval target tracking [384], and landslides monitoring [385], in which two radar signals in the S- and X-bands were handled simultaneously. One key advantage of the dual-band all-optical radar is that the generation and detection of the dual-band radar signals can be achieved by the same transmitter and receiver, which not only makes the system more compact but also ensures the coherence of the signals in the two bands due to the shared MLL, which is highly desired for simplifying the processing in multi-band data fusion.

In order to further improve the performance of the all optical radars in terms of detection, localization, and imaging, multiple transmitters and multiple receivers can be used simultaneously to construct a MIMO radar, similar to the concept based on the optoelectronic hybrid structure. The benefits of implementing the MIMO radar using all-optical structure include the low-loss fiber distribution as well as the coherence and stable clock provided by the MLL. Thus, signals from all the distributed nodes can be processed in a central unit, which guarantees the coherence among different nodes and yields favorable system performance. Fig. 38 depicts the structure of an all-optical 2×2 MIMO radar, consisting of two radar headers and a photonic core with an MLL serving as the optical master clock. In-field demonstration

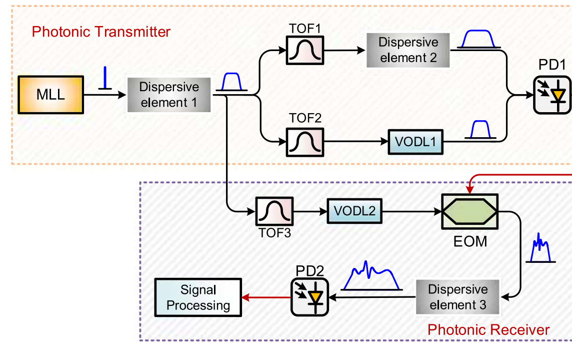

Fig. 39. The schematic of the photonic time-stretch coherent radar system.

of the radar system has been successfully conducted [386], in which a 100-MHz LFM signal in the X band is used to observe a collaborative target.

To avoid the use of the electrical baseband source in [323], a photonic time-stretch coherent radar system has been proposed [328]. The structure of the photonic time-stretch coherent radar is depicted in Fig. 39. The ultrashort pulses generated by the MLL are sent into a dispersive element with a relatively large dispersion value, so they are broadened in the time domain. The broadened pulses are then divided and introduced into the signal generation and reception channels. In the signal generation channel, the pulses are further split into two arms. Two tunable optical filters with different center frequencies are incorporated into the two arms respectively to select a certain part of the optical spectra. A second dispersive element is added into one of the two arms to introduce a dispersion difference between the two arms. After beating the signals in the two arms at a PD, pulsed LFM microwave signals would be generated. In the receiver, the optical pulses are modulated by the received echoes in the EOM and sent to the third dispersive element, so they are further stretched in the time domain. After OE conversion, the received echoes are compressed in the frequency domain. As a result, high-range resolution detection can be achieved without the need for high-speed electrical ADCs. A dual-target detection experiment based on the photonic time-stretch coherent radar was conducted in the X band, by which a range resolution of ∼5.5 cm was achieved. The main advantage of this radar is its strict coherence within the whole system since only one MLL is used as the signal source.

The performance of the photonic time-stretch coherent radar was further improved by later studies [388]–[390]. The SNR of the time-stretching receiver in the radar was analyzed in [388], and a photonic time-stretch coherent radar system operating at the W band with a bandwidth of 12 GHz was experimentally demonstrated, achieving a range resolution of 1.48 cm. To overcome the measurement range restriction due to the relatively-narrow pulsed LFM signal, an optical switch was added in the transmitter [389], which reduces the pulse repetition rate tenfold. As a result, the measurement range was improved to more than 40 m with a range resolution of ∼4 cm. Furthermore, a phase diversity scheme based on a dual-output MZM was employed to decrease the frequency response fluctuation induced by dispersion [390]. Experiment results showed that the frequency response fluctuation was reduced by 9.7 dB and the peak power in single target detection was increased by 6.7 dB.

In addition, MLLs can be exploited to generate broadband coherent radar signals through the frequency-to-time mapping approach [391], which can be used for radar detection with high resolution as well. In one such system, a waveform generator composed of an MLL, a high-resolution optical pulse shaper and a variable delay line (VDL) produced an LFM waveform from 110 GHz down to 70 GHz [211]. By using this waveform, multi-target ranging with a resolution of 3.9 mm and unambiguous detection over a range of more than 5 m was achieved. Compared with other all-optical radar systems, the radar signal in [211] had an ultra-broad bandwidth, and the resolution can be significantly increased. However, the time duration of the waveform is usually about several nanoseconds (∼ns), resulting in a limited detection range.

C. Multifunction Microwave Photonic Radar System

Due to the broad bandwidth and various multiplexing methods provided by the photonic technologies, multiple signals can be manipulated in the transceiver simultaneously, which enables multifunctional radars with reduced hardware and cost. Some novel microwave photonic radar transceivers have integrated extra functional modules to generate or process signals for communication or electronic warfare purpose. For example, in [392] the photonics-based receiver concurrently down-converts both the radar echoes and the communication signals with different frequency bands, in which the experimental results verified the penalty-free reception of S-band radar echoes and a C-band 54Gbps 64-QAM OFDM communication signal. Similarly, the optoelectronic hybrid radar transmitter in [393] can also act as a communication transmitter by encoding an amplitude shift keying signal onto a radar signal. An imaging resolution up to $\sim$1.8 cm $\times$ 2 cm and a communication rate of 100 Mbit/s were simultaneously achieved. Electronic warfare is another kind of function that can be integrated into the microwave photonic radars. A typical system of this kind has been proposed in [394], in which fast frequency measurement and high-resolution radar imaging can be implemented simultaneously. Ka-band frequency measurement with a 40-MHz measurement resolution and a 100-kHz refresh rate was achieved along with Ku-band ISAR imaging. Lidars can be integrated with microwave photonic radars as well. In [395], a coherent radar-lidar system based on a shared MLL is proposed for speed measurement, in which different comb lines are allocated to lidar and radar, respectively.

D. Distributed Microwave Photonic Radars

The aforementioned microwave photonic radars are generally monostatic, of which the sensitivity is limited by the transmission power and antenna aperture, and the positioning accuracy will be affected by the radar observation angle, leading to issues like speed ambiguity and false alarm. Meanwhile, threats such as electronic jamming and stealth aircrafts are also plaguing monostatic radar system. Thanks to the distinct features associated with flexible array, large synthetic aperture, accumulated observation angles and data fusion, distributed coherent radar network is proved to have the potential to overcome the above limitations and to improve the detection accuracy in the observation area.

Due to the low transmission loss, light weight, immunity to EMI, and bidirectional transmission capability, optical fiber is considered as the best signal transmission medium between multiple base stations in the distributed radar network. Thus, photonics-assisted distributed radar networks have attracted a lot of attentions [396]. In [397], a broadband distributed coherent aperture radar system consisted of a central controlling system, several remotely distributed transceivers, and a fiber-based time synchronization network was reported. The central controlling system performs multichannel orthogonal LFM signal generation and processing, the time synchronization network achieves time synchronization among different remote transceivers, and the remote transceivers perform OE/EO conversion as well as transmission and reception of the RF signals. An X-band two-cell all-optical radar system with a bandwidth of 3 GHz is verified experimentally. When full coherence is achieved, the signal-to-noise ratio (SNR) gain can reach 8.33 dB, which is consistent with the theoretical prediction, indicating the distance detection accuracy may improve by 2.6 times. In addition, fiber-distributed radar network utilizing ultra-wideband [398] and chaotic [399] signals based on WDM structure were previously proposed, which achieved high-precision positioning of targets. MIMO radars introduced in the previous parts [386] can also be regarded as a kind of distributed radars.

V. Discussion and Conclusion

The distinct features of microwave photonics in terms of broad bandwidth, low loss transmission, multidimensional multiplexing, flat response, fast analog signal processing, highly coherent pulse source, and EMI immunity have stimulated significant interests to apply photonics-based technologies to radars. Different techniques for generation, transmission, processing, and control of radar signals were proposed and investigated, some of which have shown superior performance or potential as compared to their electronic counterpart and are close to practical application. The investigation of these techniques leads to two typical microwave photonic radar architectures, i.e., optoelectronic hybrid structure and all-optical structure. Field trial experiments of the prototype radars in both categories have verified or envisioned the following benefits brought by photonics: (1) the broad instantaneous bandwidth and large frequency range enable high-resolution 2D or 3D imaging, accurate target identification, and multi-band, multi-signal and multi-function operation; (2) the low phase noise of the photonic LO generator significantly enhances the detection performance of weak Doppler-shifted signals in strong clutter environment; (3) the exceptional reconfigurability of the photonic techniques enables the generation and processing of various and complicated waveforms for adaptive radars or cognitive radars; (4) the optical analog signal processing reduces the data amount to the DSP which dramatically accelerates the response of radars; and (5) the high coherence of the pulsed laser and stable RF delivery improve the SNR of radar systems, especially the distributed

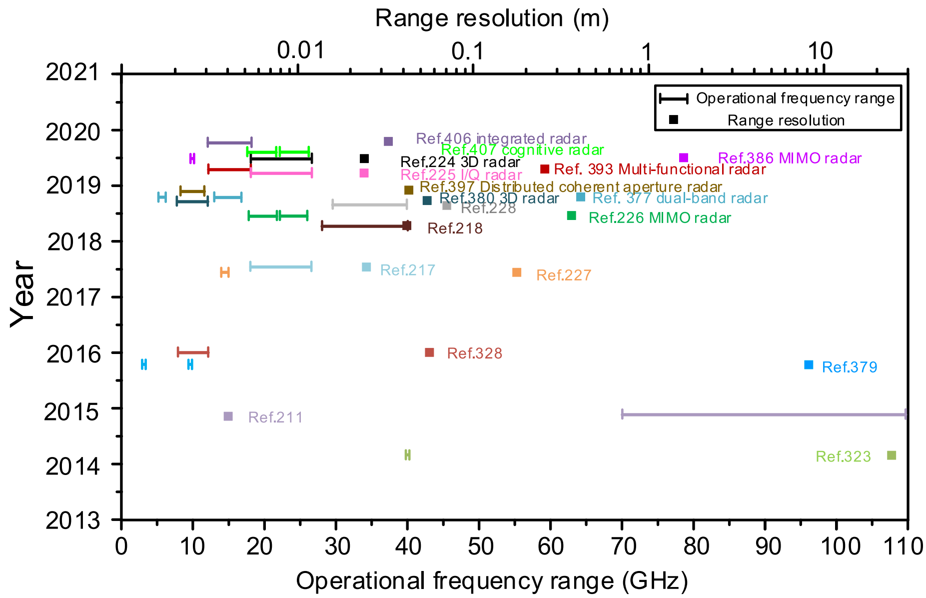

Fig. 40. The key performances of the recently reported photonic microwave radars.

and MIMO radars. Fig. 40 summarizes the key performances of the reported photonic microwave radars in the literature.

Although a certain degree of maturity has been achieved in the microwave photonic radar and related techniques, there are few breakthrough applications that attract direct industrial interest and investment. A considerable room for improvement still exists. Several expected future developments are discussed as follows.

What concerns the researchers in the field of microwave photonic radars most might be the photonic integration. Although many progresses have shown the inspiring potential of microwave-photonic radar systems, most of them are constructed based on discrete optical components, leading to a bulky system with low reliability. High-density integration is of critical importance for arrayed radar systems and miniaturized platforms such as unmanned aerial vehicles (UAVs), autonomous vehicles or even mobile devices. Up to now, many achievements have been reported on the photonic integrated circuits for possible radar applications [400]. In particular, a variety of integrated optical beamformers have been demonstrated based on optical ring resonators [71], Mach-Zehnder delay interferometer [401], and arrayed waveguide grating [402]; integrated OEOs were also reported although the phase noise performance still needs improvement [403]. In addition, some multifunctional building blocks such as reflective-type microring resonator [404] and programmable 2D mesh network [405] have been demonstrated, which might be useful for reconfigurable or software-defined microwave photonic radar. Recently, we demonstrated a chip-based broadband microwave-photonic imaging radar occupying the full Ku-band [406], as shown in Fig. 41. Both the wideband signal generator and the de-chirp receiver are integrated on a 1.45 mm$\times$2.5 mm silicon-on-insulator chip. A high precision range measurement with a resolution of 2.7 cm and an error of less than 2.75 mm were obtained. ISAR imaging of multiple targets with complex profiles was also implemented. Despite so, we have to say, the performance of most of the integrated

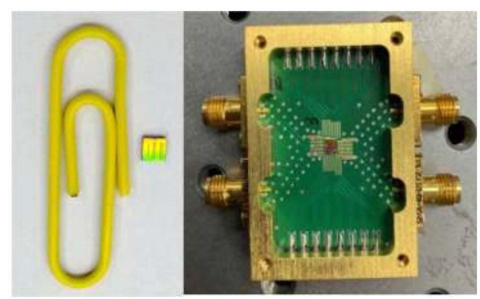

Fig. 41. The pictures of the chip-based microwave photonic radar

microwave photonic chip is not satisfactory for practical radar applications. Development in this area is still at the initial stage and advancement on chip-based microwave-photonic radars is highly welcomed.

Since monolithic integration of key microwave photonic subsystems does not have sufficient maturity for practical applications, co-packaging or hybrid integration of the devices fabricated at their optimal integration platforms is of great interest. At the present stage, indium phosphide, silicon nitride, and silicon-on-insulator are three leading photonic integration platforms [400]. Each platform has its strengths and weaknesses. Indium phosphide based-material inherently supports lasers, optical amplifier, modulator, detector, and most passive functionalities, but suffers from the large component footprint, high propagation loss, elevated charge carrier noise, and complex fabrication process. Silicon nitride waveguide has an ultralow propagation loss, hence it is particularly suitable for the optical delay lines and high Q optical cavity. However, the silicon nitride material cannot implement active optical devices such as lasers, modulators and detectors. Silicon-on-insulator is an attractive platform due to its capability of integrating modulators, PDs, passive components, and the excellent compatibility with standard CMOS processing. But the lack of light sources and amplifiers is the main challenge. In addition, the poor linearity and the tremendous loss of a pure silicon modulator would significantly degrade the dynamic range and sensitivity of the microwave photonic radar. Except for the three materials, thin-film lithium niobate (for modulators), chalcogenide glass (for stimulated Brillouin scattering based devices), gallium arsenide (for polarization modulators) and other materials are also attractive to implement special microwave photonic functions [7]. Packaging of these devices may significantly reduce the SWaP of the microwave photonic radars as compared to those based on discrete components, and enable high performance as compared to the monolithically integrated ones.

As the essential components in microwave photonic systems, EO and OE conversion devices provide the performance baseline for microwave photonic radars. Continuous efforts should be devoted to the improvement of them with respect to the conversion efficiency, noise figure, and linearity. Although some high-performance analog photonic links were reported, they are usually complicated, costly, unstable or work only in some specific scenarios. To compensate the loss introduced by the EO/OE conversion, low-noise optical amplifiers that bring as small intensity and phase noise as possible to the system are highly desired. It is worth mentioning that in some kinds of radar systems, pulse compression of broadband signals would bring considerable gain to the system, which may compensate for the dynamic range degradation due to the EO/OE conversion. Optical switch is another important device for microwave photonic radars. High speed, low insertion loss and high extinction ratio optical switches would introduce considerable design flexibility. The current optical switching techniques based on optical micro-electromechanical systems (MEMS), thermal-optic effects, acousto-optic effects, electro-optic effects, magneto-optic effects, liquid crystals and other effects seem to have tradeoff between the speed and extinction ratio, which could not well fulfill the requirement of large-scale OBFNs and reconfigurable or programmable radars.

The system-level investigation of the microwave photonic radar is still insufficient. For the microwave photonic radar based on the optoelectronic hybrid structure, one key issue is the compatibility of different microwave photonic subsystems. The photonic LO generation, waveform generation, mixing, filtering, beamforming, ADC, Fourier transform and interference cancellation are currently implemented based on different types of laser sources (i.e., CW, tunable, comb and pulsed laser sources), modulation schemes (i.e., phase modulation, intensity modulation, polarization modulation, and parallel or cascaded electrooptic modulation) and detection methods (i.e., direct detection, coherent detection, single-end or balanced detection). Some implementations require optical filtering, which may affect the realization of other microwave photonic functions. For the all-optical structure, increasing the instantaneous bandwidth is difficult since an MLL with a high repetition rate is needed while the MLL with a high repetition rate usually exhibits a large timing jitter. Direct generation of the radar waveform using the ultrashort pulse may breakthrough the bandwidth limit but the time duration is small and the quality is usually inferior due to the nonlinearity and high-order dispersion of the dispersive elements. Therefore, elegant microwave photonic radar architectures that could give full play to the advantages of photonics would be highly expected.

Another serious issue associated with the microwave photonic radars is the very scarce spectrum resource available under Ka and lower band, which could not support wideband radar detection. One way to deal with this problem is cognitive access with multi-band data fusion. Recently, we have proposed a cognitive microwave photonic radar [407], which can adaptively select the proper operation band for target detection according to the detected electromagnetic environmental information by a spectrum sensing module. A self-adaptive anti-jamming ISAR imaging is experimentally demonstrated in the presence of interference.

Acknowledgment

There are many impressive and vital works on microwave photonic technologies that are possibly applied for radar applications. However, due to the limited space, only a few are included in this tutorial.

The author would like to thank the following individuals from the Key Laboratory of Radar Imaging and Microwave Photonics, Nanjing University of Aeronautics and Astronautics, including but not limited to Xingwei Ye for contribution to Section III and section IV; Shifeng Liu for contribution to Section II and Section III; Hao Chen, Wenjuan Chen, Bowen Zhang, Huashan Yang, Pei Zhou for contribution to Section III; Bindong Gao, Jingzhan Shi, Cong Ma, Beichen Fan for contribution to Section IV; Zhaoyu Li, Ting Qing for contribution to Section II; and Simin Li for contribution to Section V.

References

[1] M. Skolnik, *Radar Handbook*, 3rd ed. USA: McGraw-Hill, 2008.
[2] J. Capmany and D. Novak, "Microwave photonics combines two worlds," *Nature Photon.*, vol. 1, no. 6, pp. 319–330, Jun. 2007.
[3] J. Yao, "Microwave photonics," *J. Lightw. Technol.*, vol. 27, no. 3, pp. 314–335, Feb. 2009.
[4] S. Pan, D. Zhu, and F. Zhang, "Microwave photonics for modern radar systems," *Trans. Nanjing Univ. Aeronaut. Astronaut.*, vol. 31, no. 3, pp. 219–240, Jun. 2014.
[5] A. Seeds and K. Williams, "Microwave photonics," *J. Lightw. Technol.*, vol. 24, no. 12, pp. 4628–4641, Dec. 2006.
[6] V. Urick, K. Williams, and J. McKinney, *Fundamentals of Microwave Photonics*. USA: John Wiley & Sons, 2015.
[7] A. Marpaung, C. Roeloffzen, R. Heideman, A. Leinse, S. Sales, and J. Capmany, "Integrated microwave photonics," *Laser Photon. Rev.*, vol. 7, no. 4, pp. 506–538, Jan. 2013.
[8] X. Yao and L. Maleki, "Optoelectronic oscillator for photonic systems," *IEEE J. Quantum Electron.*, vol. 32, no. 7, pp. 1141–1149, July 1996.
[9] J. Yao, "Arbitrary waveform generation," *Nature Photon.*, vol. 4, no. 2, pp. 79–80, Feb. 2010.
[10] Z. Tang, Y. Li, J. Yao, and S. Pan, "Photonics-based microwave frequency mixing: methodology and applications," *Laser Photon. Rev.*, vol. 14, no. 1, Jan. 2020.
[11] W. Ng, A. Walston, G. Tangonan, J. Lee, I. Newberg, and N. Bernstein, "The first demonstration of an optically steered microwave phased array antenna using true-time delay," *J. Lightw. Technol.*, vol. 9, no. 9, pp. 1124–1131, Sep. 1991.
[12] T. Jannson, "Real-time Fourier transformation in dispersive optical fibers," *Opt. Lett.*, vol. 8, no. 4, p. 232, Apr. 1983.
[13] G. Valley, "Photonic analog-to-digital converters," *Opt. Express*, vol. 15, no. 5, pp. 1955–1982, Mar. 2007.

[14] H. Heckscher and J. Rossi, “Flashlight-size external cavity semiconductor laser with narrow-linewidth tunable output,” *Appl. Opt.*, vol. 14, no. 1, pp. 94–96, Jan. 1975.

[15] Z. Zhao, J. Liu, Y. Liu, and N. Zhu, “High-speed photodetectors in optical communication system,” *J. Semicond.*, vol. 38, no. 12, pp. 121001-1–121001-7, Dec. 2017.

[16] K. Ho, J. Walker, and J. Kahn, “External optical feedback effects on intensity noise of vertical-cavity surface-emitting lasers,” *IEEE Photon. Technol. Lett.*, vol. 5, no. 8, pp. 892–895, Aug. 1993.

[17] *Ultra Low-Relative Intensity Noise Analog DFB Laser Module*, APIC Corp., USA [Online]. Available: http://www.cybel-llc.com/wp-content/uploads/2018/10/Ultra-Low-RIN-Analog-DFB-Laser-CWL-series-Ver-1-30-Aug-2018.pdf. Accessed on: Feb. 2020.

[18] D. G. Matei *et al.*, “1.5um Lasers with Sub-10 mHz Linewidth,” *Phys. Rev. Lett.*, vol. 118, pp. 263202-1–263202-6, Jun. 2017.

[19] R. Mears, L. Reekie, S. Poole, and D. Payne, “Neodymium-doped silica single-mode fibre lasers,” *Electron. Lett.*, vol. 21, no. 17, pp. 738–740, Aug. 1985.

[20] M. Gorjan, M. Marinček, and M. Čopič, “High-power pulsed diode-pumped Er: ZBLAN fiber laser,” *Opt. Lett.*, vol. 36, no. 10, pp. 1923–1925, Mar. 2011.

[21] D. Hall, A. Yariv, and E. Garmire, “Optical guiding and electro-optic modulation in GaAs epitaxial layers,” *Opt. Commun.*, vol. 1, no. 9, pp. 403–405, Apr. 1970.

[22] Y. Shi, C. Zhang, H. Zhang, J. H. Bechtel, L. R. Dalton, B. H. Robinson, and W. H. Steier, “Low (sub-1-volt) halfwave voltage polymeric electro-optic modulators achieved by controlling chromophore shape,” *Science*, vol. 288, no. 5463, pp. 119–122, Apr. 2000.

[23] F. Chen, “Modulators for optical communications,” *Proc. IEEE*, vol. 58, no. 10, pp. 1440–1457, Oct. 1970.

[24] A. Mercante, S. Shi, P. Yao, L. Xie, R. Weikle, and D. W. Prather, “Thin film lithium niobate electro-optic modulator with terahertz operating bandwidth,” *Opt. Express*, vol. 26, no. 11, pp. 14810–14816, May 2018.

[25] H. Ito, T. Furuta, Y. Muramoto, T. Ito, and T. Ishibashi, “Photonic millimetre-and sub-millimetre-wave generation using J-band rectangular-waveguide-output uni-travelling-carrier photodiode module,” *Electron. Lett.*, vol. 42, no. 24, pp. 1424–1425, Nov. 2006.

[26] J. Shi, Y. Wu, C. Wu, P. Chiu, and C. Hong, “High-speed, high-responsivity, and high-power performance of near-ballistic uni-traveling-carrier photodiode at 1.55-μm wavelength,” *IEEE Photon. Technol. Lett.*, vol. 17, no. 9, pp. 1929–1931, Aug. 2005.

[27] J. Klamkin *et al.*, “High output saturation and high-linearity uni-traveling-carrier waveguide photodiodes,” *IEEE Photon. Technol. Lett.*, vol. 19, no. 3, pp. 149–151, Mar. 2007.

[28] H. Oohashi *et al.*, “46.9-nm wavelength-selectable arrayed DFB lasers with integrated MMI coupler and SOA,” in *2001 Int. Conf. Indium Phosphide and Related Materials (13th IPRM)*, Nara, Japan, 2001, pp. 575–578.

[29] S. Park *et al.*, “16-arrayed electrooptic polymer modulator,” *IEEE Photon. Technol. Lett.*, vol. 16, no. 8, pp. 1834–1836, July 2004.

[30] L. Chen, C. Doerr, L. Buhl, Y. Baeyens, and R. Aroca, “Monolithically integrated 40-wavelength demultiplexer and photodetector array on silicon,” *IEEE Photon. Technol. Lett.*, vol. 23, no. 13, pp. 869–871, Apr. 2011.

[31] E. Ackerman *et al.*, “Signal-to-noise performance of two analog photonic links using different noise reduction techniques,” in *2007 IEEE/MTT-S Int. Microwave Symp. (IMS)*, Honolulu, USA, 2007, pp. 51–54.

[32] F. Zhang, Q. Guo, and S. Pan, “Photonics-based real-time ultra-high-range-resolution radar with broadband signal generation and processing,” *Sci. Rep.*, vol. 7, no. 1, pp. 1–8, Oct. 2017.

[33] T. Perry, “In search of the future of air traffic control,” *IEEE Spectrum*, vol. 34, no. 8, pp. 18–35, Aug. 1997.

[34] K. L. Koester and W. Vaillancourt, “TALONS 95 GHz radar sensor for autonomous landing guidance,” *IEEE Aerosp. Electron. Syst. Mag.*, vol. 7, no. 7, pp. 40–44, July 1992.

[35] G. H. Pettengill and I. I. Shapiro, “Radar astronomy,” *Ann. Rev. Astron. Astrophys.*, vol. 3, no. 1, pp. 377–411, Jan. 1965.

[36] C. Elachi, “Space imaging radar in planetary exploration and earth observation,” *AIAA J.*, vol. 39, no. 4, pp. 553–563, Apr. 2001.

[37] L. Andreone, F. Tango, U. Scheunert, H. Cramer, G. Wanielik, and A. Amditis, “A new driving supporting system, integrating an infrared camera and an anti-collision micro-wave radar: the EUCLIDE project,” in *Intell. Vehicle Symp., 2002. IEEE*, Versailles, France, 2002, vol. 2, pp. 519–526.

[38] N. Bobrinsky and L. Del Monte, “The space situational awareness program of the European Space Agency,” *Cosmic Res.*, vol. 48, no. 5, Oct. 2010.

[39] P. Kollias, E. Clothiaux, M. Miller, B. Albrecht, G. Stephens, and T. Ackerman, “Millimeter-wavelength radars: New frontier in atmospheric cloud and precipitation research,” *Bull. Amer. Meteorol. Soc.*, vol. 88, no. 10, pp. 1608–1624, Oct. 2007.

[40] J. Crétaux and C. Birkett, “Lake studies from satellite radar altimetry,” *Comp. Rendus Geosci.*, vol. 338, no. 14–15, pp. 1098–1112, Nov. 2006.

[41] L. Conyers and D. Goodman, *Ground-Penetrating Radar: An Introduction for Archaeologist*. USA: AltaMira Press, 1997, pp. 131–159.

[42] M. Davis, “A history of battlefield surveillance radar,” in *2015 IEEE Radar Conf. (RadarCon)*, Arlington, USA, 2015, pp. 1345–1350.

[43] S. Blackman, *Multiple-Target Tracking with Radar Applications*. Dedham, 1986, pp. 463.

[44] A. Madni, P. McDonald, R. Hansen, and L. Wan, “High-dynamic-range airborne tracking and fire control radar subsystem,” *IEEE Trans. Microw. Theory Technol.*, vol. 37, no. 12, pp. 1942–1948, Dec. 1989.

[45] J. Levinson *et al.*, “Towards fully autonomous driving: systems and algorithms,” in *2011 IEEE Intell. Vehicles Symp. (IV)*, Baden, Germany, 2011, pp. 163–168.

[46] B. Skinner, J. Donohoe, and F. Ingels, “Simplified performance estimation of FSK/PSK hybrid signaling radar systems,” in *Proc. IEEE 1993 National Aerospace and Electronics Conf.-NAECON 1993*, Dayton, USA, 1993, vol. 1, pp. 255–261.

[47] H. Harmuth, “Frequency-sharing and spread-spectrum transmission with large relative bandwidth,” *IEEE Trans. Electromagn. Compat.*, no. 1, pp. 232–239, Feb. 1978.

[48] *ALL-Wave Optical Fiber-Zero Water Peak*, OFS Corp., USA [Online]. Available: https://www.ofsoptics.com/wp-content/uploads/AllWave-117-web-7.pdf. Accessed on: Feb. 2020.

[49] *Corning SMF-28 Ultra Optical Fiber*, Corning, USA [Online]. Available: https://www.corning.com/media/worldwide/coc/documents/Fiber/SMF-28%20Ultra.pdf. Accessed on: Feb. 2020.

[50] T. Kato, Y. Koyano, and M. Nishimura, “Temperature dependence of chromatic dispersion in various types of optical fiber,” *Opt. Lett.*, vol. 25, no. 16, pp. 1156–1158, Aug. 2000.

[51] K. Y. Lau and G. F. Lutes, “Planetary radar imaging and RF-over-fiber,” *Opt. Photon. News*, vol. 25, pp. 44–51, 2014.

[52] G. Grosche *et al.*, “Optical frequency transfer via 146 km fiber link with 10^{-19} relative accuracy,” *Opt. Lett.*, vol. 34, no. 15, pp. 2270–2272, Aug. 2009.

[53] B. Wang *et al.*, “Precise and continuous time and frequency synchronisation at the 5×10^{-19} accuracy level,” *Sci. Rep.*, vol. 2, p. 556, Aug. 2012.

[54] S. Droste *et al.*, “Optical-frequency transfer over a single-span 1840 km fiber link,” *Phys. Rev. Lett.*, vol. 111, no. 11, p. 110801, Sept. 2013.

[55] K. Y. Lau, G. F. Lutes, and R. L. Tjoelker, “Ultra-stable RF-over-fiber transport in NASA antennas, phased arrays and radars,” *J. Lightw. Technol.*, vol. 32, no. 20, pp. 3440–3451, Oct. 2014.

[56] T. Farr *et al.*, “The shuttle radar topography mission,” *Rev. Geophys.*, vol. 45, no. 2, pp. RG2004, Jun. 2007.

[57] X. Wang *et al.*, “High-accuracy optical time delay measurement in fiber link [Invited],” *Chin. Opt. Lett.*, vol. 17, no. 6, Jun. 2019.

[58] S. Li *et al.*, “Optical fiber transfer delay measurement based on phase-derived ranging,” *IEEE Photon. Technol. Lett.*, vol. 31, no. 16, pp. 1351–1354, Aug. 2019.

[59] K. Hill and G. Meltz, “Fiber Bragg grating technology fundamentals and overview,” *J. Lightw. Technol.*, vol. 15, no. 8, pp. 1263–1276, Aug. 1997.

[60] W. Gruener, J. Toernig, and P. Fielding, “Active-electronically-scanned-array based radar system features,” in *Radar 97 (Conf. Publ. No. 449)*, Edinburgh, UK, 1997, pp. 339–343.

[61] E. Cohen, “Trends in the development of MMICs and packages for active electronically scanned arrays (AESAs),” in *Proc. Int. Symp. Phased Array Systems and Technology*, Boston, USA, 1996, pp. 1–4.

[62] D. Bliss and K. Forsythe, “Multiple-input multiple-output (MIMO) radar and imaging: degrees of freedom and resolution,” in *The Thirty-Seventh Asilomar Conf. Signals, Systems & Computers, 2003*, Pacific Grove, USA, 2003, vol. 1. pp. 54–59.

[63] K. Forsythe, D. Bliss, and G. Fawcett, “Multiple-input multiple-output (MIMO) radar: performance issues,” in *Conf. Record of the Thirty-Eighth Asilomar Conf. on Systems, Signals and Computers, 2004*, Pacific Grove, USA, 2004, vol. 1, pp. 310–315.

[64] N. Kees, E. Schmidhammer, and J. Detlefsen, "Improvement of angular resolution of a millimeterwave imaging system by transmitter location multiplexing," in *IEEE NTC, Conf. Proc. Microwave Systems Conf.*, Orlando, USA, 1995, pp. 105–108.
[65] A. Zwanetski and H. Rohling, "Continuous wave MIMO radar based on time division multiplexing," in *2012 13th Int. Radar Symp.*, Warsaw, Poland, 2012, pp. 119–121.
[66] K. Rambach and B. Yang, "MIMO radar: time division multiplexing vs. code division multiplexing," in *Int. Conf. Radar Systems (Radar 2017)*, Belfast, UK, 2017, pp. 1–5.
[67] M. Sebt, A. Sheikhi, and M. Nayebi, "Orthogonal frequency-division multiplexing radar signal design with optimised ambiguity function and low peak-to-average power ratio," *IET Radar Sonar Navig*., vol. 3, no. 2, pp. 122–132, Apr. 2009.
[68] D. Bleh *et al.*, "W-band time-domain multiplexing FMCW MIMO radar for far-field 3-D imaging," *IEEE Trans. Microw. Theory Technol.*, vol. 65, no. 9, pp. 3474–3484, Sept. 2017.
[69] T. Yao, D. Zhu, D. Ben, and S. Pan, "Distributed MIMO chaotic radar based on wavelength-division multiplexing technology," *Opt. Lett.*, vol. 40, no. 8, pp. 1631–1634, Apr. 2015.
[70] S. Park, C. Lee, K. Jeong, H. Park, J. Ahn, and K. Song, "Fiber-to-the-home services based on wavelength-division-multiplexing passive optical network," *J. Lightw. Technol.*, vol. 22, no. 11, pp. 2582–2591, Nov. 2004.
[71] M. Burla *et al.*, "Multiwavelength-integrated optical beamformer based on wavelength division multiplexing for 2-D phased array antennas," *J. Lightw. Technol.*, vol. 32, no. 20, pp. 3509–3520, Oct. 2014.
[72] P. Mamyshev and L. Mollenauer, "Pseudo-phase-matched four-wave mixing in soliton wavelength-division multiplexing transmission," *Opt. Lett.*, vol. 21, no. 6, pp. 396–398, Mar. 1996.
[73] T. Kuri, H. Toda, J. Olmos, and K. Kitayama, "Reconfigurable dense wavelength-division-multiplexing millimeter-waveband radio-over-fiber access system technologies," *J. Lightw. Technol.*, vol. 28, no. 16, pp. 2247–2257, Aug. 2010.
[74] J. Capmany, B. Ortega, and D. Pastor, "A tutorial on microwave photonic filters," *J. Lightw. Technol.*, vol. 24, no. 1, pp. 201–229, Jan. 2006.
[75] C. Deng, J. Suo, Y. Wang, Z. Zhang, and Q. Dai, "Single-shot thermal ghost imaging using wavelength-division multiplexing," *Appl. Phys. Lett.*, vol. 112, no. 5, Jan. 2018.
[76] S. Evangelides, L. Mollenauer, J. Gordon, and N. Bergano, "Polarization multiplexing with solitons," *J. Lightw. Technol.*, vol. 10, no. 1, pp. 28–35, Jan. 1992.
[77] D. Qian, N. Cvijetic, J. Hu, and T. Wang, "108 Gb/s OFDMA-PON with polarization multiplexing and direct detection," *J. Lightw. Technol.*, vol. 28, no. 4, pp. 484–493, Feb. 2010.
[78] Y. Zhang and S. Pan, "Broadband microwave signal processing enabled by polarization-based photonic microwave phase shifters," *IEEE J. Quantum Electron.*, vol. 54, no. 4, pp. 0700112, Aug. 2018.
[79] Z. Tang and S. Pan, "A full-duplex radio-over-fiber link based on a dual-polarization Mach-Zehnder modulator," *IEEE Photon. Technol. Lett.*, vol. 28, no. 8, pp. 852–855, Apr. 2016.
[80] M. Huang, D. Zhu, and S. Pan, "Optical RF interference cancellation based on a dual-parallel polarization modulator," in *Asia Communications and Photonics Conf. 2014*, Nov. 2014, p. ATh1F.6.
[81] S. Liu, D. Zhu, Z. Wei, and S. Pan, "Photonic generation of widely tunable phase-coded microwave signals based on a dual-parallel polarization modulator," *Opt. Lett.*, vol. 39, no. 13, pp. 3958–3961, Jul. 2014.
[82] J. Yu, X. Li, J. Zhang, and J. Xiao, "432-Gb/s PDM-16QAM signal wireless delivery at W-band using optical and antenna polarization multiplexing," in *2014 The Eur. Conf. Optical Communication (ECOC)*, Cannes, France, 2014, pp. 1–3.
[83] Y. Deng, A. Burr, and G. White, "Performance of MIMO systems with combined polarization multiplexing and transmit diversity," in *2005 IEEE 61st Vehicular Technology Conf.*, Stockholm, Sweden, 2005, vol. 2, pp. 869–873.
[84] K. Kikuchi, "Performance analyses of polarization demultiplexing based on constant-modulus algorithm in digital coherent optical receivers," *Opt. Express*, vol. 19, no. 10, pp. 9868–9880, May 2011.
[85] P. Marchal *et al.* "Spatial division multiplexing: a novel approach for guaranteed throughput on NoCs," in *2005 Third IEEE/ACM/IFIP Int. Conf. Hardware/Software Codesign and System Synthesis (CODES+ISSS)*, Jersey City, USA, 2005, pp. 81–86.
[86] D. Richardson, J. Fini, and L. Nelson, "Space-division multiplexing in optical fibres," *Nature Photon*., vol. 7, no. 5, pp. 354–362, Apr. 2013.
[87] Y. Awaji, N. Wada, Y. Toda, and T. Hayashi, "World first mode/spatial division multiplexing in multi-core fiber using Laguerre-Gaussian mode," in *2011 37th Eur. Conf. Optical Communication (ECOC)*, Geneva, Switzerland, 2011, pp. We.10.P1.55.
[88] T. Morioka, "New generation optical infrastructure technologies: "EXAT initiative" towards 2020 and beyond," in *2009 14th OptoElectronics and Communications Conf. (OECC)*, Vienna, Austria, 2009, pp. 1–2.
[89] Y. Sasaki *et al.*, "Few-mode multicore fibers for long-haul transmission line," *Opt. Fiber Technol.*, vol. 35, pp. 19–27, Feb. 2017.
[90] R. Uden *et al.*, "Ultra-high-density spatial division multiplexing with a few-mode multicore fibre," *Nature Photon*., vol. 8, no. 11, pp. 865, Oct. 2014.
[91] G. Wang *et al.*, "Ultrafast optical imaging using multimode fiber based compressed sensing and photonic time stretch," 2018, arXiv preprint, *arXiv:1803.03061*.
[92] H. Wen *et al.*, "Few-mode fibre-optic microwave photonic links," *Light Sci. Appl.*, vol. 6, no. 8, pp. e17021–e17021, Feb. 2017.
[93] K. Saitoh and S. Matsuo, "Multicore fiber technology," *J. Lightw Technol.*, vol. 34, no. 1, pp. 55–66, Jan. 2016.
[94] W. Zhang *et al.*, "Mode division multiplexing communication using microwave orbital angular momentum: An experimental study," *IEEE Trans. Wireless Commun.*, vol. 16, no. 2, pp. 1308–1318, Feb. 2017.
[95] N. Bozinovic *et al.*, "Terabit-scale orbital angular momentum mode division multiplexing in fibers," *Science*, vol. 340, no. 6140, pp. 1545–1548, Jun. 2013.
[96] M. Koshiba, K. Saitoh, and Y. Kokubun, "Heterogeneous multi-core fibers: proposal and design principle," *IEICE Electron. Express*, vol. 6, no. 2, pp. 98–103, Jan. 2009.
[97] T. Birks, I. Gris-Sánchez, S. Yerolatsitis, S. Leon-Saval, and R. Thomson, "The photonic lantern," *Adv. Opt. Photon.*, vol. 7, pp. 107–167, 2015.
[98] D. Noordegraaf, P. Skovgaard, M. Nielsen, and J. Hawthorn, "Efficient multi-mode to single-mode coupling in a photonic lantern," *Opt. Express*, vol. 17, no. 3, pp. 1988–1994, Feb. 2009.
[99] I. Gasulla *et al.*, "Spatial division multiplexed microwave signal processing by selective grating inscription in homogeneous multicore fibers," *Sci. Rep.*, vol. 7, no. 1, pp. 1–10, Jan. 2017.
[100] I. Gasulla and J. Capmany, "Microwave photonics applications of multicore fibers," *IEEE Photon. J.*, vol. 4, no. 3, pp. 877–888, Jun. 2012.
[101] X. Zou *et al.*, "Microwave photonics for featured applications in high-speed railways: communications, detection, and sensing," *J. Lightw. Technol.*, vol.36, no. 19, pp. 4337–4346, Oct. 2018.
[102] I. Gasulla, D. Barrera, and S. Sales, "Microwave photonic devices based on multicore fibers," in *2014 16th Int. Conf. Transparent Optical Networks (ICTON)*, Graz, Austria, 2014, pp. 1–4.
[103] Y. Zhao *et al.*, "Super-channel oriented routing, spectrum and core assignment under crosstalk limit in spatial division multiplexing elastic optical networks," *Opt. Fiber Technol.*, vol. 36, pp. 249–254, Jul. 2017.
[104] C. Caloz, S. Gupta, Q. Zhang, and B. Nikfal, "Analog signal processing: A possible alternative or complement to dominantly digital radio schemes," *IEEE Microw. Mag.*, vol. 14, no. 6, pp. 87–103, Jun. 2013.
[105] R. Yarlagadda, *Analog and Digital Signals and Systems*. USA: Springer, 2010.
[106] E. Palushani *et al.*, "OTDM-to-WDM conversion based on time-to-frequency mapping by time-domain optical Fourier transformation," *IEEE J. Sel. Topics Quantum Electron.*, vol. 18, no. 2, pp. 681–688, Mar. 2012.
[107] J. Azana, N. Berger, B. Levit, and B. Fischer, "Spectra-temporal imaging of optical pulses with a single time lens," *IEEE Photon. Technol. Lett.*, vol. 16, no. 3, pp. 882–884, Mar. 2004.
[108] Y. Dai, J. Li, Z. Zhang, F. Yin, W. Li, and K. Xu, "Real-time frequency-to-time mapping based on spectrally-discrete chromatic dispersion," *Opt. Express*, vol. 25, no. 14, pp. 16660–16671, May 2017.
[109] X. Xu *et al.*, "Photonic RF phase-encoded signal generation with a microcomb source," *J. Lightw. Technol.*, early access, 2019.
[110] P. Xiang, X. Zheng, H. Zhang, Y. Li, and Y. Chen, "A novel approach to photonic generation of RF binary digital modulation signals," *Opt. Express*, vol. 21, no. 1, pp. 631–639, Jan. 2013.
[111] Y. Han and B. Jalali, "Photonic time-stretched analog-to-digital converter: Fundamental concepts and practical considerations," *J. Lightw. Technol.*, vol. 21, no. 12, pp. 3085–3103, Dec. 2003.
[112] T. Nagashima, M. Hasegawa, and T. Konishi, "40 GSample/s all-optical analog to digital conversion with resolution degradation prevention," *IEEE Photon. Technol. Lett.*, vol. 29, no. 1, pp. 74–77, Jan. 2017.

[113] W. Hao *et al.*, "Frequency-oriented subsampling by photonic Fourier transform and I/Q demodulation," *IEEE Photon. J.*, vol. 9, no. 6, pp. 5503508, Dec. 2017.

[114] V. Supradeepa *et al.*, "Comb-based radiofrequency photonic filters with rapid tunability and high selectivity," *Nature Photon*., vol. 6, no. 3, pp. 186–194, Mar 2012.

[115] X. Xu *et al.*, "Reconfigurable microwave photonic transversal filter based on an integrated optical micro-comb source," in *Integrated Optics: Devices, Materials, and Technologies XXIII*, San Francisco, USA, 2019, vol. 10921, pp. 1092104.

[116] X. Zhu, F. Chen, H. Peng, and Z. Chen, "Novel programmable microwave photonic filter with arbitrary filtering shape and linear phase," *Opt. Express*, vol. 25, no. 8, pp. 9232–9243, Apr. 2017.

[117] Z. Wang, B. Wang, D. Zhao, and R. Wang, "Full analog broadband time-reversal module for ultra-wideband communication system," *IEEE Photon. Technol. Lett.*, vol. 11, no. 5, pp. 1–10, Oct. 2019.

[118] M. Cornet, J. Degert, E. Abraham, and E. Freysz, "Frequency resolved cross-correlation between optical and terahertz pulses: application to ultrashort laser pulse characterization," *Opt. Express*, vol. 24, no. 3, pp. 3003–3010, Feb. 2016.

[119] K. Goda, K. Tsia, and B. Jalali, "Amplified dispersive fourier-transform imaging for ultrafast displacement sensing and barcode reading," *Appl. Phys. Lett.*, vol. 93, no. 13, pp. 131109-1–131109-3, Sept. 2008.

[120] K. Goda, K. Tsia, and B. Jalali, "Serial time-encoded amplified imaging for real-time observation of fast dynamic phenomena," *Nature*, vol. 458, pp. 1145–1150, Apr. 2009.

[121] J. Zhao, Y. E, K. Williams, X. Zhang, and R. W. Boyd, "Spatial sampling of terahertz fields with sub-wavelength accuracy via probe-beam encoding," *Light Sci. Appl.*, vol. 8, pp. 55, Jun. 2019.

[122] Y. Huang, W. Zhang, F. Yang, J. Du, and Z. He, "Programmable matrix operation with reconfigurable time-wavelength plane manipulation and dispersed time delay," *Opt. Express*, vol. 27, no. 15, pp. 20456–20467, Jul. 2019.

[123] N. Janosik, C. Qixiang, M. Glick, H. Yishen, and K. Bergman, "High-resolution silicon microring based architecture for optical matrix multiplication," in *2019 Conf. Lasers and Electro-Optics (CLEO)*, San Jose, USA, 2019, pp. SM2J.3.

[124] M. Pagani, D. Marpaung, D. Choi, S. Madden, B. Davies, and B. Eggleton, "Tunable wideband microwave photonic phase shifter using on-chip stimulated Brillouin scattering," *Opt. Express*, vol. 22, no. 23, pp. 28810–28818, Nov. 2014.

[125] S. Pan and Y. Zhang, "Tunable and wideband microwave photonic phase shifter based on a single-sideband polarization modulator and a polarizer," *Opt. Lett.*, vol. 37, no. 21, pp. 4483–4485, Nov. 2012.

[126] M. Lei, Z. Zheng, J. Qian, M. Xie, X. Gao, and S. Huang, "Photonics-assisted super-octave microwave phase shifter," *IEEE Photon. J.*, vol. 11, no. 1, pp. 1–11, Feb. 2019.

[127] F. Yang *et al.*, "A microwave photonic phase-tunable mixer with local oscillator frequency doubling," *Opt. Commun.*, vol. 438, pp. 141–146, May 2019.

[128] Y. Zhang and S. Pan, "Generation of phase-coded microwave signals using a polarization-modulator-based photonic microwave phase shifter," *Opt. Lett.*, vol. 38, no. 5, pp. 766–768, Mar. 2013.

[129] Z. Li, M. Li, H. Chi, X. Zhang, and J. P. Yao, "Photonic generation of phase-coded millimeter-wave signal with large frequency tunability using a polarization-maintaining fiber Bragg grating," *IEEE Microw. Wireless Compon. Lett.*, vol. 21, no. 12, pp. 694–696, Dec. 2011.

[130] J. Yan, L. Li, X. Yi, and S. Chew, "Widely tunable single band-pass microwave photonic filter based on dual-fiber stimulated Brillouin scattering," *Microw. Opt. Technol. Lett.*, vol. 61, no. 4, pp. 954–958, Apr 2019.

[131] N. Shi, T. Hao, W. Li, N. Zhu, and M. Li, "A reconfigurable microwave photonic filter with flexible tunability using a multi-wavelength laser and a multi-channel phase-shifted fiber Bragg grating," *Opt. Commun.*, vol. 407, pp. 27–32, Jun. 2018.

[132] Y. Zhang and S. Pan, "An electrically-tunable microwave photonic filter based on polarization modulation," in *2014 IEEE MTT-S Int. Microwave Symp. (IMS)*, Tampa, USA, 2014, pp. 1–3.

[133] H. Chatellus, L. Cortés, and J. Azaña, "Optical real-time Fourier transformation with kilohertz resolutions," *Optica*, vol. 3, no. 1, pp. 1–8, Jan. 2016.

[134] C. Schnebelin and H. Chatellus, "Agile photonic fractional Fourier transformation of optical and RF signals," *Optica*, vol. 4, no. 8, pp. 907–910, Aug. 2017.

[135] Y. Zhang and S. Pan, "Experimental demonstration of frequency-octupled millimeter-wave signal generation based on a dual-parallel Mach-Zehnder modulator," in *2012 IEEE MTT-S Int. Microwave Workshop Series on Millimeter Wave Wireless Technology and Applications*, Nanjing, China, 2012, pp. 1–4.

[136] Z. Zhu, S. Zhao, X. Chu, and Y. Dong, "Optical generation of millimeter-wave signals via frequency 16-tupling without an optical filter," *Opt. Commun.*, vol. 354, pp. 40–47, Nov. 2015.

[137] Y. Gao *et al.*, "Microwave generation with photonic frequency sextupling based on cascaded modulators," *IEEE Photon. Technol. Lett.*, vol. 26, no. 12, pp. 1199–1202, Jun. 2014.

[138] G. Picardi, S. Sorge, R. Seu, G. Fedele, and R. Jordan, "Coherent cancellation of surface clutter for radar sounding," in *IEEE 1999 Int. Geoscience and Remote Sensing Symp. (IGARSS)*, Hamburg, Germany, 1999, vol. 5, pp. 2678–2680.

[139] X. Guo, H. Sun, and T. Yeo, "Interference cancellation for high-frequency surface wave radar," *IEEE Trans. Geosci. Remote Sens.*, vol. 46, no. 7, pp. 1879–1891, Jul. 2008.

[140] A. Singh and V. Lubecke, "Adaptive noise cancellation for two frequency radar using frequency doubling passive RF tags," *IEEE Trans. Microw. Theory Techn.*, vol. 61, no. 8, pp. 2975–2981, Aug. 2013.

[141] D. Zhu, J. Chen, and S. Pan, "Multi-octave linearized analog photonic link based on a polarization-multiplexing dual-parallel Mach-Zehnder modulator," *Opt. Express*, vol. 24, no. 10, May 2016.

[142] M. Huang, J. Fu, and S. Pan, "Linearized analog photonic links based on a dual-parallel polarization modulator," *Opt. Lett.*, vol. 37, no. 11, pp. 1823–1825, Jun. 2012.

[143] F. Wang, S. Shi, and D. Prather, "Microwave photonic link with improved SFDR using two parallel MZMs and a polarization beam combiner," *J. Lightw. Technol.*, vol. 37, no. 24, pp. 6156–6164, Dec. 2019.

[144] Y. Cui *et al.*, "Intermodulation distortion suppression for intensity-modulated analog fiber-optic link incorporating optical carrier band processing," *Opt. Express*, vol. 21, no. 20, pp. 23433–23440, Oct. 2013.

[145] P. Li *et al.*, "Improvement of linearity in phase-modulated analog photonic link," *Opt. Lett.*, vol. 38, no. 14, pp. 2391–2393, Jul. 2013.

[146] D. Zhu, W. Chen, and S. Pan, "Photonics-enabled balanced Hartley architecture for broadband image-reject microwave mixing," *Opt. Express*, vol. 26, no. 21, pp. 28022–28029, Oct. 2018.

[147] Z. Meng *et al.*, "Dual-band dechirping LFMCW radar receiver with high image rejection using microwave photonic I/Q," *Opt. Express*, vol. 25, no. 18, pp. 22055–22065, Sept. 2017.

[148] Z. Shi, S. Zhu, M. Li, N. Zhu, and W. Li, "Reconfigurable microwave photonic mixer based on dual-polarization dual-parallel Mach-Zehnder modulator," *Opt. Commun.*, vol. 428, pp. 131–135, Dec. 2018.

[149] Z. Tu, A. Wen, W. Zhang, Z. Xiu, and G. Yu, "All-optical image-reject frequency down-conversion based on cascaded electro-optical modulators," *Opt. Commun.*, vol. 430, pp. 158–162, Jan. 2019.

[150] C. Xie, D. Zhu, W. Chen and S. Pan, "Microwave photonic channelizer based on polarization multiplexing and photonic dual output image reject mixer," *IEEE Access*, vol. 7, pp. 158308–158316, Oct. 2019.

[151] Y. Gao, A. Wen, W. Chen, and X. Li, "All-optical, ultra-wideband microwave I/Q mixer and image-reject frequency down-converter," *Opt. Lett.*, vol. 42, no. 6, pp. 1105–1108, Mar. 2017.

[152] T. Li, H. Chan, X. Wang, X. Feng, B. Guan, and J. Yao, "Broadband photonic microwave signal processor with frequency up/down conversion and phase shifting capability," *IEEE Photon. J.*, vol. 9, no. 6, Dec. 2017.

[153] K. Kolodziej, S. Yegnanarayanan, and B. Perry, "Photonic-enabled RF canceller for wideband in-band full-duplex wireless systems," *IEEE Trans. Microw. Theory Technol.*, vol. 67, no. 5, pp. 2076–2086, May 2019.

[154] M. Chang, C. Lee, B. Wu, and P. Prucnal, "Adaptive Optical Self-Interference Cancellation Using a Semiconductor Optical Amplifier," *IEEE Photon. Technol. Lett.*, vol. 27, no. 9, pp. 1018–1021, May 2015.

[155] G. Li, Y. Xiang, and S. Pan, "Wideband optical cancellation of RF interference with phase change," in *2017 16th Int. Conf. Optical Communications and Networks (ICOCN)*, Wuzhen, China, 2017, pp. 1–3.

[156] Y. Xiang, G. Li, and S. Pan, "Ultrawideband optical cancellation of RF interference with phase change." *Opt. Express*, vol. 25, no. 18, pp. 21259–21264, Sept. 2017.

[157] V. Urick, J. Diehl, and J. Mckinney, "Nonlinear optical angle modulation for suppression of RF interference." *IEEE Trans. Microw. Theory Technol.*, vol. 64, no. 7, pp. 1–7, Jul. 2016.

[158] J. Suarez, K. Kravtsov, and P. Prucnal, "Incoherent method of optical interference cancellation for radio-frequency communications," *IEEE J. Quantum Electron.*, vol. 45, no. 4, pp. 402–408, Apr. 2009.

[159] W. Zhou, P. Xiang, Z. Niu, M. Wang, and S. Pan, "Wideband optical multipath interference cancellation based on a dispersive element," *IEEE Photon. Technol. Lett.*, vol. 28, no. 8, pp. 849–851, Apr. 2016.

[160] Q. Guo, F. Zhang, P. Zhou, and S. Pan, "Dual-band LFM signal generation by optical frequency quadrupling and polarization multiplexing," *IEEE Photon. Technol. Lett.*, vol. 29, no. 16, pp. 1320–1323, Aug. 2017.

[161] Y. Zhang, F. Zhang, and S. Pan, "Generation of frequency-multiplied and phase-coded signal using an optical polarization division multiplexing modulator," *IEEE Trans. Microw. Theory Technol.*, vol. 65, no. 2, pp. 651–660, Feb. 2017.

[162] W. Li and J. Yao, "Investigation of photonically assisted microwave frequency multiplication based on external modulation," *IEEE Trans. Microw. Theory Technol.*, vol. 58, no. 11, pp. 3259–3268, Nov. 2010.

[163] K. Kolodziej, B. Perry, and J. McMichael, "Multitap RF canceller for in-band full-duplex wireless communications," *IEEE Trans. Wireless Commun.*, vol. 15, no. 6, pp. 4321–4334, Jun. 2016.

[164] C. Albert, C. Huang, and E. Chan, "Intensity noise suppression using dual-polarization dual-parallel modulator and balanced detector," *IEEE Photon. J.*, vol. 10, no. 2, Apr. 2018.

[165] J. Kim and Y. Song, "Ultralow-noise mode-locked fiber lasers and frequency combs: principles, status, and applications," *Adv. Opt. Photon.*, vol. 8, no. 3, pp. 465–540, Sept. 2016.

[166] X. Xie *et al.*, "Photonic microwave signals with zeptosecond-level absolute timing noise," *Nature Photon*., vol. 11, no. 1, pp. 44–47, Jan. 2017.

[167] T. Fortier *et al.*, "Generation of ultrastable microwaves via optical frequency division," *Nature Photon*., vol. 5, no. 7, pp. 425–429, Jul. 2011.

[168] A. Khilo *et al.*, "Photonic ADC: overcoming the bottleneck of electronic jitter," *Opt. Express*, vol. 20, no. 4, pp. 4454–4469, Feb. 2012.

[169] J. Chou, O. Boyraz, D. Solli, and B. Jalali, "Femtosecond real-time single-shot digitizer," *Appl. Phys. Lett.*, vol. 91, no. 16, p. 161105, Oct. 2007.

[170] K. Goda and B. Jalali, "Dispersive Fourier transformation for fast continuous single-shot measurements," *Nature Photon*., vol. 7, no. 2, pp. 102–112, Feb. 2013.

[171] K. Goda *et al.*, "Hybrid dispersion laser scanner," *Sci. Rep.*, vol. 2, Jun. 2012.

[172] C. Jeon, Y. Na, B. Lee, and J. Kim, "Simple-structured, subfemtosecond-resolution optical-microwave phase detector," *Opt. Lett.*, vol. 43, no. 16, pp. 3997–4000, Aug. 2018.

[173] M. Peng, A. Kalaydzhyan, and F. Kartner, "Balanced optical-microwave phase detector for sub-femtosecond optical-RF synchronization," *Opt. Express*, vol. 22, no. 22, pp. 27102–27111, Nov. 2014.

[174] J. Wei, S. Zhang, J. Kim, and S. Pan, "Compact phase detector for optical-microwave synchronization using polarization modulation," *J. Lightw. Technol.*, vol. 36, no. 19, pp. 4267–4272, Oct. 2018.

[175] J. Lee, Y. Kim, K. Lee, S. Lee, and S. Kim, "Time-of-flight measurement with femtosecond light pulses," *Nature Photon*., vol. 4, no. 10, pp. 716–720, Oct. 2010.

[176] M. Xin *et al.*, "Attosecond precision multi-kilometer laser-microwave network," *Light Sci. Appl.*, vol. 6, Jan. 2017.

[177] D. Holshouser, H. Foerster, and G. Člark, "Microwave modulation of light using the Kerr effect," *J. Opt. Soc. Am.*, vol. 51, pp. 1360–1365, Dec. 1961.

[178] I. Kaminow, "Microwave modulation of the electro-optic effect in KH2PO4," *Phys. Rev. Lett.*, vol. 6, pp. 528–530, May 1961.

[179] A. Levine, "Fiber optics for radar and data system," *Proc. SPIE*, vol. 150, 1978.

[180] K. Garenaux *et al.*, "Recent breakthroughs in RF photonics for radar systems," *IEEE Aerosp. Electron. Syst. Mag.*, vol. 22, no. 2, pp. 3–8, Feb. 2007.

[181] M. Loïc *et al.*, "Optical functions for microwave signal processing in radar, communications and surveillance systems," in *2009 Int. Radar Conf. "Surveillance for a Safer World" (RADAR)*, Bordeaux, France, 2009, pp. 1–5.

[182] J. McKinney, "Photonics illuminates the future of radar," *Nature*, vol. 507, no. 7492, pp. 310–312, Mar. 2014.

[183] G. Serafino *et al.*, "Toward a new generation of radar systems based on microwave photonic technologies," *J. Lightw. Technol.*, vol. 37, no. 2, pp. 643–650, Jan. 2019.

[184] C. Cox, *Analog Optical Links: Theory and Practice*. UK: Cambridge University Press, 2006.

[185] K. Alameh, "Frequency downconverter for high-capacity fibre grating based beamformers for phased arrays," *Electron. Lett.*, vol. 35, no. 1, pp. 66–67, Jan. 1999.

[186] A. Agarwal, T. Banwell, and T. Woodward, "Optically filtered microwave photonic links for RF signal processing applications," *J. Lightw. Technol.*, vol. 29, no. 16, pp. 2394–2401, Aug. 2011.

[187] C. Brès, S. Zlatanovic, A. Wiberg, and S. Radic, "Reconfigurable parametric channelized receiver for instantaneous spectral analysis," *Opt. Express*, vol. 19, no. 4, pp. 3531–3541, Feb. 2011.

[188] A. Poddar, U. Rohde, V. Madhavan, A. Apte, and S. Koul, "Ka-Band metamaterial Möbius Oscillator (MMO) circuit," in *2016 IEEE MTT-S Int. Microwave Symp. (IMS)*, San Francisco, USA, 2016, pp. 1–4.

[189] J. Fontana and R. Pantell, "Theoretical considerations on millimeter wave generation by optical frequency mixing," *Proc. IRE*, vol. 50, no. 8, pp. 1796–1800, Aug. 1962.

[190] J. Yao, "Microwave photonics: Photonic generation of microwave and millimeter-wave signals," *Int. J. Microw. Opt. Technol.*, vol. 5, no. 1, pp. 16–21, Jan. 2010.

[191] U. Gliese *et al.*, "A wideband heterodyne optical phase-locked loop for generation of 3-18 GHz microwave carriers," *IEEE Photon. Technol. Lett.*, vol. 4, no. 8, pp. 936–938, Aug. 1992.

[192] J. Li, H. Lee, and K. Vahala, "Microwave synthesizer using an on-chip Brillouin oscillator," *Nat. Commun.*, vol. 4, no. 2097, pp. 1–7, Jun. 2013.

[193] G. Schneider, J. Murakowski, C. Schuetz, S. Shi, and D. Prather, "Radiofrequency signal-generation system with over seven octaves of continuous tuning," *Nature Photon*., vol. 7, pp. 118–122, Jan. 2013.

[194] W. Liang *et al.*, "High spectral purity Kerr frequency comb radio frequency photonic oscillator," *Nature Commun*., vol. 6, no. 7957, pp. 1–8, Aug. 2015.

[195] W. Zhou and G. Blasche, "Injection-locked dual opto-electronic oscillator with ultra-low phase noise and ultra-low spurious level," *IEEE Trans. Microw. Theory Technol.*, vol. 53, no. 3, pp. 929–933, Mar. 2005.

[196] C. Lin, J. Chen, S. Dai, P. Peng, and S. Chi, "Impact of nonlinear transfer function and imperfect splitting ratio of MZM on optical up-conversion employing double sideband with carrier suppression modulation," *J. Lightw. Technol.*, vol. 26, no. 15, pp. 2449–2459, Aug. 2008.

[197] G. Qi, J. Yao, J. Seregelyi, C. Bélisle, and S. Paquet, "Generation and distribution of a wide-band continuously tunable mm-wave signal with an optical external modulation technique," *IEEE Trans. Microw. Theory Technol.*, vol. 53, no. 10, pp. 3090–3097, Oct. 2005.

[198] M. Hasan, R. Guemri, R. Basilio, F. Lucarz, J. Tocnaye, and T. Hall, "Theoretical analysis and modeling of a photonic integrated circuit for frequency 8-tupled and 24-tupled millimeter wave signal generation," *Opt. Lett.*, vol. 39, no. 24, pp. 6950–6953, Dec. 2014.

[199] J. Kim, J. Cox, J. Chen, and F. Kartner, "Drift-free femtosecond timing synchronization of remote optical and microwave sources," *Nature Photon*., vol. 2, pp. 733–736, Dec 2008.

[200] J. Wei, D. Kwon, S. Zhang, S. Pan, and J. Kim, "All-fiber-photonics-based ultralow-noise agile frequency synthesizer for X-band radars," *Photon. Res.*, vol. 6, no. 1, pp. 12–17, Jan. 2018.

[201] X. S. Yao and L. Maleki, "High frequency optical subcarrier generator," *Electron. Lett.*, vol. 30, no. 18, pp. 1525–1526, Sept. 1994.

[202] D. Eliyahu, D. Seidel, and L. Maleki, "Phase noise of a high performance OEO and an ultra low noise floor cross-correlation microwave photonic homodyne system," in *2008 IEEE Int. Frequency Control Symp.*, Honolulu, USA, 2008, pp. 811–814.

[203] A. Savchenkov *et al.*, "Whispering-gallery mode based opto-electronic oscillators," in *2010 EEE Int. Frequency Control Symp.*, Newport Beach, USA, 2010, pp. 554–557.

[204] M. Bagnell, J. Rodriguez, and P. Delfyett, "Millimeter-wave generation in an optoelectronic oscillator using an ultrahigh finesse etalon as a photonic filter," *J. Lightw. Technol.*, vol. 32, no. 6, pp. 1063–1067, Mar. 2014.

[205] S. Liu *et al.*, "Ultralow phase noise optoelectronic oscillator and its application to a frequency synthesizer," (in Chinese), *J. Radars*, vol. 8, no. 2, pp. 245–250, Apr. 2019.

[206] C. Wang and J. P. Yao, "Photonic generation of chirped microwave pulses using superimposed chirped fiber Bragg gratings," *IEEE Photon. Technol. Lett.*, vol. 20, no. 9–12, pp. 882–884, May-Jun 2008.

[207] C. Wang and J. Yao, "Chirped microwave pulse generation based on optical spectral shaping and wavelength-to-time mapping using a Sagnac loop mirror incorporating a chirped fiber bragg grating," *J. Lightw. Technol.*, vol. 27, no. 16, pp. 3336–3341, Aug. 2009.

[208] M. Li, L. Shao, J. Albert, and J. Yao, "Tilted fiber bragg grating for chirped microwave waveform generation," *IEEE Photon. Technol. Lett.*, vol. 23, no. 5, pp. 314–316, Mar. 2011.

[209] W. Wang *et al.*, "Photonic generation of pulsed microwave signal based on phase shifted lyot optical filter," *IEEE Photon. Technol. Lett.*, vol. 27, no. 17, pp. 1845–1848, Sept. 2015.

[210] F. Zhang, X. Ge, and S. Pan, "Background-free pulsed microwave signal generation based on spectral shaping and frequency-to-time mapping," *Photon. Res.*, vol. 2, no. 4, pp. B5–B10, Aug. 2014.

[211] Y. Li, A. Rashidinejad, J. Wun, D. Leaird, J. Shi, and A. Weiner, "Photonic generation of W-band arbitrary waveforms with high time-bandwidth products enabling 3.9 mm range resolution," *Optica*, vol. 1, no. 6, pp. 446–454, Dec. 2014.

[212] A. Rashidinejad and A. Weiner, "Photonic radio-frequency arbitrary waveform generation with maximal time-bandwidth product capability," *J. Lightw. Technol.*, vol. 32, no. 20, pp. 3383–3393, Oct. 2014.

[213] P. Zhou, F. Zhang, Q. Guo, and S. Pan, "Linearly chirped microwave waveform generation with large time-bandwidth product by optically injected semiconductor laser," *Opt. Express*, vol. 24, no. 16, pp. 18460–18467, Aug. 2016.

[214] P. Zhou, F. Zhang, Q. Guo, S. Li, and S. Pan, "Reconfigurable radar waveform generation based on an optically injected semiconductor laser," *IEEE J. Sel. Topics Quantum Electron.*, vol. 23, no. 6, pp. 1801109, Nov. 2017.

[215] B. Zhang, D. Zhu, P. Zhou, C. Xie, and S. Pan, "Tunable triangular frequency modulated microwave waveform generation with improved linearity using an optically injected semiconductor laser," *Appl. Opt.*, vol. 58, no. 20, pp. 5479–5485, Jul. 2019.

[216] P. Zhou, F. Zhang, X. Ye, Q. Guo, and S. Pan, "Flexible frequency-hopping microwave generation by dynamic control of optically injected semiconductor laser," *IEEE Photon. J.*, vol. 8, no. 6, pp. 5501909, Dec. 2016.

[217] F. Z. Zhang *et al.*, "Photonics-based broadband radar for high-resolution and real-time inverse synthetic aperture imaging," *Opt. Express*, vol. 25, no. 14, pp. 16274–16281, Jul. 2017.

[218] Y. Yao *et al.*, "Demonstration of ultra-high-resolution photonics-based Ka-band inverse synthetic aperture radar imaging," in *2018 Optical Fiber Commun. Conf. and National Fiber Optic Engineers Conf. (OFC)*, San Diego, USA, 2018, pp. Th3G.5.

[219] W. Chen, D. Zhu, C. Xie, T. Zhou, X. Zhong, and S. Pan, "Photonics-based reconfigurable multi-band linearly frequency-modulated signal generation," *Opt. Express*, vol. 26, no. 25, pp. 32491–32499, Dec. 2018.

[220] B. D. Gao, F. Z. Zhang, and S. L. Pan, "Experimental demonstration of arbitrary waveform generation by a 4-bit photonic digital-to-analog converter," *Opt. Commun.*, vol. 383, pp. 191–196, Jan. 2017.

[221] J. D. Li *et al.* "A segmented photonic digital-to-analog converter with a high effective number of bits," *2019 Int. Topical Meeting on Microwave Photonics (MWP)*, Ottawa, ON, Canada,7-10 Oct. 2019.

[222] S. Peng *et al.*, "High-resolution W-band ISAR imaging system utilizing a logic-operation based photonic digital-to-analog converter," *Opt. Express*, vol. 26, no. 2, pp. 1978–1987, Jan. 2018.

[223] S. Cundiff and A. Weiner, "Optical arbitrary waveform generation," *Nature Photon*., vol. 4, no. 11, p. 760, 2010.

[224] X. Ye, F. Zhang, Y. Yang, D. Zhu, and S. Pan, "Photonics-based high-resolution 3D inverse synthetic aperture radar imaging," *IEEE Access*, vol. 7, pp. 79503–79509, Jul. 2019.

[225] X. Ye, F. Zhang, Y. Yang, and S. Pan, "Photonics-based radar with balanced I/Q de-chirping for interference-suppressed high-resolution detection and imaging," *Photon. Res.*, vol. 7, no. 3, pp. 265–272, Mar. 2019.

[226] F. Zhang, B. Gao, and S. Pan, "Photonics-based MIMO radar with high-resolution and fast detection capability," *Opt. Express*, vol. 26, no. 13, pp. 17529–17540, Jun. 2018.

[227] R. Li *et al.*, "Demonstration of a microwave photonic synthetic aperture radar based on photonic assisted signal generation and stretch processing," *Opt. Express*, vol. 25, no. 13, pp. 14334–14340, Jun. 2017.

[228] A. Wang *et al.*, "Ka-band microwave photonic ultra-wideband imaging radar for capturing quantitative target information," *Opt. Express*, vol. 26, no. 16, pp. 20708–20717, Aug. 2018.

[229] T. A. Schaffer, H. P.Warren, M. J. Bustamante, and K. W.Kong, "A 2 GHz 12-bit digital-to-analog converter for direct digital synthesis applications," *Techn. Digest GaAs Ie Symp.*, 1996, pp. 61–64.

[230] A. Yacoubian and P. K. Das, "Digital-to-analog conversion using electrooptic modulators," *IEEE Photon. Technol. Lett.*, vol. 15, no. 1, pp. 117–119, 2003.

[231] M. Currie and J. W. Lou, "Weighted, summing photonic digital-to-analog converter," *Electron. Lett.*, vol. 42, no. 1, pp. 54–55, 2006.

[232] X. Yu, K. Wang, X. Zheng, and H. Zhang, "Incoherent photonic digital-to-analogue converter based on broadband optical source," *Electron. Lett.*, vol. 43, no. 19, pp. 1044–1045, 2007.

[233] A. Leven *et al.*, "High speed integrated InP photonic digital-to-analog converter," in *Proc. Indium Phosphide and Related Materials Conf.*, 2006, pp. 14–15.

[234] A. Leven, J. Lin, J. Lee, K.-Y. Tu, Y. Baeyens, and Y. K. Chen, "A 12.5G sample/s optical digital-to-analog converter with 3.8 effective bits," in *Proc. 17th Ann. Meet. IEEE Lasers and Electro-Optics Society*, Puerto Rico, 2004, pp. 270–271.

[235] S. Oda and A. Maruta, "All-optical digital-to-analog conversion using nonlinear optical loop mirrors," *IEEE Photon. Technol. Lett.*, vol. 18, no. 5, pp. 703–705, 2006.

[236] F. Zhang, B. Gao, and S. Pan, "Two-bit photonic digital-to-analog conversion unit based on polarization multiplexing," *Opt. Eng.*, vol. 55, no. 3, pp. 031115-1-4, 2016.

[237] J. Ding *et al.*, "Optical digital-to-analog converter based on microring switches," *IEEE Photon. Technol. Lett.*, vol. 26, no. 20, pp. 2066–2069, 2014.

[238] J. Liao *et al.*, "Novel bipolar photonic digital-to-analog conversion employing differential phase shift keying modulation and balanced detection," *IEEE Photon. Technol. Lett.*, vol. 25, no. 2, pp. 126–128, 2013.

[239] T. Saida, K. Okamoto, K. Uchiyama, K. Takiguchi, T. Shibata, and A. Sugita, "Integrated optical digital-to-analogue converter and its application to pulse pattern recognition," *Electron. Lett.*, vol. 37, no. 20, pp. 1237–1238, 2001.

[240] T. Nishitani, T. Konishi, H. Furukawa, and K. Itoh, "All-optical digital-to-analog conversion using pulse pattern recognition based on optical correlation processing," *Opt. Express*, vol. 13, no. 25, pp. 10310–10315, 2005.

[241] Y. Peng *et al.*, "Photonic digital-to-analog converter based on summing of serial weighted multiwavelength pulses," *IEEE Photon. Technol. Lett.*, vol. 20, no. 24, pp. 2135–2137, 2008.

[242] Y. Zhang, X. Ye, Q. Guo, F. Zhang, and S. Pan, "Photonic generation of linear-frequency-modulated waveforms with improved time-bandwidth product based on polarization modulation," *J. Lightw. Technol.*, vol. 35, no. 10, pp. 1821–1829, May 2017.

[243] Y. Dai and J. Yao, "Arbitrary phase-modulated RF signal generation based on optical pulse position modulation," *J. Lightw. Technol.*, vol. 26, no. 17–20, pp. 3329–3336, Sept. 2008.

[244] J. Wun, C. Wei, J. Chen, C. Goh, S. Set, and J. Shi, "Photonic chirped radio-frequency generator with ultra-fast sweeping rate and ultra-wide sweeping range," *Opt. Express*, vol. 21, no. 9, pp. 11475–11481, May 2013.

[245] M. Richards, J. A. Scheer, and W. A. Holm, *Principle of Modern Radar: Basic Principle*. SciTech Publishing, 2010.

[246] J. Hasch, E. Topak, R. Schnabel, T. Zwick, R. Weigel, and C. Waldschmidt, "Millimeter-wave technology for automotive radar sensors in the 77 GHz frequency band," *IEEE Trans. Microw. Theory Tech.* vol. 60, no. 3, pp. 845–860, 2012.

[247] Z. Li and K. Wu, "On the leakage of FMCW radar front-end receiver," in *Global Symp. Millimeter Waves*, IEEE, 2008, pp. 127–130.

[248] G. Gopalakrishnan, W. Burns, and C. Bulmer, "Microwave-optical mixing in LiNbO3 modulators," *IEEE Trans. Microw. Theory Technol.*, vol. 41, no. 12, pp. 2383–2391, Dec. 1993.

[249] C. Bohemond, T. Rampone, and A. Sharaiha, "Performances of a photonic microwave mixer based on cross-gain modulation in a semiconductor optical amplifier," *J. Lightw. Technol.*, vol. 29, no. 16, pp. 2402–2409, Aug. 15, 2011.

[250] J. Seo, C. Choi, W. Choi, Y. Kang, Y. Chung, and J. Kim, "Remote optoelectronic frequency down-conversion using 60-GHz optical heterodyne signals and an electro-absorption modulator," *IEEE Photon. Technol. Lett.*, vol. 17, no. 5, pp. 1073–1075, May 2005.

[251] S. Constant, Y. Guennec, G. Maury, M. Lourdiane, and B. Cabon, "Directly modulated laser diode in the nonlinear regime for low-cost digital frequency up-conversion," *Microw. Opt. Technol. Lett.*, vol. 50, no. 5, pp. 1214–1219, May 2008.

[252] V. Pagán, B. Haas, and T. Murphy, "Linearized electrooptic microwave downconversion using phase modulation and optical filtering," *Opt. Express*, vol. 19, no. 2, pp. 883–95, Jan. 2011.

[253] D. Zhu and S. Pan, "Photonics-based microwave image-reject mixer," *MDPI Photon*., vol. 5, no. 2, pp. 6-1-12, Jun. 2018.

[254] S. Strutz and K. Williams, "An 8-18-GHz all-optical microwave downconverter with channelization," *IEEE Trans. Microw. Theory Technol.*, vol. 49, no. 10, pp. 1992–1995, Oct. 2001.

[255] S. Strutz and K. Williams, "A 0.8-8.8-GHz image rejection microwave photonic downconverter," *IEEE Photon. Technol. Lett.*, vol. 12, no. 10, pp. 1376–1378, Oct. 2002.

[256] Z. Tang and S. Pan, “A reconfigurable photonic microwave mixer using a 90° optical hybrid,” *IEEE Trans. Microw. Theory Technol.*, vol. 64, no. 9, pp. 3017–3025, Sept. 2016.
[257] Z. Tang and S. Pan, “Image-reject mixer with large suppression of mixing spurs based on a photonic microwave phase shifter,” *J. Lightw. Technol.*, vol. 34, no. 20, pp. 4729–4735, Oct. 2016.
[258] D. Hunter, L. Edvell, and M. Englund, “Wideband microwave photonic channelised receiver,” in *2005 Int. Topical Meeting on Microwave Photonics (MWP)*, Seoul, Korea, 2005, pp. 249–252.
[259] X. Gu, D. Zhu, S. Li, Y. Zhao, and S. Pan, “Photonic RF channelization based on series-coupled asymmetric double-ring resonator filter,” in *The 7th IEEE/Int. Conf. on Advanced Infocomm Technology*, Fuzhou, China, 2014, pp. 240–244.
[260] X. Xie *et al.*, “Broadband photonic radio-frequency channelization based on a 39-GHz optical frequency comb,” *IEEE Photon. Technol. Lett.*, vol. 24, no. 8, pp. 661–663, Apr. 2012.
[261] G. Anderson, D. Webb, A. Spezio, and J. Lee, “Advanced channelization for RF, microwave, and millimeterwave applications,” *Proc. IEEE*, vol. 79, no. 3, pp. 355–388, Mar. 1991.
[262] Z. Tang, D. Zhu, and S. Pan, “Coherent optical RF channelizer with large instantaneous bandwidth and large in-band interference suppression,” *J. Lightw. Technol.*, vol. 36, no. 19, pp. 4219–4226, Oct. 2018.
[263] W. Chen, D. Zhu, C. Xie, J. Liu, and S. Pan, “Microwave channelizer based on a photonic dual-output image-reject mixer,” *Opt. Lett.*, vol. 44, no. 16, pp. 4052–4055, Aug. 2019.
[264] H. Zmuda and E. N. Toughlian, *Photonic Aspects of Modern Radar*. USA: Artech House, 1994.
[265] R. Minasian, “Photonic signal processing of microwave signals,” *IEEE Trans. Microw. Theory Technol.*, vol. 54, no. 2, pp. 832–846, Feb. 2006.
[266] J. Capmany, J. Mora, I. Gasulla, J. Sancho, J. Lloret, and S. Sales, “Microwave photonic signal processing,” *J. Lightw. Technol.*, vol. 31, no. 4, pp. 571–586, Feb. 2013.
[267] M. Fok and J. Ge, “Tunable multiband microwave photonic filters,” *MDPI Photon.*, vol. 4, no. 4, Dec. 2017.
[268] X. Zou, P. Li, W. Pan, and L. S. Yan, “Photonic microwave filters with ultra-high noise rejection [Invited],” *Chin. Opt. Lett.*, vol. 17, no. 3, Mar. 2019.
[269] E. Heyde and R. Minasian, “A solution to the synthesis problem of recirculating optical delay line filters,” *IEEE Photon. Technol. Lett.*, vol. 6, no. 7, pp. 833–835, Jul. 1994.
[270] V. Polo, B. Vidal, J. Corral, and J. Marti, “Novel tunable photonic microwave filter based on laser arrays and N x N AWG-based delay lines,” *IEEE Photon. Technol. Lett.*, vol. 15, no. 4, pp. 584–586, Apr. 2003.
[271] X. K. Yi, F. Wei, N. Hong, and L. Chao, “Tunable microwave filter design using wavelength conversion technique and high dispersion time delays,” *IEEE Photon. Technol. Lett.*, vol. 13, no. 8, pp. 857–859, Aug. 2001.
[272] S. Sales, J. Capmany, J. Marti, and D. Pastor, “Experimental demonstration of fibre-optic delay line filters with negative coefficients,” *Electron. Lett.*, vol. 31, no. 13, pp. 1095–1096, Jun. 1995.
[273] F. Zeng, J. Wang, and J. Yao, “All-optical microwave bandpass filter with negative coefficients based on a phase modulator and linearly chirped fiber Bragg gratings,” *Opt. Lett.*, vol. 30, no. 17, pp. 2203–2205, Sep. 2005.
[274] J. Yao and Q. Wang, “Photonic microwave bandpass filter with negative coefficients using a polarization modulator,” *IEEE Photon. Technol. Lett.*, vol. 19, no. 9–12, pp. 644–646, May 2007.
[275] A. Loayssa, J. Capmany, M. Sagues, and J. Mora, “Demonstration of incoherent microwave photonic filters with all-optical complex coefficients,” *IEEE Photon. Technol. Lett.*, vol. 18, no. 13–16, pp. 1744–1746, Jul. 2006.
[276] M. Sagues, R. Olcina, A. Loayssa, S. Sales, and J. Capmany, “Multi-tap complex-coefficient incoherent microwave photonic filters based on optical single-sideband modulation and narrow band optical filtering,” *Opt. Express*, vol. 16, no. 1, pp. 295–303, Jan. 2008.
[277] Y. Dai and J. Yao, “Nonuniformly-spaced photonic microwave delay-line filter,” *Opt. Express*, vol. 16, no. 7, pp. 4713–4718, Mar. 2008.
[278] X. K. Yi, T. Huang, and R. Minasian, “Tunable and reconfigurable photonic signal processor with programmable all-optical complex coefficients,” *IEEE Trans. Microw. Theory Techn.*, vol. 58, no. 11, pp. 3088–3093, Nov. 2010.
[279] W. Xue, S. Sales, J. Mork, and J. Capmany, “Widely tunable microwave photonic notch filter based on slow and fast light effects,” *IEEE Photon. Technol. Lett.*, vol. 21, no. 1–4, pp. 167–169, Jan. 2009.
[280] X. Li, J. Dong, Y. Yu, and X. Zhang, “A tunable microwave photonic filter based on an all-optical differentiator,” *IEEE Photon. Technol. Lett.*, vol. 23, no. 5, pp. 308–310, Mar. 2011.
[281] J. Lloret *et al.*, “Tunable complex-valued multi-tap microwave photonic filter based on single silicon-on-insulator microring resonator,” *Opt. Express*, vol. 19, no. 13, pp. 12402–12407, Jun. 2011.
[282] Y. Zhang and S. Pan, “Complex coefficient microwave photonic filter using a polarization-modulator-based phase shifter,” *IEEE Photon. Technol. Lett.*, vol. 25, no. 2, pp. 187–189, Jan. 2013.
[283] Y. Zhang and S. Pan, “Tunable multitap microwave photonic filter with all complex coefficients,” *Opt. Lett.*, vol. 38, no. 5, pp. 802–804, Mar. 2013.
[284] W. Li, N. H. Zhu, and L. X. Wang, “Continuously tunable microwave photonic notch filter with a complex coefficient,” *IEEE Photon. J.*, vol. 3, no. 3, pp. 462–467, Jun. 2011.
[285] W. Li, W. Wang, W. Sun, J. Liu, and N. Zhu, “Microwave photonic notch filter with complex coefficient based on DDMZM,” *IEEE Photon. Technol. Lett.*, vol. 26, no. 18, pp. 1859–1862, Sept. 2014.
[286] H. Wen, M. Li, W. Li, and N. Zhu, “Ultrahigh-Q and tunable single-passband microwave photonic filter based on stimulated Brillouin scattering and a fiber ring resonator,” *Opt. Lett.*, vol. 43, no. 19, pp. 4659–4662, Oct. 2018.
[287] S. Hu, L. W. Li, X. Yi, and F. Teng, “Tunable dual-passband microwave photonic filter based on stimulated Brillouin scattering,” *IEEE Photon. Technol. Lett.*, vol. 29, no. 3, pp. 330–333, Feb. 2017.
[288] Z. Zeng *et al.*, “Freely tunable dual-passband microwave photonic filter based on phase-to-intensity modulation conversion by stimulated Brillouin scattering,” *IEEE Photon. J.*, vol. 11, no. 1, Feb. 2019.
[289] J. Fandino, P. Munoz, D. Domenech, and J. Capmany, “A monolithic integrated photonic microwave filter,” *Nature Photon.*, vol. 11, no. 2, pp. 124–129, Feb. 2017.
[290] C. Porzi *et al.*, “High-capacity single-sideband suppressed-carrier modulation with integrated optical filter in silicon-on-insulator technology,” in *2019 Int. Workshop on Fiber Optics in Access Networks (FOAN)*, Sarajevo, Bosnia and Herzegovina, 2019, pp. 29–33.
[291] E. Norberg, R. Guzzon, J. Parker, L. Johansson, and L. Coldren, “Programmable photonic microwave filters monolithically integrated in InP-InGaAsP,” *J. Lightw. Technol.*, vol. 29, no. 11, pp. 1611–1619, Jun. 2011.
[292] X. Xue *et al.*, “Programmable single-bandpass photonic RF filter based on kerr comb from a microring,” *J. Lightw. Technol.*, vol. 32, no. 20, pp. 3557–3565, Oct. 2014.
[293] X. Xu *et al.*, “Advanced adaptive photonic RF filters with 80 taps based on an integrated optical micro-comb source,” *J. Lightw. Technol.*, vol. 37, no. 4, pp. 1288–1295, Feb. 2019.
[294] D. Marpaung *et al.*, “Low-power, chip-based stimulated Brillouin scattering microwave photonic filter with ultrahigh selectivity,” *Optica*, vol. 2, no. 2, pp. 76–83, Feb. 2015.
[295] Y. Xie *et al.*, “System-level performance of chip-based Brillouin microwave photonic bandpass filters,” *J. Lightw. Technol.*, vol. 37, no. 20, pp. 5246–5258, Oct. 2019.
[296] A. Levine, “Fiber optic phased array antenna system for RF transmission,” U.S. Patent 4 028 702, Jun. 7, 1977.
[297] I. Frigyes and A. J. Seeds, “Optically generated true-time delay in phased-array antennas,” *IEEE Trans. Microw. Theory Technol.*, vol. 43, no. 9, pp. 2378–2386, Sept. 1995.
[298] A. Goutzoulis, K. Davies, J. Zomp, P. Hrycak, and A. Johnson, “Development and field demonstration of a hardware-compressive fiber-optic true-time-delay steering system for phased-array antennas,” *Appl. Opt.*, vol. 33, no. 35, pp. 8173–8185, Dec. 1994.
[299] D. Dolfi, P. Joffre, J. Antoine, J. P. Huignard, D. Philippet, and P. Granger, “Experimental demonstration of a phased-array antenna optically controlled with phase and time delays,” *Appl. Opt.*, vol. 35, no. 26, pp. 5293–5300, Sept. 1996.
[300] X. Ye, D. Zhu, Y. Zhang, S. Li, and S. Pan, “Analysis of photonics-based RF beamforming with large instantaneous bandwidth,” *J. Lightw. Technol.*, vol. 35, no. 23, pp. 5010–5019, Dec. 2017.
[301] S. Dug, L. Song, and K. Gyoun, “Optical true time-delay feeder for X-band phased array antennas composed of 2x2 optical MEMS switches and fiber delay lines,” *IEEE Photon. Technol. Lett.*, vol. 16, no. 5, pp. 1364–1366, May 2004.
[302] R. Moreira *et al.*, “Integrated ultra-low-loss 4-bit tunable delay for broadband phased array antenna applications,” *IEEE Photon. Technol. Lett.*, vol. 25, no. 12, pp. 1165–1168, Jun. 2013.
[303] Y. Liu, A. Choudhary, D. Marpaung, and B. Eggleton, “Gigahertz optical tuning of an on-chip radio frequency photonic delay line,” *Optica*, vol. 4, no. 4, pp. 418–423, Apr. 2017.

[304] R. Bonjour *et al.*, "Ultra-fast millimeter wave beam steering," *IEEE J. Quantum Electron.*, vol. 52, no. 1, p. 0600708, Jan. 2016.
[305] Miniature Motorized Optical Variable Delay Line, General Photonics Corp., USA [Online]. Available: http://www.generalphotonics.com/wp-content/uploads/2017/12/MDL-002-spec-12-17-17.pdf. Accessed on: Feb. 2020.
[306] X. Yi, L. Li, T. Huang, and R. Minasian, "Programmable multiple true-time-delay elements based on a Fourier-domain optical processor," *Opt. Lett.*, vol. 37, no. 4, pp. 608–610, Apr. 2012.
[307] Y. Liu, J. Yang, and J. Yao, "Continuous true-time-delay beamforming for phased array antenna using a tunable chirped fiber grating delay line," *IEEE Photon. Technol. Lett.*, vol. 14, no. 8, pp. 1172–1174, Apr. 2002.
[308] J. Cardenas *et al.*, "Wide-bandwidth continuously tunable optical delay line using silicon microring resonators," *Opt. Express*, vol. 18, no. 25, pp. 26525–26534, Dec. 2010.
[309] I. Aryanfar *et al.*, "Chip-based Brillouin radio frequency photonic phase shifter and wideband time delay," *Opt. Lett.*, vol. 42, no. 7, pp. 1313–1316, Apr. 2017.
[310] T. Tatoli, D. Conteduca, F. Dell'Olio, C. Ciminelli, and M. Armenise, "Graphene-based fine-tunable optical delay line for optical beamforming in phased-array antennas," *Appl. Opt.*, vol. 55, no. 16, pp. 4342–4349, Jun. 2016.
[311] J. Cruz *et al.*, "Chirped fibre Bragg gratings for phased-array antennas," *Electron. Lett.*, vol. 33, no. 7, pp. 545–546, Mar. 1997.
[312] P. Matthews, L. Pao-Lo, J. Medberry, M. Franekl, and R. Esman, "Demonstration of a wide-band fiber-optic nulling system for array antennas," *IEEE Trans. Microw. Theory Technol.*, vol. 47, no. 7, pp. 1327–1331, Jul. 1999.
[313] M. Chen, H. Subbaraman, and R. Chen, "Photonic crystal fiber beamformer for multiple X-band phased-array antenna transmissions," *IEEE Photon. Technol. Lett.*, vol. 20, no. 5, pp. 375–377, Mar. 2008.
[314] X. Xue *et al.*, "Microcomb-based true-time-delay network for microwave beamforming with arbitrary beam pattern control," *J. Lightw. Technol.*, vol. 36, no. 12, pp. 2312–2321, 2018.
[315] N. Shi, W. Li, N. Zhu, and M. Li, "Optically controlled phase array antenna," *Chin. Opt. Lett.*, vol. 17, no. 5, p. 052301, May 2019.
[316] P. Wu, S. Tang, and D. Raible, "A prototype high-speed optically-steered X-band phased array antenna," *Opt. Express*, vol. 21, no. 16, pp. 32599–32604, Dec. 2013.
[317] X. Ye, F. Zhang, and S. Pan, "Optical true time delay unit for multi-beamforming," *Opt. Express*, vol. 23, no. 8, pp. 10002–10008, Apr. 2015.
[318] X. Ye, F. Zhang, and S. Pan, "Compact optical true time delay beamformer for a 2D phased array antenna using tunable dispersive elements," *Opt. Lett.*, vol. 41, no. 17, pp. 3956–3959, Sept. 2016.
[319] I. Visscher *et al.*,"Broadband true time delay microwave photonic beamformer for phased array antennas," in *2019 13th Eur. Conf. on Antennas and Propagation (EuCAP)*, Krakow, Poland, 2019, pp. 1–5.
[320] R. Rotman, O. Raz, S. Barzilay, S. R. Rotman, and M. Tur, "Wideband antenna patterns and impulse response of broadband RF phased arrays with RF and photonic beamforming," *IEEE Trans. Antennas Propag.*, vol. 55, no. 1, pp. 36–44, Jan. 2007.
[321] X. Ye, B. Zhang, Y. Zhang, D. Zhu, and S. Pan, "Performance evaluation of optical beamforming-based wideband antenna array," *Chin. Opt. Lett.*, vol. 15, no. 1, p. 010013, Jan. 2017.
[322] Z. Zhang, H. Li, S. Zhang, and Y. Liu, "Analog-to-digital converters using photonic technology," *Chin. Sci. Bull.*, vol. 59, no. 22, pp. 2666–2671, Aug. 2014.
[323] P. Ghelfi *et al.*, "A fully photonics-based coherent radar system," *Nature*, vol. 507, no. 7492, pp. 341–345, 2014.
[324] F. Laghezza, F. Scotti, P. Ghelfi, A. Bogoni, and S. Pinna, "Jitter-limited photonic analog-to-digital converter with 7 effective bits for wideband radar applications," in *2013 IEEE Radar Conf. (RadarCon)*, Ottawa, Canada, 2013, pp. 1–5.
[325] A. Fard, S. Gupta, and B. Jalali, "Photonic time-stretch digitizer and its extension to real-time spectroscopy and imaging," *Laser Photon. Rev.*, vol. 7, no. 2, pp. 207–263, Feb. 2013.
[326] G. Sefler, J. Chou, J. Conway, and G. Valley, "Distortion correction in a high-resolution time-stretch ADC scalable to continuous time," *J. Lightw. Technol.*, vol. 28, no. 10, pp. 1468–1476, May 2010.
[327] Y. Han, O. Boyraz, and B. Jalali, "Ultrawide-band photonic time-stretch A/D converter employing phase diversity," *IEEE Trans. Microw. Theory Technol.*, vol. 53, no. 4, pp. 1404–1408, Apr. 2005.
[328] W. Zou, H. Zhang, X. Long, S. Zhang, Y. Cui, and J. Chen, "All- optical-central-frequency-programmable and bandwidth-tailorable radar," *Sci. Rep.*, vol. 6, Jan. 2016.
[329] A. Johnstone, M. Lewis, J. D. Hares, and P. Kellet, "High-speed opto-electronic transient waveform digitiser," *Comput. Standards Interfaces*, vol. 23, no. 2, pp. 73–84, 2001.
[330] H. Zmuda *et al.*, "Optically assisted high-speed, high resolution analog-to-digital conversion," in *Enabling Photonics Technologies for Defense, Security, and Aerospace Applications*, Orlando, USA, 2005, pp. 51–61.
[331] X. Zhu, D. Zhu, and S. Pan,"A photonic analog-to-digital converter with multiplied sampling rate using a fiber ring," in *2017 Int. Topical Meeting on Microwave Photonics (MWP)*, Beijing, China, 2017, pp. 1–3.
[332] J. Chou, J. Conway, G. Sefler, G. Valley, and B. Jalali, "Photonic bandwidth compression front end for digital oscilloscopes," *J. Lightw. Technol.*, vol. 27, no. 22, pp. 5073–5077, Nov. 2009.
[333] W. Haur *et al.*, "Photonic time-stretched analog-to-digital converter amenable to continuous-time operation based on polarization modulation with balanced detection scheme," *J. Lightw. Technol.*, vol. 29, no. 2, pp. 3099–3106, Jan. 2011.
[334] S. Haykin, "Cognitive radar: a way of the future," *IEEE Signal Proc. Mag.*, vol. 23, no. 1, pp. 30–40, Jan. 2006.
[335] P. Welch, "The use of fast Fourier transform for the estimation of power spectra: A method based on time averaging over short, modified periodograms," *IEEE Trans. Audio Electroacoust.*, vol. 15, no. 2, pp. 70–73, Jul. 1967.
[336] M. F. Salem, and A. Gaeta, "Application of space–time duality to ultrahigh-speed optical signal processing," *Adv. Opt. Photon.*, vol. 5, pp. 274–317, Aug. 2013.
[337] M. Muriel, J. Azana, and A. Carballar, "Real-time Fourier transformer based on fiber gratings," *Opt. Lett.*, vol. 24, no. 1, p. 1, Jan. 1999.
[338] Y. Zheng, J. Li, Y. Dai, F. Yin, and K. Xu, "Real-time Fourier transformation based on the bandwidth magnification of RF signals," *Opt. Lett.*, vol. 43, no. 2, pp. 194–197, Jan. 2018.
[339] R. Saperstein, D. Panasenko, and Y. Fainman, "Demonstration of a microwave spectrum analyzer based on time-domain optical processing in fiber," *Opt. Lett.*, vol. 29, no. 5, pp. 501–503, Mar. 2004.
[340] R. Saperstein and Y. Fainman, "Information processing with longitudinal spectral decomposition of ultrafast pulses," *Appl. Opt.*, vol. 47, no. 4, pp. A21–A31, Feb. 2008.
[341] M. Li, C. Wang, W. Li, and J. Yao, "An imbalanced temporal pulse-shaping system for chirped microwave waveform generation," *IEEE Trans. Microw. Theory Technol.*, vol. 58, no. 11, pp. 2968–2975, Nov. 2010.
[342] M. Li, Y. Han, S. Pan, and J. Yao, "Experimental demonstration of symmetrical waveform generation based on amplitude-only modulation in a fiber-based temporal pulse shaping system," *IEEE Photon. Technol. Lett.*, vol. 23, no. 11, pp. 715–717, Jun. 2011.
[343] Y. Duan, L. Chen, H. Zhou, X. Zhou, C. Zhang, and X. Zhang, "Ultrafast electrical spectrum analyzer based on all-optical Fourier transform and temporal magnification," *Opt. Express*, vol. 25, no. 7, pp. 7520–7529, Apr. 2017.
[344] Y. Duan, L. Chen, L. Zhang, X. Zhou, C. Zhang, and X. Zhang, "Temporal radio-frequency spectrum analyzer, based on asynchronous optical sampling assisted temporal convolution," *Opt. Express*, vol. 26, no. 16, pp. 20735–20743, Aug. 2018.
[345] C. Schnebelin and H. Chatellus, "Fractional Fourier transform-based description of the Talbot effect: application to analog signal processing," *Appl. Opt.*, vol. 56, no. 1, pp. A62–A68, Jan. 2017.
[346] H. Chatellus, L. Cortés, C. Schnébelin, M. Burla, and J. Azaña, "Reconfigurable photonic generation of broadband chirped waveforms using a single CW laser and low-frequency electronics," *Nature Commun.*, vol. 9, no. 1, p. 2438, Jun. 2018.
[347] C. Schnébelin, J. Azaña, and H. Chatellus, "Programmable broadband optical field spectral shaping with megahertz resolution using a simple frequency shifting loop," *Nature Commun.*, vol. 10, no. 1, pp. 1–11, Oct. 2019.
[348] A. Sabharwal, P. Schniter, D. Guo, D. Bliss, S. Rangarajan, and R. Wichman, "In-band full-duplex wireless: Challenges and opportunities," *IEEE J. Sel. Areas Commun.*, vol. 32, no. 9, pp. 1637–1652, Sep. 2014.
[349] N. Shi, Q. Song, J. Tang, W. Li, N. Zhu, and M. Li, "A switchable self-interference cancellation system for dual-band IBFD system using a monolithic integrated DML array." *Opt. Commun.*, vol. 447. pp. 55–60, Feb. 2019.

[350] Y. Chen and S. L. Pan, "Photonics-assisted radio-frequency self-interference cancellation and fiber transmission using a DP-QPSK modulator," in *2018 Int. Topical Meeting on Microwave Photonics (MWP)*, Toulouse, France, 2018, pp. 1–4.
[351] Z. Tu, A. Wen, X. Li, and H. Zhang, "A photonic pre-distortion technique for RF self-interference cancellation." *IEEE Photon. Technol. Lett.*, vol. 30, no. 14. pp. 1297–1300, July. 2018.
[352] X. Han, B. Huo, Y. Shao, and M. Zhao, "Optical RF self-interference cancellation for full-duplex communication using an integrated DP-MZM," in *2017 Progress in Electromagnetics Research Symp.-Spring (PIERS)*, St. Petersburg, Russia, 2017, pp. 2240–2244.
[353] Y. Yu, Y. Zhang, L. Huang, and S. Xiao, "Performance analysis of an optical self-interference cancellation system with a directly modulated laser-based demonstration." *Appl. Opt.*, vol. 57, no. 6, pp. 1284–1291, Feb. 2018.
[354] X. Han, B. Huo, Y. Shao, C. Wang, and M. Zhao, "RF self-interference cancellation using phase modulation and optical sideband filtering." *IEEE Photon. Technol. Lett.*, vol. 29, no. 11, pp. 917–920, June. 2017.
[355] Y. Zhang, S. Xiao, and H. Feng, "Self-interference cancellation using dual-drive Mach-Zehnder modulator for in-band full-duplex radio-over-fiber system." *Opt. Express*, vol. 23, no. 26, pp. 33205, Dec. 2015.
[356] Q. Zhou, H. Feng, and G. Scott, "Wideband co-site interference cancellation based on hybrid electrical and optical techniques." *Opt. Lett.*, vol. 39, no. 22, pp. 6357–6540, Nov. 2014.
[357] M. Pagani, D. Marpaung, D. Choi, S. Madden, B. Davies, and B. Eggleton, "Tunable wideband photonic microwave phase shifter using on-chip stimulated Brillouin scattering," *Opt. Express*, vol. 22, no. 23, pp. 28810–28818, Nov. 2014.
[358] J. Sancho, J. Lloret, I. Gasulla, S. Sales, and J. Capmany, "Fully tunable 360° photonic microwave phase shifter based on a single semiconductor optical amplifier," *Opt. Express*, vol. 19, no. 18, pp. 17421–17426, Sept. 2011.
[359] W. Xue, S. Sales, J. Capmany, and J. Mørk, "Wideband 360° photonic microwave phase shifter based on slow light in semiconductor optical amplifiers," *Opt. Express*, vol. 18, no. 6, pp. 6156–6163, Mar. 2010.
[360] H. Shahoei and J. P. Yao, "Tunable photonic microwave phase shifter based on slow and fast light effects in a tilted fiber Bragg grating," *Opt. Express*, vol. 20, no. 13, pp. 14009–14014, Jun. 2012.
[361] M. Pu *et al.*, "Widely tunable microwave phase shifter based on silicon-on-insulator dual-microring resonator," *Opt. Express*, vol. 18, no. 6, pp. 6172–6182, Mar. 2010.
[362] P. Qu *et al.*, "Design of a vector-sum integrated photonic microwave phase shifter in silicon-on-insulator waveguides," *Appl. Opt.*, vol. 50, no. 17, pp. 2523–2530, Sept. 2011.
[363] L. Bui, A. Mitchell, K. Ghorbani, and T. Chio, "Wide-band RF photonic second order vector sum phase-shifter," *IEEE Microw. Wireless Compon. Lett.*, vol. 15, no. 5, May 2005.
[364] X. Wang, T. Niu, E. Chan, X. Feng, B. Guan, and J. Yao, "Photonics-based wideband microwave phase shifter," *IEEE Photon. J.*, vol. 9, no. 3, pp. 5501710, Jun. 2017.
[365] W. Li, W. Zhang, and J. Yao, "A wideband 360° photonic-assisted microwave phase shifter using a polarization modulator and a polarization-maintaining fiber Bragg grating," *Opt. Express*, vol. 20, no. 28, pp. 29838–29843, Dec. 2012.
[366] W. Li, W. Sun, W. Wang, L. Wang, J. Liu, and N. Zhu, "Photonic-assisted microwave phase shifter using a DMZM and an optical bandpass filter," *Opt. Express*, vol. 22, no. 5, pp. 5522–5527, Mar. 2014.
[367] E. Chan, W. Zhang, and R. Minasian, "Photonic RF phase shifter based on optical carrier and RF modulation sidebands amplitude and phase control," *J. Lightw. Technol.*, vol. 30, no. 23, pp. 3672–3678, Dec.2012.
[368] S. Pan and Y. Zhang, "Tunable and wideband photonic microwave phase shifter based on a single sideband polarization modulator and a polarizer," *Opt. Lett.*, vol. 37, no. 21, pp. 4483–4485, Nov. 2012.
[369] Y. Zhang and S. Pan, "Frequency-multiplying microwave photonic phase shifter for independent multichannel phase shifting," *Opt. Lett.*, vol. 41, no. 6, pp. 1261–1264, Mar. 2016.
[370] Y. Zhang and S. Pan, "A photonics-based multi-function analog signal processor based on a polarization division multiplexing Mach-Zehnder modulator," *Opt. Lett.*, vol. 42, no. 23, pp. 5034–5037, Dec. 2017.
[371] N. Riza, "Liquid crystal-based optical time delay units for phased array antennas," *J. Lightw. Technol.*, vol. 12, no. 8, pp. 1440–1447, Aug. 1994.
[372] J. Lee *et al.*, "Photonic wideband array antennas," *IEEE Trans. Antennas Propagat.*, vol. 43, no. 9, pp. 966–982, Sept. 1995.
[373] J. Roman *et al.*, "Fiber-optic remoting of an ultrahigh dynamic range radar," *IEEE Trans. Microw. Theory Technol.*, vol. 46, no. 12, pp. 2317–2323, Dec. 1998.
[374] *OEwaves' micro-opto-electronic oscillator supports successful mina true interceptor test flight*, OEwaves Inc., USA [Online]. Available: https://www.microwavejournal.com/articles/19733-oewaves-micro-opto-electronic-oscillator-supports-successful-mina-true-interceptor-test-flight. Accessed on: Feb. 2020.
[375] F. Z. Zhang *et al.*, "Photonics-based real-time and high-resolution ISAR imaging of non-cooperative target," *Chin. Opt. Lett.*, vol. 15, no. 11, Nov. 2017.
[376] B. Gao, F. Zhang, E. Zhao, D. Zhang, and S. Pan, "High-resolution phased array radar imaging by photonics-based broadband digital beamforming," *Opt. Express*, vol. 27, no. 9, pp. 13194–13203, Apr. 2019.
[377] J. Cao *et al.*, "Photonic deramp receiver for dual-band LFM-CW Radar," *J. Lightw. Technol.*, vol. 37, no. 10, pp. 2403–2408, May 2019.
[378] X. Ye, F. Zhang, Y. Yang, and S. Pan, "Photonics-based radar transceiver for full-polarimetric inverse synthetic aperture imaging," in *2018 Int. Topical Meeting on Microwave Photonics (MWP)*, Toulouse, France, 2018, pp. 1–4.
[379] P. Ghelfi *et al.*, "Photonics for radars operating on multiple coherent bands," *J. Lightw. Technol.*, vol. 34, no. 2, pp. 500–507, Jan. 2016.
[380] D. Wu, S. Li, X. Xue, X. Xiao, S. Peng, and X. Zheng, "Photonics based microwave dynamic 3D reconstruction of moving targets," *Opt. Express*, vol. 26, no. 21, pp. 27659–27667, Nov. 2018.
[381] T.-F. Tseng, J.-M. Wun, W. Chen, S.-W. Peng, J.-W. Shi, and C.-K. Sun, "High-depth-resolution 3-dimensional radar-imaging system based on a few-cycle W-band photonic millimeter-wave pulse generator," *Opt. Express*, vol. 21, pp. 14109–14119, 2013.
[382] F. Scotti, D. Onori, and F. Laghezza, "Fully coherent S-and X-band photonics-aided radar system demonstration," *IEEE Microw. Compon. Lett.*, vol. 25, no. 11, pp. 757–759, Nov. 2015.
[383] F. Laghezza, F. Scotti, D. Onori, and A. Bogoni, "ISAR imaging of non-cooperative targets via dual band photonics-based radar system," in *2016 17th Int. Radar Symp. (IRS)*, Krakow, Poland, 2016, pp. 1–4.
[384] F. Scotti, F. Laghezza, D. Onori, and A. Bogoni, "Field trial of a photonics-based dual-band fully coherent radar system in a maritime scenario," *IET Radar Sonar Navig.*, vol. 11, pp. 420–425, Mar. 2017.
[385] S. Melo *et al.*, "Photonics-based dual-band radar for landslides monitoring in presence of multiple scatterers," *J. Lightw. Technol.*, vol. 36, no. 12, pp. 2337–2343, Jun. 2018.
[386] L. Lembo *et al.*, "In-field demonstration of a photonic coherent MIMO distributed radar network," in *2019 IEEE Radar Conf. (RadarCon)*, Boston, MA, USA, 2019, pp. 1–6.
[387] S. Maresca *et al.*, "Photonics for coherent MIMO radar: an experimental multi-target surveillance scenario," in *2019 20th Int. Radar Symp. (IRS)*, Ulm, Germany, 2019, pp. 1–6.
[388] N. Qian, W. Zou, S. Zhang, and J. Chen, "Signal-to-noise ratio improvement of photonic time-stretch coherent radar enabling high-sensitivity ultrabroad W-band operation," *Opt. Lett.*, vol. 43, no. 23, pp. 5869–5872, Dec. 2018.
[389] S. Zhang, W. Zou, N. Qian, and J. Chen, "Enlarged range and filter-tuned reception in photonic time-stretched microwave radar," *IEEE Photon. Technol. Lett.*, vol. 30, no. 11, pp. 1028–1031, Jun. 2018.
[390] S. Zhang, X. Li, J. Chen, and W. Zou, "Maintenance of broadband detection in photonic time-stretched coherent radar employing phase diversity," *Opt. Express*, vol. 27, no. 23, pp. 32892–32899, Nov. 2019.
[391] J. Lin *et al.*, "Photonic generation and detection of W-Band chirped millimeter-wave pulses for Radar," *IEEE Photon. Technol. Lett.*, vol. 24, pp. 1437–1439, Aug 15 2012.
[392] S. Melo *et al.*, "Dual-use system combining simultaneous active radar & communication, based on a single photonics-assisted transceiver," in *2016 17th Int. Radar Symp. (IRS)*, Krakow, Poland, 2016, pp. 1–4.
[393] H. Nie, F. Zhang, Y. Yang, and S. Pan, "Photonics-based integrated communication and radar system," in *2019 Int. Topical Meeting on Microwave Photonics (MWP)*, Ottawa, Canada, 2019, pp. 1–4.
[394] J. Shi, F. Zhang, X. Ye, Y. Yang, D. Ben, and S. Pan, "Photonics-based dual-functional system for simultaneous high-resolution radar imaging and fast frequency measurement," *Opt. Lett.*, vol. 44, no. 9, pp. 1948–1951, Apr. 2019.

[395] F. Scotti, D. Onori, M. Scaffardi, E. Lazzeri, A. Bogoni, and F. Laghezza, “Multi-frequency lidar/radar integrated system for robust and flexible doppler measurements,” *IEEE Photon. Technol. Lett.*, vol. 27, no. 21, pp. 2268–2271, Nov. 2015.

[396] S. L. Pan and J. P. Yao, “Photonics-based broadband microwave measurement,” *IEEE/OSA J. Lightw. Technol.*, vol. 35, no. 16, pp. 3498–3513, Aug. 2017.

[397] X. Xiao *et al.*, “Photonics-based wideband distributed coherent aperture radar system,” *Opt. Express*, vol. 26, no. 26, pp. 33783–33796, Dec. 2018.

[398] J. Fu, F. Zhang, D. Zhu, and S. Pan, “Fiber-distributed ultra-wideband radar network based on wavelength reusing transceivers,” *Opt. Express*, vol. 26, no. 14, pp. 18457–18469, Jul. 2018.

[399] T. Yao, D. Zhu, D. Ben, and S. Pan, “Distributed MIMO chaotic radar based on wavelength-division multiplexing technology,” *Opt. Lett.*, vol. 40, no. 8, pp. 1631–1634, Apr. 2015.

[400] D. Marpaung, J. Yao, and J. Capmany, “Integrated microwave photonics,” *Nature Photon*., vol. 13, no. 2, pp. 80–90, Feb. 2019.

[401] V. Duarte *et al.*, “Modular and smooth introduction of photonics in high-throughput communication satellites-perspective of project BEACON,” in *Int. Conf. on Space Optics -ICSO 2018*, Chania, Greece, 2018, pp. 1118079.

[402] G. Hu *et al.*, “Optical beamformer based on diffraction order multiplexing (DOM) of an arrayed waveguide grating,” *J. Lightw. Technol.*, vol. 37, no. 13, pp. 2898–2904, Jul. 2019.

[403] J. Tang *et al.*, “Integrated optoelectronic oscillator,” *Opt. Express*, vol. 26, no. 9, pp. 12257–12265, Apr. 2018.

[404] S. Pan, Z. Tang, M. Huang, and S. Li, “Reflective-type microring resonator for on-chip reconfigurable microwave photonic systems,” *IEEE J. Sel. Top. Quantum Electron.*, vol. 26, no. 5, pp. 1–12, Sept.-Oct. 2020

[405] L. Zhuang, C. Roeloffzen, M. Hoekman, K. Boller, and A. Lowery, “Programmable photonic signal processor chip for radiofrequency applications,” *Optica*, vol. 2, no. 5, pp. 854–859, Oct. 2015.

[406] S. Li *et al.*, “Chip-based photonic radar for high-resolution imaging,” 2019, arXiv preprint, *arXiv:1905.12802*.

[407] S. Pan and D. Zhu, “Broadband cognitive radio enabled by photonics,” in *the 45th Eur. Conf. Exhib. Optical Communications (ECOC)*, Dublin, Ireland, 2019.

Shilong Pan (Senior Member, IEEE) received the B.S. and Ph.D. degrees in electronic engineering from Tsinghua University, Beijing, China, in 2004 and 2008, respectively. From 2008 to 2010, he was a “Vision 2010” Postdoctoral Research Fellow at the Microwave Photonics Research Laboratory, University of Ottawa, Canada. He joined the College of Electronic and Information Engineering, Nanjing University of Aeronautics and Astronautics, China, in 2010, where he is currently a Full Professor and an Executive Director of the Key Laboratory of Radar Imaging and Microwave Photonics, the Ministry of Education. His research has focused on microwave photonics, which includes optical generation and processing of microwave signals, analog photonic links, photonic microwave measurement, and integrated microwave photonics. Prof. Pan has authored or co-authored over 420 research papers, including more than 230 articles in peer-reviewed journals and 190 papers in conference proceedings. Prof. Pan is currently an Associate Editor of *Electronics Letters*, a Topical Editor of *Chinese Optics Letters*, and is a Technical Committee Member of IEEE MTT-3 MICROWAVE PHOTONICS. He is a Steering Committee Member of IEEE International Topical Meeting on Microwave Photonics and International Conference on Optical Communications and Networks. Prof. Pan has also served as a Chair of a number of international conferences, symposia, and workshops, including the TPC Chair of the International Conference on Optical Communications and Networks in 2015 and TPC Co-chair of IEEE International Topical Meeting on Microwave Photonics in 2017. Prof. Pan is a Fellow of OSA, SPIE and IET, and a Senior Member of IEEE. He was selected as an IEEE Photonics Society Distinguished Lecturer in 2019.

Yamei Zhang (Member, IEEE) received the B.S. and Ph.D. degrees from the Nanjing University of Aeronautics and Astronautics, Nanjing, China, in 2012 and 2018, respectively.She is currently with the Key Laboratory of Radar Imaging and Microwave Photonics and the Ministry of Education, Nanjing University of Aeronautics and Astronautics, Nanjing, China. Her research interests include microwave photonic signal generation and processing and ultra-fast microwave photonics.